Radio over Fibre Distribution Systems for Ultra Wideband and Millimetre Wave Applications

A Thesis Submitted in Partial Fulfilment of the
Requirements for the Degree of Doctor of Philosophy in the
School of Electronic Engineering

By

Haymen Shams
B.Sc., M.Sc., SMIEEE

School of Electronic Engineering
Faculty of Engineering and Computing
Dublin City University

Research Supervisor

Prof. Liam Barry

April 2011

APPROVAL

Candidate: Haymen Shams

Degree: Doctor of Philosophy

Thesis Title: Radio over Fibre Distribution Systems for Ultra Wideband and Millimetre wave Applications

Examining Committee:

Chairperson: Dr. Patrick J. McNally
School of Electronic Engineering, DCU

External Examiner: Dr. Roberto Llorente
University of Valencia, Spain

Internal Examiner: Dr. Conor Brennan
School of Electronic Engineering, DCU

Supervisor: Prof. Dr. Liam P. Barry
School of Electronic Engineering, DCU

DECLARATION

I hereby certify that this material, which I now submit for assessment on the programme of study leading to the award of Doctor of Philosophy is entirely my own work, that I have exercised reasonable care to ensure that the work is original, and does not to the best of my knowledge breach any law of copyright, and has not been taken from the work of others save and to the extent that such work has been cited and acknowledged within the text of my work.

Signed: _____

ID No.: _____

Date: _____

ACKNOWLEDGMENT

First, I am very grateful to my gracious God for granting me patience and perseverance to get through the entire journey of my PhD and also meet and work with some of the finest people I have known in my entire life.

I would like to begin with expressing my gratitude from all my heart and soul to my supervisor, Prof. Liam P. Barry, for his academic guidance, support, and constant encouragement. Words just fall short in evincing how honoured I feel to have such kind helpful supervisor who helped me to develop as a researcher and I did learn from him. I would also like to thank my co-supervisor, Dr. Philip Perry for his continuous support, and advice throughout my Ph.D. He provided me with necessary suggestion, and improvements. Special thanks and appreciation is devoted to Dr. Prince Anadarajah for his continuous guidance, and support to me. I really feel honour to work with them in a team during my research study for Ph.D.

My appreciation also goes to my colleagues, the existence and left people, in the photonic research lab for their friendly academic atmosphere and help. Specially, Dr. Aleksandra Kaszubowska-Anandarajah is never forgiven for her guidance, and support at the beginning of my research work. I am in debt to my friend and advisor Dr. Amr Arisha for his assistance and continuous encouragement. He was always there when I needed him and offered his support in many of ways and inspires me throughout the long journey of Ph.D. I hold also my gratitude to all my friends in Dublin for their love and support.

At last but never the least, my parents I hope you know how much your love inspired me through and I owe you every success in life. I hope I make you proud. I am thankful to my brothers Ramez, and Mohammed, and my little sister Ayat. My family; I would have never been there without your love and encouragement.

ABSTRACT

Short range wireless technology such as ultra-wideband (UWB) and 60 GHz millimetre wave (mm-wave) play a key role for wireless connectivity in indoor home, office environment or large enclosed public areas. UWB has been allocated at the frequency band 3.1-10.6 GHz with an emission power below -41.3 dBm. Mm-wave signals around 60 GHz have also attracted much attention to support high-speed data for short range wireless applications. The wide bandwidth and high allowable transmit power at 60 GHz enable multi-Gbps wireless transmission over typical indoor distances. Radio-over-fibre (RoF) systems are used to extend the propagation distance of both UWB and mm-wave signals over hundred of meters inside a building. UWB or mm-wave signals over fibre can be generated first at the central office before being distributed to the remote access points through optical fibre.

In this work, we investigate two new techniques to generate and distribute UWB signals. These techniques are based on generating Gaussian pulse position modulation (PPM) using a gain switched laser (GSL). The simulation and experimental results have been carried out to show the suitability of employing gain switching in UWB over fibre systems (UWBoF) to develop a reliable, simple, and low cost technique for distributing UWB pulses. The second part of this work proposes two configurations for optical mm-wave generation and transmission of 3 Gbps downstream data based on GSL. We investigate the distribution of these two methods over fibre with wireless link, and demonstrate the system simplicity and cost efficiency for mm-wave over fibre systems. Both configurations are simulated to verify our obtained results and show system performance at higher bit rates. In the third part, we generate phase modulated mm-waves by using an external injection of a modulated light source into GSL. The performance of this system is experimentally investigated and simulated for different fiber links.

TABLE OF CONTENTS

LIST OF FIGURES

LIST OF TABLES

LIST OF ACRONYMS

2G	Second generation
3G	Third generation
4G	Fourth generation
APD	Avalanche photodiode
ASE	Amplified spontaneous emission
AWG	Arbitrary waveguide grating
BER	Bit error rate
BERT	Bit error rate tester
BPF	Bandpass filter
BPSK	Binary phase shift keying
BPSK	Binary phase shift keying
BS	Base station
BTB	Back-to-Back
CEPT	European conference of postal and telecommunications
CO	Centre office
CW	Continuous wave
DAS	Distributed antenna system
DBR	Distributed Bragg refelector
DC	Direct current
DFB-LD	Distributed feedback laser diode
DM	Direct modulated
DR	Dynamic range
DR	Dynamic range
DSB	Double sideband
DSF	Dispersion shifted fibre
DVD	Digital versatile disc
EAM	Electro-absorption modulator
ECC	Electronic communication committee
EDFA	Eribum doped fiber amplifier

EI	External injection
EIRP	Equivalent isotropic radiation power
EOM	Electro-optic intensity modulator
EOPM	Electro-optic phase modulator
EPON	Ethernet passive optical network
ETSI	European telecommunications standards institute
FBG	Fiber Bragg grating
FCC	Federal communication commission
FFT	Fast Fourier transform
FP-LD	Fabry Perot laser diode
FTTH	Fiber to the home
FTTP	Fiber to the premise
FWA	Fixed wireless access
GPON	Gigabit passive optical network
GPRS	General packet radio service
GPS	Global positioning system
GS-DFB	Gain switched distributed feedback
GSL	Gain switched laser
GSM	Global system for mobile communications
GVD	Group velocity dispersion
HDMI	High definition multimedia interface
HDTV	High definition television
HNA	Home networking area
IEEE	Institute of electrical and electronics engineers
IF	Intermediate frequency
IFFT	Inverse fast Fourier transform
IM	Intensity modulation
IM3	Third intermodulation product
IM-DD	Intensity modulation and direct detection
IMT	International mobile telecommunication
IR-UWB	Impulse radio Ultra-wide band
ISI	Intersymbol interference
LD	Laser diode

LNA	Low noise amplifier
LO	Local oscillator
LOS	Line-of-sight
LTE+	Advanced long term evolution
MAN	Metropolitan area network
MIMO	Multiple input multiple output
MMF	Multi-mode fiber
Mm-wave	Millimetre wave
MPN	Mode partition noise
MQW	Multiple quantum well
MU	Mobile unit
MZM	Mach Zehnder modulator
NLOS	Non-line-of-sight
NRZ	Non-return to zero
OBPF	Optical bandpass filter
ODC	Optical distribution centre
ODL	Optical delay line
OFDM	Orthogonal frequency division multiplexing
OIL	Optical injection locking
OIPL	Optical injection phase locking
OLT	Optical line terminal
ONU	Optical network unit
OOK	On-off keying
OPLL	Optical phase locked loop
OSSR	Optical sidebands suppression ratio
P2MP	Point-to-multipoint
P2P	Point-to-point
PAM	Pulse amplitude modulation
PD	Photo-diode
PIN-PD	p-i-n photodetector
PM	Phase modulation
PPM	Pulse position modulation
PRBS	Pseudo random bit sequence

PSD	Power spectral density
PSK	Phase shift keying
R&O	the First Report and Order
RAU	Remote antenna unit
RF	Radio frequency
RIN	Relative intensity noise
RN	Remote node
RoF	Radio over fiber
ROP	Received optical power
RT	Radio terminal
RZ	Return to zero
SFDR	Superior free dynamic range
SMF	Single mode fiber
SMSR	Side mode suppression ratio
SNR	Signal to noise ratio
SSMF	Standard single mode fiber
TDM	Time Division multiplexing
TFC	Time frequency coding
TLM	Transmission line model
UMTS	Universal mobile telecommunication system
UWB	Ultra wideband
UWBoF	Ultra-wideband over fiber
VCSEL	Vertical cavity surface emitting laser
VCSEL	Vertical cavity surface emitting laser
WDM	Wavelength division multiplexing
WiMax	Worldwide Interoperability for Microwave Access
WLAN	Wireless local area network
WPAN	Wireless personal area network

Chapter 1 – Introduction

1.1 Wireless Access Networks

Wireless access networking is one of the fastest growing technologies in the area of telecommunications and computer systems. The advances in wireless technologies and the existence of inexpensive wireless equipment have contributed much to the tremendous growth of wireless access networks during the last decades. These networks have changed the way people use computers and other personal electronic devices at work, home, and when they are travelling.

Nowadays, there are many wireless access technologies that vary according to bandwidth, range, and speed as shown in Fig. 1.1. The first and second generation (1G and 2G) of wireless mobile telephone were intended for voice transmission. The main difference between these generations is that 1G used analogue signals and the 2G uses digital signals. The global system for mobile (GSM) is the most popular digital cellular network standard and allocated in radio spectrum around 900, and 1800 MHz. The initial GSM standard allowed only 13 kbps for voice transmission and 9.6 kbps for data transmission [1]. An extension to the GSM standard was defined by the general packet radio service (GPRS) which offers data transmission up to 160 kbps [2]. The third generation of wireless cellular phone such as universal mobile telecommunication system (UMTS) provides both voice and data applications [3]. This allows people to make phone calls, send text and multimedia messages, and browse the internet. The fourth generation (4G) offers higher data speeds and more mobility such as advanced long term evolution (LTE+), and worldwide interoperability for microwave access (WiMax). The 4G system provides a comprehensive and secure all IP based mobile broadband to smartphones, laptop computer and other mobile devices. The use of multiple input multiple output (MIMO) technology improves communication performance and increases the potential throughput by using additional antennas at both the transmitter and receiver end. The requirement speed of 4G services by international mobile telecommunication advanced (IMT-advanced) standard is targeted to reach a peak

download at 100 Mbit/s for high mobility communication in a moving vehicle and 1 Gbit/s for low mobility communication (such as pedestrians and stationary users) [4].

Wireless local area networks (WLAN) or IEEE standards 802.11 a/b/g/n provide wireless coverage in one or more rooms in a building. The cost, data speed, and easy integration of WLAN have gained great popularity. IEEE 802.11 series standards have different speed and frequency ranges, shown in summary table 1.1 [5], and the range of these varies from 30 -100 m based on location.

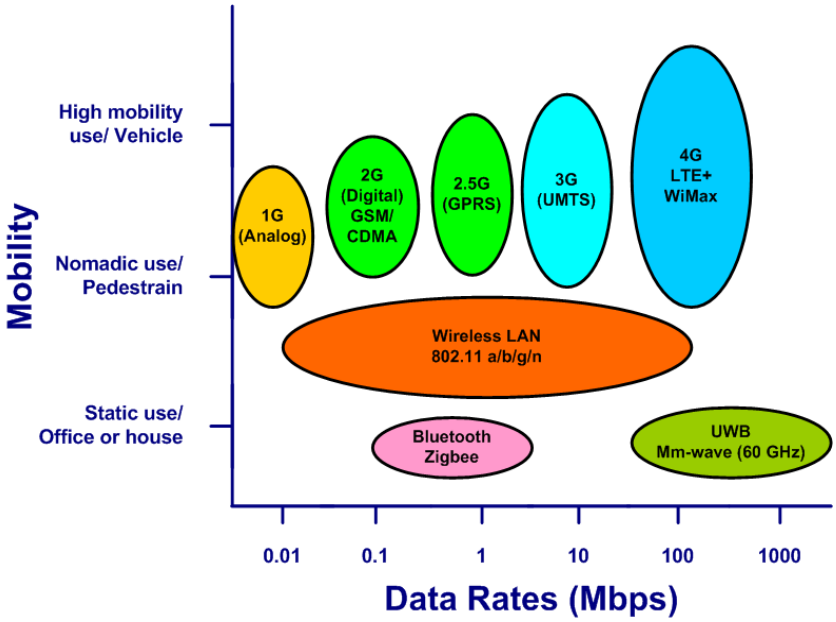

Fig. 1.1. Wireless access technologies

Wireless personal area network (WPANs) is another paradigm that provides short range wireless connectivity between consumer electronic devices such as personal digital assistants (PDA), and mobile phones. Bluetooth (IEEE standard 802.15.1) was the first low data rate standard for WPAN networks [6]. It enables wireless connectivity between mobile phones, computers, and electronic appliances with data rates up to 3 Mbps. ZigBee (IEEE standard 802.15.4) wireless technology is designed for data rates up to 250 kbps, primarily for wireless sensor applications [7]. This technology is mainly devoted for low data rate, low power consumption, and low cost wireless networking. Other exciting technologies in this area are ultra wideband (UWB) and millimetre waves (mm-waves) at 60 GHz. These are of particular importance to the work presented in this thesis.

UWB wireless technology is intriguing as it lies in the frequency band 3.1- 10.6 GHz and has low power consumption [8]. It is designed for short range applications in fast home networks for video or audio data transport. Mm-wave communication systems are another growing wireless technology that enables transmission of data at speeds of more than 1 Gbps. This is possible due to the huge and unexploited bandwidth available, combined with advances of low cost fabrication technology and low loss packaging material. Mm-waves use the frequency band 30 -300 GHz, which corresponds to the wavelengths from 10 – 1 mm and within that range, the frequency band around 60 GHz has been assigned globally for unlicensed use. The goal of the 60 GHz system is for future "super broadband" data services delivery in terms of data rate and power consumption. Compared to lower frequency bands, the radio signals in this mm-wave band are extremely susceptible to attenuation from atmospheric oxygen absorption. In addition, the free space loss increases quadratically with signal frequency giving up to 21 dB more loss than a signal at 5 GHz. This classifies mm-waves for short range applications but it also means dense frequency reuse patterns [9].

Table 1.1. Summary of wireless access networks.

Technology	**Frequency band**	**Bit rate**	**Signal range**	**Typical usage**
GSM	900/1800 MHz	9.6 kbps	35 km	Voice and data
GPRS	900/1800 MHz	160 kbps	35 km	Data and WAP
UMTS	873/1900 MHz	2 Mbps	2 km	Voice, data, and multimedia
Bluetooth	2.4 GHz	2.1 Mbps	10 m	WPAN
ZigBee	2.4 GHz	250 kbps	10 m	WPAN
ÙWB	3.1 – 10.6 GHz	> 100 Mbps	10 m	WPAN
Mm-wave (60 GHz)	57- 64 GHz	> 1Gbps	10 m	WPAN
802.11a	5 GHz	54 Mbps	100 / 30 m	WLAN
802.11b	2.4 GHz	11 Mbps	110/ 35 m	WLAN
802.11g	2.4 GHz	54 Mbps	110/ 35 m	WLAN
802.11n	2.4 / 5 GHz	600 Mbps	250/ 70 m	WLAN

1.2 Optical Fibre Access Networks

The growing demands for broadband internet connection at home are increasing nowadays in most countries. Services and multimedia applications such as internet video, video communication, and video on demand are now available and need much greater bandwidth than that is offered today. At the same time, new services such as high definition television (HDTV) and interactive video have been developed and are becoming commercially available in many countries. These applications and services drive the need for new connections that can carry the increased bitrates inside homes, or buildings.

Single mode optical fibre provides huge transmission bandwidth over extremely long distances, compared to the existing access networks such as digital subscriber lines (DSL), and cable modems. The end goal is to provide this fibre connection to each customer's home or premises. Fibre to the home/premises (FTTH/P) is a solution to open up the "last mile" bandwidth bottleneck and enables the increasing delivery of high speed services to the final users' front door [10]. The number of FTTH subscribers in Europe (including Russia) has reached 4.5 million with more than 25 million homes/buildings passed, according to the latest figures from FTTH council [11]. While Japan continues to lead the world in terms of the number of FTTH/P subscribers, and South Korea has the highest penetration in the world and is the first country in the world to reach over 50% penetration of households using FTTH/P.

The broadband market is expected to steadily grow in the coming years to reach close to 140 million subscribers around the globe by 2014 [12]. FTTH/P installation is achieved by using either a point-to-point (P2P) or point-to-multipoint (P2MP) topology [13]. In the case of P2P topology, optical networks rely on a variety of electronically enabled equipment to distribute the signal such as switches, routers, or multiplexers. However, there is a growing attention to P2MP passive optical network (PON) architectures due to the 20 - 35% expense reduction from sharing the fibre and all passive optical components, in addition to the low maintenance requirement for passive modules. The basic configuration of a PON connects the telecom central office (CO) to businesses and residential users by using one wavelength channel in

the downstream direction. A single feeder fibre is used in PON to connect an optical line terminal (OLT) at the CO to multiple drop fibres that go to each home. At the subscriber end, the drop fibre terminates at an optical network unit (ONU) that converts the optical signals to electrical signals for use by various devices such as phones, computers, HDTVs, etc.

A PON configuration reduces the required amount of fibre and does not have any active elements in the signal's path compared to P2P topology. The only elements used in such a network are passive combiners, couplers, and splitters. There are several multiple-access techniques that are used in a single PON architecture. The most promising candidate techniques are time division multiplexing PON (TDM-PON) and wavelength division multiplexing PON (WDM-PON) as shown in Fig. 1.2 [14].

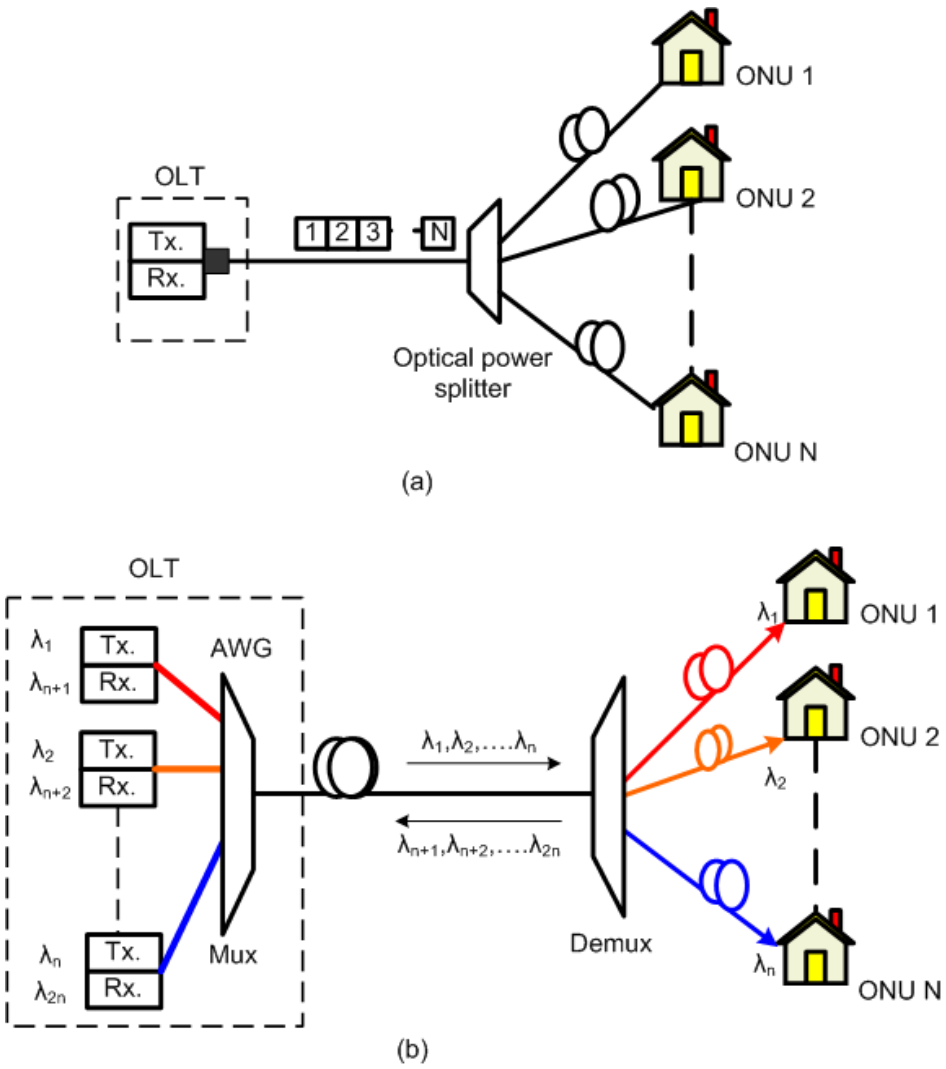

Fig. 1.2. PON configurations for FTTH/P; (a) TDM-PON and (b) WDM-PON.

A TDM-PON shares a single transmission channel with multiple subscribers in the time domain. A passive optical splitter is used to split the downstream signals to multiple ONUs. Each ONU selects its destined packets, and discards the packets addressed to the other ONUs. This scheme has low installation and maintenance cost, however, the number of ONUs is limited by the splitting loss, and by the bit rate of the transceiver in the OLT. Several TDM-PON standards have been developed for 16 ONUs or more with a maximum transmission distance up to 20 km such as; Gigabit PON (GPON) with 2.5/1.25 Gbps down/upstream and Ethernet PON (EPON) with 1.25 Gbps for both directions. Another new commercial standard available now is 10GPON which supports up to 10 Gbps downstream and 2.5 Gbps upstream.

In a WDM-PON the bandwidth of the fibre is shared between the subscribers, and each subscriber is assigned a pair of wavelength channels for up/down links. This means that each subscriber gets a dedicated point-to-point optical channel to the OLT and can send data at any time independent of other subscribers, although they are sharing a common point-to multipoint physical architecture. A WDM multiplexer/demultiplexer or array waveguide grating (AWG) is used to combine/separate the multiple-wavelength signals instead of the optical power splitter in a TDM-PON configuration. This decreases the insertion power loss in WDM-PONs and improves its ability to scale up to serve a large number of users sharing a single PON. However, there are some challenges in developing a practical system since each ONU requires a specified wavelength source and ‘N’ separate transceivers at the OLT to realize a connection to each subscriber.

1.3 Objective and Major Contribution

Fibre connections to the home provide a reliable distributed signal, but they are not flexible enough to allow convenient roaming connection inside homes. Therefore, the combined technology between wireless and optical fibre can provide access solutions that offer portability and flexibility to users. This technology is known as radio over fibre (RoF) and is the most promising solution to increase the capacity coverage, bandwidth and mobility in environments such as conference centres, airports, hotels, shopping malls, and ultimately to home and small offices [15].

Furthermore, the use of photonic technologies in optical wireless generation is desirable and can greatly reduce the cost and the requirement of high frequency electrical components for signal processing in these short range radios.

The objective of this thesis is to investigate a number of simple and cost effective RoF systems for delivering future high speed wireless signals over optical fibres and air links. The main contributions of this thesis are to present novel techniques for optical generation of short range wireless signals as follows.

- Two optical transmitter schemes for generating an electro-optic impulse radio (IR-UWB) signal based on gain switched laser (GSL) and pulse position modulation (PPM) at 1.625 Gbps are proposed in chapter 4.

    - The first setup uses a single gain switched optical source with two optical Mach-Zehnder modulators (MZM) [16, 17].
    - The second setup has two optical sources driven with a signal composed of an NRZ data and an RF sinusoid signal [18].

- Two setups for optical generation and distribution over fibre of mm-waves at 60 GHz with bit rates up to 3 Gbps are demonstrated in chapter 5. These two schemes are based on optical comb generation of the GSL. The optical 60 GHz signal is produced by selecting two optical tones from the optical comb.

    - The first setup uses an external modulator to modulate the selected tones with NRZ data signal [19].
    - The second setup drives the laser with the RF sinusoidal and data signal coupled together [20].

- Another alternative way for generating an optical modulated mm-wave signal is proposed in chapter 6 by externally injecting OOK modulated light into a GSL and selecting two signals separated by 60GHz [21].

1.4 Thesis Organization

The rest of this thesis is organized as follows. Chapter 2 mainly focuses on an overview of radio over fibre (RoF) technology and its basic components. The conventional structure of a RoF system and its main optical components are described in detail. RoF networks are described for different applications such as cellular networks, and indoor distribution. Furthermore, the main limitation factors such as optical noise and nonlinear distortion that affect the performance of RoF systems are discussed in this chapter.

In chapter 3, optical generation and distribution of short range wireless communication signals over optical fibres are described for ultra wideband (UWB), and mm-waves at 60 GHz. Regulation and spectrum allocation for these signals are defined. Several recent reported schemes for optical generation, processing, and distribution of these short range signals are also presented in this chapter.

Chapter 4 proposes and demonstrates two different optical generation techniques for electro-optical impulse radio (IR-UWB) signals based on a GSL and pulse position modulation (PPM) scheme at a bit rate of 1.625 Gbps. The system performance of the two setups is evaluated by using experimental implementations and simulations for different optical transmitter configurations and different fibre links. Then, a comparison between both setups is presented to show the trade-off between the cost/complexity of the transmitter configuration in a UWB over fibre system, and the required reach and performance of the distribution network.

In chapter 5, two novel optical transmitter schemes are proposed for generation and distribution of mm-waves at bit rates up to 3 Gbps. Experimental investigations and simulations are carried out to assess the system performance in both cases. Comparison between the two setups is also discussed to show the advantages and disadvantages of both systems.

Chapter 6 investigates another novel technique for optical generation of a phase modulated mm-wave at 60 GHz by using external injection into GSL with a

modulated light source. The experimental setup is implemented and analysed at 1.25 and 2.5 Gbps data rates and simulation work is also carried out to validate the obtained results.

Finally, chapter 7 provides a brief summary of the thesis and the possible future research opportunities.

References

[1] M. P. Clark and M. Clarke, Wireless Access Networks: Fixed Wireless Access and WLL Networks--Design and Operation, John Wiley \& Sons, Inc, New York, NY, USA, 2000.

[2] T. Halonen, J. Melero and J. R. Garcia, GSM, GPRS and EDGE Performance: Evolution Toward 3G/UMTS, Halsted Press, New York, NY, USA, 2002.

[3] B. Walke, R. Seidenberg, M. P. Althoff, UMTS: The Fundamentals, Wiley & Sons, England, 2003.

[4] International Telecommunication Union. IMT-Advanced (4G) Mobile wireless broadband on the anvil [Online]. Available: http://www.itu.int/newsroom/press releases/2009/48.html. [accessed: 3/2/2011]

[5] Wi-Fi Alliance. Wi-Fi CERTIFIED™ n: Longer-Range, Faster-Throughput, Multimedia-Grade Wi-Fi® Networks [Online]. Available: http://www.wi-fi. org/register.php?file=wp_Wi-Fi_CERTIFIED_n_Industry.pdf. [accessed: 2/2/2011]

[6] IEEE 802.15 WPAN Task Group 1 (TG1). IEEE 802.15 Bluetooth standard for wireless personal area network [Online]. Available: http://ieee802.org/15/pub/ TG1 .html. [accessed: 2/2/2011]

[7] IEEE 801.15 WPAN Task Group 4 (TG4). IEEE 802.15.4 Standard for Low Rate Wireless Personal Area Networks (WPAN) [Online]. [accessed: http:\\www:ieee802.org\15\pub\TG4.html]

[8] IEEE 801.15 WPAN Task Group 3 (TG3), IEEE 802.15.3 Standard for High Rate Wireless Personal Area Networks. [Online]. Available: http:\\www.ieee802.org\ 15 \pub\TG3.html. [accessed: 2/2/2011]

[9] C. Park and T. S. Rappaport, "Short-range wireless communications for next-generation networks: UWB, 60 GHz millimeter-wave WPAN, and ZigBee," *Wireless Communications, IEEE*, vol. 14, no. 4, pp. 70-78, 2007.

[10] P. W. Shumate, "Fiber-to-the-home: 1977-2007," *Lightwave Technology, Journal of*, vol. 26, no. 9, pp. 1093-1103, 2008.

[11] TelecomPaper, FTTH/B subscribers in Europe up 22 percent in H1 [Online]. http://www.telecompaper.com/news/ftthb-subscribers-in-europe-up-22-percent-in-h1. [accessed: 2/2/2011]

[12] IDATE Consulting and Research: Telecoms, Internet, Media [Online].

Available: http://www.idate.org/en/News/Inventory-of-FTTH-in-Europe-Middle-East625.html. [accessed: 3/18/2010]

[13] P. E. Green, "Fiber to the home: The next big broadband thing," *Communications Magazine, IEEE*, vol. 42, no. 9, pp. 100-106, 2004.

[14] C. H. Lee, W. V. Sorin, and B. Y. Kim, "Fiber to the home using a PON infrastructure," *Lightwave Technology, Journal of*, vol. 24, no. 12, pp. 4568-4583, 2006.

[15] R. Gaudino, D. Cardenas, M. Bellec, B. Charbonnier, N. Evanno, P. Guignard, S. Meyer, A. Pizzinat, I. Mollers, and D. Jager, "Perspective in next-generation home networks: Toward optical solutions?" *Communication Magazine, IEEE*, vol. 48, no. 2, pp. 39-47, 2010.

[16] A. Kaszubowska-Anandarajah, P. Perry, L. P. Barry, and H. Shams, "An IR-UWB photonic distribution system," *Photonics Technology Letters, IEEE*, vol. 20, no. 22, pp. 1884-1886, 2008.

[17] H. Shams, A. Kaszubowska-Anandarajah, P. Perry, and L. Barry, "Demonstration and optimization of an optical impulse radio ultrawideband distribution system using a gain-switched laser transmitter," *Optical Networks, Journal of*, vol. 8, no. 2, pp. 179-187, 2009.

[18] H. Shams, A. Kaszubowska-Anandarajah, P. Perry, P. Anandarajah, and L. P. Barry, "Electro-optical generation and distribution of ultrawideband signals based on the gain switching technique," *Optical Communications and Networking, IEEE/OSA Journal of,* vol. 2, no. 3, pp. 122-130, 2010.

[19] H. Shams, P. M. Anandarajah, P. Perry, and L. Barry, "Optical generation and wireless transmission of 60 GHz OOK signals using gain switched laser," *presented at Optical Fiber Communication and National Fiber Optic Engineers Conference (OFC/NFOEC 2010)*, pp. OThO7, 21- 25th March, San Diego, USA.

[20] H. Shams, P. M. Anandarajah, P. Perry, and L. P. Barry, "Optical generation of modulated millimeter waves based on a gain-switched laser," *Microwave Theory and Techniques, IEEE Transactions on*, vol. 58, no. 11, pp. 3372-3380, 2010.

[21] H. Shams, P. Perry, P. Anandarajah, and L. Barry, "Modulated millimeter-wave generation by external injection of a gain switched laser," *Photonics Technology Letters, IEEE*, vol. 23, no. 7, pp. 447-449, 2011.

Chapter 2 –Radio over Fibre Technologies

2.1 Introduction

The combination of wireless and fibre optics was first introduced in the early 1980s in the United States for military applications. Fibre cables were used to connect the control or central station to distant antennas in the development of radar systems. The RF signals were conventionally transported via bulky copper cables and waveguides where all high frequency elements of a system have to be placed together to minimize the RF losses. Therefore, the low optical loss and large bandwidth features of the fibre made it an efficient transmission medium for transporting high frequency radio signals. In addition, optical fibre cables have substantially less weight over the coaxial cable and are cost effective for long link lengths [1]. In late 1980s, radio over fibre (RoF) systems were then developed by Cooper for cordless and mobile communications [2]. Following this many research centres and scientists across the world have developed new techniques to send wireless signals over fibre.

RoF systems are now being used in many RF applications for transporting the radio signal from a central office (CO) to a remote antenna site such as cellular networks, indoor distributed antenna systems, and wireless local area networks (WLANs). When utilizing a large number of distributed remote terminals, the corresponding remote antenna units (RAUs) should be simple, small in size, light and low cost. Equally, the system components should be arranged in such a way that most of the expensive and high frequency equipment such as that required for coding, modulation, multiplexing, and up-conversion process are localized at the central station [3].

This chapter is divided up into eight sections. The electrical and optical methods for RF distribution are introduced in sections 2.2 and 2.3. The basic bi-directional RoF transmission systems are described in section 2.4. In section 2.5, the optical link components in RoF systems are discussed in terms of their operating principles and

characteristics. Section 2.6 represents the network architectures for RoF and its applications. Then, the limitations on RoF system are discussed in section 2.7. Finally, the chapter summary is outlined in section 2.8.

2.2 Electrical Methods for RF Signal Distribution

The electrical distribution of radio signals such as VHF, UHF, microwave, or millimetre wave is challenging due to the very high loss and high cost of such cables or waveguides. This means that the central generation and distribution of the radio signals is not practical, and the data signals must be distributed in a baseband or a low intermediate frequency (IF) to the base station. Then, the baseband or IF signal would have to be upconverted to the required RF frequency at each base station, amplified, and radiated. This leads to a rather complex base station system that has very tight performance requirements.

The typical electrical distribution system is shown in Fig. 2.1. The system design includes a number of repeaters along the transmission lines to counteract the cable loss and maintain an appropriate value of signal to noise ratio. However, the number of stages and thus the covered area from a switching centre are limited due to the degradation in the signal fidelity. Coaxial cables or waveguide also suffer from moisture problems that can significantly reduce system performance. This can be addressed by replacing the affected cable with another. Once distribution has been achieved the base stations have to transform the baseband or IF signals up to the required RF frequency [4].

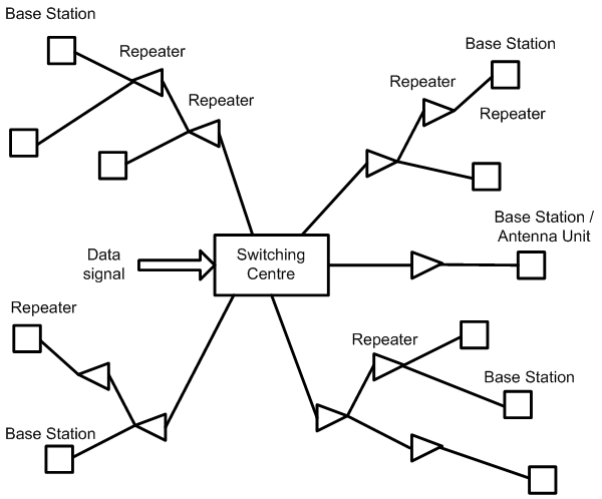

Fig. 2.1. Electrical distribution scheme for data signals.

From the above discussion, electrical methods for generation and distribution of modulated RF signals are severely limited in both performance, and cost.

2.3 Optical Methods for RF Signal Distribution

Optical fibres are used to deliver high quality radio signals directly to a point of free space radiation (antenna site). The simple system arrangement for radio signal transmission over fibre is shown in Fig. 2.2. There are three possible transmission configurations used to generate and distribute wireless signals over optical fibre links [5, 6]. These configurations depend on the required application and the hardware components in the CO and base stations. The three transmission systems are classified based on the transmission frequency bands into:

- RF-over-fibre,
- IF-over-fibre, and
- Baseband-over-fibre.

In RF-over-fibre, the radio signal is directly transmitted over the fibre link at the radio carrier transmission frequency without any need for frequency conversions at the base station. This leads to centralization of all control and electrical hardware at the CO, and reduces the complexity and the cost of the base stations. However, it is vulnerable to fibre chromatic dispersion and requires high speed optical electronic components for high frequency radio signals [5].

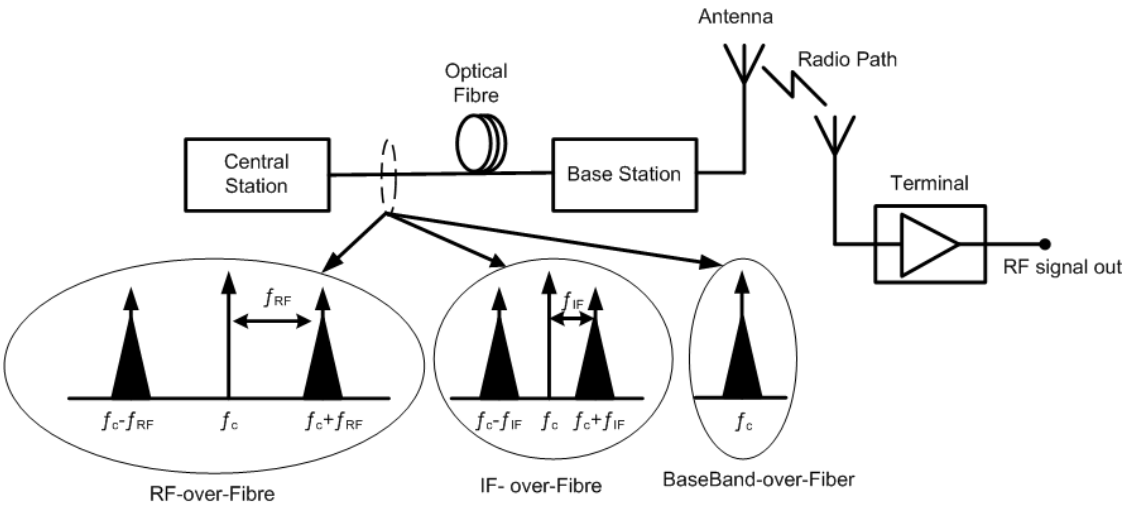

Fig. 2.2. The schematic diagram for radio signal distribution over fiber.

In order to reduce the effect of chromatic dispersion, the wireless signal for downstream transmission can be distributed from the CO to the remote terminals at a lower IF which is known as IF-over-fibre. This scheme uses lower speed opto-electronic devices and can allow transmission over the multimode fibre (MMF). This can be advantageous as MMF is cheaper than single mode fibre (SMF) and many buildings now have infrastructure networks based on MMF. At the receiver side, it requires a local oscillator (LO) and high speed electronic mixers which increase the complexity and cost of the RAU. In addition, this also results in limitations to upgrading or reconfiguring the wireless channel for different wireless frequencies. Baseband-over-fibre is the third transport technique where the data signal is transported in baseband to the remote terminal and then up-converted to the required RF signals. This greatly reduces the limitations imposed by fibre chromatic dispersion (as for IF-over-fibre scheme) and the need for high speed opto-electronic devices. However, the system complexity and cost increases due to the high LO frequency signal needed at the remote terminals. This can only be simplified if the LO signal is delivered optically from a CO.

For any transmission system, practical issues such as the size, weight, reliability, cost, and power consumption at the antenna site are of critical importance. Therefore, it is necessary to keep most of the expensive, high frequency equipment at a central location, thus allowing the remaining equipment at the base station to be simple, small sized, and requiring low power consumption. This results in easy installation, and low maintenance making it suitable for installation in remote or inaccessible places.

2.4 Basic Radio over Fibre Systems

The simplest schematic diagram of a bi-directional RoF system is shown in Fig. 2.3 [7]. In the downlink/uplink direction, the light intensity of the laser diode is directly modulated with the RF signal and then transmitted towards the photodiode through optical fibre links. The choice between MMF or SMF, depends on the application and transmission distance. The wavelength of the light can be either 1300 nm or 1550 nm for low transmission loss in silica fibre. Normally, SMF is used to carry the information in a single direction only (simplex), which means that we need to use

two optical fibre links for bi-directional (duplex) communication. However, wavelength division multiplexing (WDM) technology makes it possible to transmit the information in the two directions by using different wavelengths. The optical receiver is usually a normal Positive Intrinsic Negative (PIN) photodiode and it converts the optical signal back to the electrical signal, where the RF power output is directly proportional to the square of the input optical power. This kind of the RoF system is called intensity modulated-direct detection (IM-DD) which is widely used in cellular applications due to its simplicity and low cost. There are also other types of optical modulation used for different application, such as frequency or phase modulation which require an external modulator.

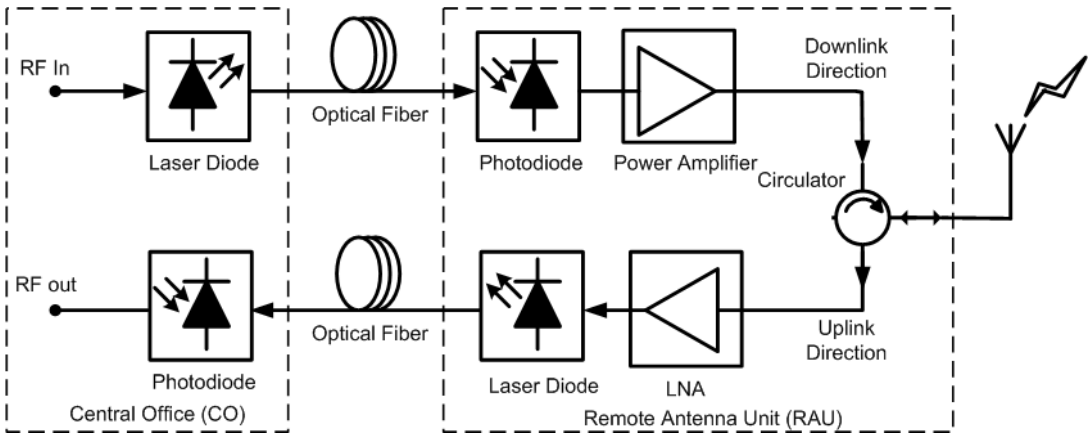

Fig. 2.3. The schematic diagram for the simple bidirectional RoF system.

In this conventional RoF system, the RAU contains a laser, photodoiode, amplifiers, circulator, control circuit, and power supplies. These components can be enclosed in a compact and integrated package. However complexity still contributes much cost to the remote terminals.

For applications that need a large number of remote terminals, the cost and power consumption are very important in the overall design. Therefore, it would be more desirable to have radio access points with zero power consumption and a low cost component. In Fig. 2.4, another proposed RAU replaces the laser, photodiode, amplifiers and circulator with a single opto-electronic device, an electro-absorption modulator (EAM) that acts as a remote transceiver [7, 8]. This means that the EAM device can be used as a photodiode for downlink and as an optical modulator for the uplink transmission. In this case, the RAU does not need a light source or control

circuit, and therefore it is much simpler and cheaper. For small radio coverage such as pico-cell networks, the RAU can be made simpler without using any RF amplifiers or DC bias [9].

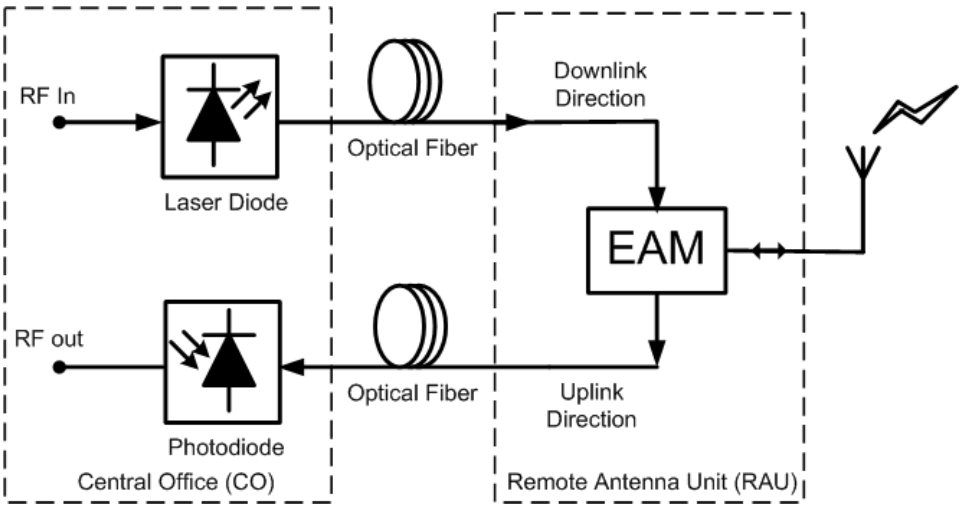

Fig. 2.4. Schematic diagram for bi-directional RoF system using an electro-absorption transceiver at the RAU.

2.5 RoF Link Components

This section describes in detail the operating principles and characteristics of the optical transmitter, receiver, and optical link that make up the RoF system.

2.5.1 Optical Transmitter

In the optical transmitter, the laser diode is an essential element in fibre optic links since it generates the optical signal that carries the information. Normally, the laser wavelengths are selected to be at 1300 nm and 1550 nm, corresponding to the lowest known values of dispersion and attenuation, respectively. The RF (10 kHz- 300 MHz) or the microwave (300 MHz- 300 GHz) signal can be carried on the laser frequency (around 200 THz) and transported over the fibre links in several ways. The simplest way is to directly modulate the injection current of a semiconductor laser diode (direct modulation) or to drive an electro-optic modulator (external modulation).

A. Direct Modulation Scheme

The direct modulation scheme and the laser light output power versus injection current (L-I) of a typical semiconductor laser are shown in Fig. 2.5. The biased laser emits a constant level of optical power P_0 if there is no RF signal. When the RF signal is applied, the optical power is deviated from bias point P_0 according to the change of the driving current. The L-I curve shows that the output laser power increases slowly at low current values up to the threshold point I_{th}. Above the threshold current level, the optical output increases rapidly until it reaches power saturation. Power saturation is basically due to heating of the laser junction which results from internal losses or current leakage at high operating power [10]. A large input current will give high optical output power and high signal to noise ratio. However, this can drive the laser into a non-linear region where distortion occurs. Another serious limitation is due to the clipping and distortion at the nonlinear region near the knee of the L-I curve. That means the laser diode should be biased at a point in the linear region where there is minimum distortion. The output laser power P_{opt} versus current I in the linear region can be given as:

$$P_{opt} = \frac{hf}{e}\eta_L (I - I_{th}); \qquad I_{th} \le I \le I_S \tag{2.1}$$

where h is Plank's constant, f is the laser frequency, e is the electron's charge, I_s is the saturation current, and η_L is the laser quantum efficiency, that is, the average number of the generated photons per electron. Semiconductor lasers are classified into a single and multimode type.

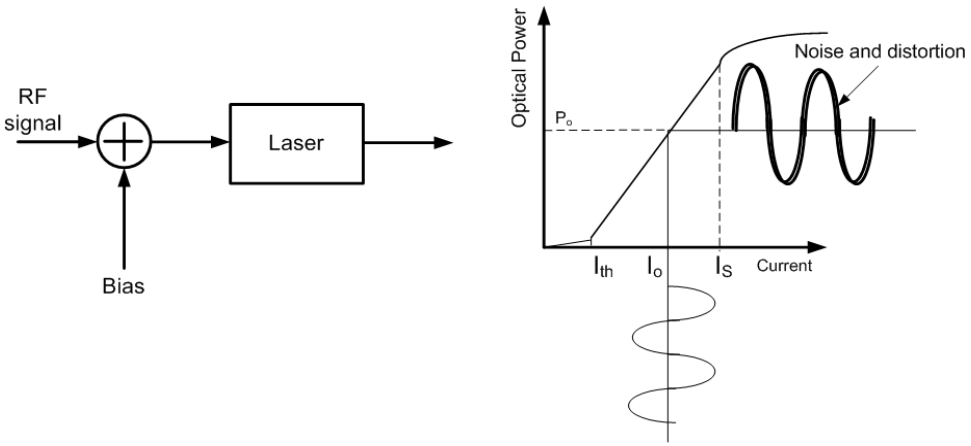

Fig. 2.5. Direct intensity modulation of the optical signal.

A Fabry Perot (FP) laser is a multimode laser and emits light in several longitudinal modes that only satisfy the condition of constructive interference of forward and backward travelling optical waves in the cavity. However, a distributed feedback laser diode (DFB-LD) lases in a single longitudinal mode generated from the coupling between the forward and backward wave. This occurs due to the periodic variation of the refractive index across one side of the active layer. There are some important factors that should be considered when semiconductor lasers are directly modulated in optical fibre communication systems.

Modulation bandwidth: In a typical semiconductor laser, the modulation bandwidth is an important parameter in a RoF system where it sets the limit on the maximum RF frequency attainable in a direct modulated laser. The modulation response for a laser is relatively flat over a wide frequency range with a peak at the relaxation oscillation frequency as shown in Fig. 2.6. This peak is due to the intrinsic response of the device, and then drops sharply for higher frequencies indicating a decrease of the laser's responsivity. Normally, this relaxation oscillation frequency increases with the bias current and hence increases the modulation bandwidth of the laser diode. A modulation bandwidth of 30 GHz was reported in multiple quantum well (MQW) laser at 1550 nm wavelength and 37 GHz for a distributed Bragg reflector (DBR) laser [11, 12]. The modulation bandwidth can also be extended further by more than five times that of the free running laser by using an injection locking technique. The improvement of the optical bandwidth is achieved by injecting the semiconductor laser with another free running laser with a specific power and detuned frequency. Recently, an enhancement in modulation bandwidth using optical injection was recorded for DFB laser at 44 GHz, and vertical cavity surface emitting laser (VCSEL) at 50 GHz [13, 14].

Laser noise: The main contribution to laser noise is due to random spontaneous emission. Each spontaneously emitted photon adds a small field component with random phase to the coherent field, and thus results in fluctuations of both the amplitude and phase of an optical source. The unwanted intensity variation is known as *relative intensity noise* (RIN) while the phase noise leads to a finite linewidth. The value of RIN is a function of the modulation frequency and degrades the signal to

noise ratio [15]. In a typical semiconductor laser at 1550 nm, the RIN increases with the modulation frequency, and peaks at the relaxation oscillation frequency. For higher frequencies, the laser can not respond to fluctuations and thus the RIN decreases rapidly. The laser phase noise is converted to intensity noise after transmission through a fibre due to fibre dispersion [16]. This noise contributes to the RIN and limits the signal to noise ratio at the receiver end.

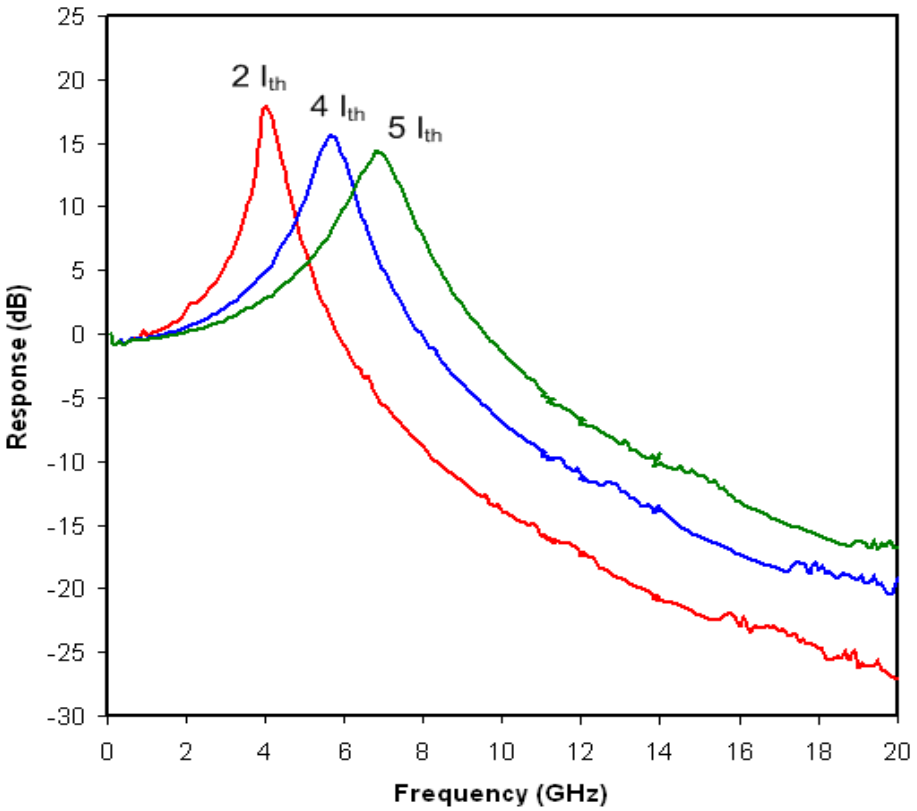

Fig. 2.6. Frequency response for 1.55 μm laser with several bias levels.

Frequency chirping: Direct modulation of a laser not only changes the output power of the laser but also the emission frequency [15]. This is due to the carrier density in the cavity varying with the changing current, which results in a change in the refractive index of the cavity. Since the laser wavelength is a function of refractive index, the emitted frequency fluctuates with the changes in the injected current. This is known as *frequency chirping* and causes optical spectral broadening [15]. Such spectral broadening affects the pulse shape at the fibre output because of fibre dispersion and limits the propagation length in optical communication systems.

Several methods have been used to reduce the chirp. One direct method is to design semiconductor lasers with small values of the linewidth enhancement factor α. Most semiconductor lasers have typical values of α in the range of 3-5. A small broadening in the linewidth under direct modulation was achieved in quantum well lasers [17], and a further reduction has been shown for strained quantum wells [18]. The chirp reduction in the high speed modulated semiconductor laser was also achieved by using injection locking with a CW laser [19]. Another way to eliminate the laser chirp is to modulate the laser output by using an external modulator.

B. External Modulation Scheme

When semiconductor lasers are not modulated, they exhibit less RIN [20], and problems such as chirp and distortion are eliminated. Therefore, an externally modulated optical system offers an alternative way to overcome the difficulties of direct laser modulation. As a results many RoF system that have been proposed use external modulators.

There are two different principles of an external optical modulator used in optical fibre communication: *electro-optic* effect, where the applied electric field changes the optical refractive index, and *electro-absorption* effect, where the optical absorption changes under the influence of electric field changes. The electro-absorption materials are semiconductors that can be easily integrated with the continuous wave (CW) laser diode [21]. In electro-optic modulators, the substrate is made of an insulating material (lithium niobate ($LiNbO_3$)) which has many advantages such as a refractive index that changes linearly with applied voltage, high electro-optic coefficient, and stability at normal electronic operating temperatures [22]. This type of modulator can handle much higher optical powers (up to 400 mW) than electro-absorption modulators (limited to a few tens of milliwatts) [23], and exhibits much higher extinction ratio (~25 dB) than EAMs (~10dB) but in general they also need higher drive voltages.

The main type of electro-optic modulator used in photonic systems is the Mach-Zehnder modulator (MZM). Figure 2.7 shows the schematic diagram for employing a MZM and its transfer function. The input light is split into two paths in the upper and

lower waveguide. The optical phase of the upper arm is shifted with respect to the phase in the lower arm according to the applied voltage. Then, the two waveguides are recombined again in the output to produce constructive or destructive interference based on the relative phase of the light in the two arms. The transfer function of the MZM is a raised cosine function as shown in Fig. 2.6 and given by:

$$P_o = P_i t_{ff}\left[1+\cos\left(\frac{\pi V}{V_\pi}+\phi_b\right)\right] \qquad 2.2$$

where t_{ff} is the optical transmission factor of the device and related to its loss, V is the applied voltage, V_π is the half wave voltage required to change the output from maximum to minimum, and Φ_b is the bias phase. This modulator has a sinusoidal transfer function, and therefore needs to be biased at the quadrature (half power point) with a small modulation index to operate in the linear region. The link gain or the slope efficiency can be enhanced by using devices with low switching voltages or increasing the input light power for a given modulation depth. The main disadvantage in this modulator is the nonlinearity of the light output power versus voltage transfer characteristics of the interferometeric intensity [24]. Other disadvantages of external modulators include optical loss, polarization sensitivity, and it is a separate component which makes its application more complex and costly.

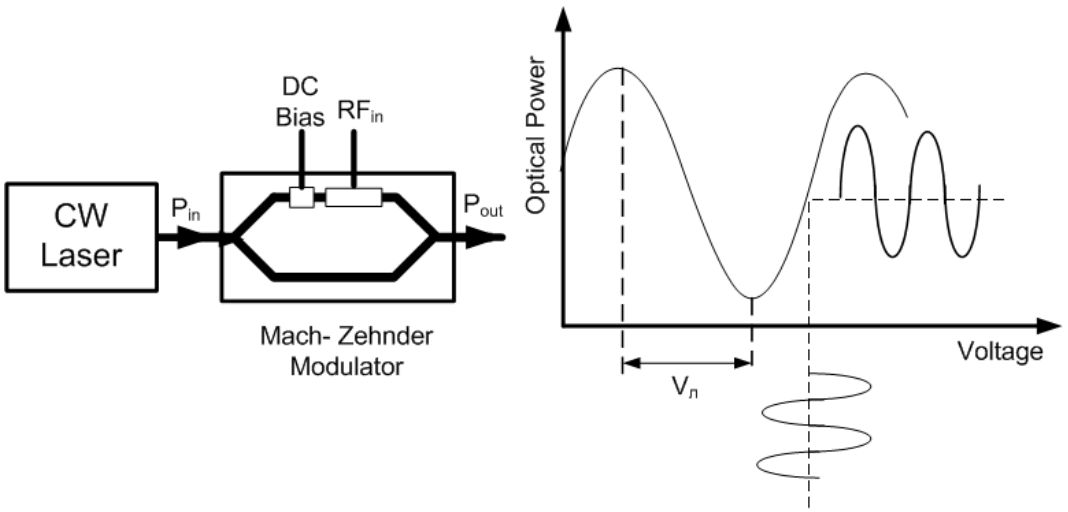

Fig. 2.7. Intensity modulation of the optical signal.

2.5.2 Optical Receiver

The function of an optical receiver is to convert the optical signal back into electrical form and has an enough large bandwidth that can handle the RF frequency used in the RoF system [22]. Optical receivers normally consist of a photodetector which is a photodiode and an amplifier. There are two common types of photodiode: the PIN and avalanche photodiode (APD). The PIN diode consists of an intrinsic layer (i-layer) inserted between a p-type layer and an n-type layer. When this structure is reverse biased, and light is incident upon it, it generates a current which is proportional to the intensity of the light. The ratio of the current generated to light absorbed is known as the responsivity and is normally around 0.5- 0.7 A/W. For PIN diodes this current is usually very small, so they are often coupled directly to a transimpedence amplifier which converts the small current to a more useable voltage.

Receiver sensitivity can be greatly improved by using an avalanche photodiode (APD). The device structure of an APD differs from that of a PIN photodiode mainly in one additional layer p-type is added between i-layer and n^+-layer. Under reverse bias, a high electric field exists in this additional layer where secondary electron-hole pairs are generated through the impact ionization process. This increases the responsivity of the detector by several orders of magnitude higher than a PIN.

The disadvantages of APDs are that they are noisier than PIN diodes and their gain is temperature dependent. In addition, the multiplication process reduces the response time and hence the bandwidth of the device. Traditionally the bandwidth of APDs was limited to less than 5 GHz but advances in the technology have yielded APDs with bandwidths of more than 10 GHz. In optical fibre communications, the PIN device is cheaper, less sensitive to temperature and requires lower reverse bias voltage than the APD. However, the APD is generally preferred when the system is loss limited, as occurs for long distance links.

2.5.3 Optical fibre links

The communication channel in most lightwave systems is the optical fibre which transports the optical signal from the transmitter to receiver. Therefore, it is

important to consider the effect of the fibre during the propagation of the optical signal. Optical fibre attenuation and dispersion are very important factors that degrade the system performance due to a reduction in signal to noise ratio or result in an increase in the signal distortion.

Fibre attenuation is an important design issue in optical fibre systems and is relatively low, typically 0.5 dB/km or 0.2 dB/km for 1330 nm and 1550 nm windows, respectively. This attenuation is mainly caused by the absorption of the light by impurities in the glass (primarily OH ions), and by light scattering due to the interactions between the photons and silica molecules, known as Rayleigh scattering [15]. This attenuation decreases the signal to noise ratio at the optical receiver and limits the transmission distance of the fibre optic communication systems. In some optical systems, optical amplifiers such as erbium doped fibre amplifiers (EDFAs) which can easily provide gain of 20 dB or more are used to increase the link length or provide distribution to a large number of users but this decreases the signal to noise ratio.

Fibre dispersion is another important issue which leads to the broadening of data pulses as the optical signal travels along the fibre causing intersymbol interference (ISI) between bits. There are three types of dispersion in the fibre. *Intermodal dispersion* results from the modes of a multimode fibre propagating with different velocities. This is also called modal dispersion and does not occur in the single mode fibre. The second dispersion is *material dispersion* or *chromatic dispersion*.

The refractive index of the fibre material is a function of wavelength. The material dispersion means that each wavelength travels with a different velocity and arrives at different times. This dispersion occurs in all transmission systems since the light source and data signal has finite bandwidth. The third type of dispersion is *waveguide dispersion* and results from the waveguide characteristics such as fibre indices and the shape of the fibre core and cladding. This type of dispersion is very small and can be neglected in the transmission link. The combination of the material and waveguide dispersion can be reduced to zero by operating at 1330 nm or at 1550 nm in dispersion shifted fibre (DSF). Another way to decrease the effects of

dispersion is to use a compensating fibre with a strong negative dispersion known as dispersion compensation fibre (DCF) [25, 26].

The effect of chromatic dispersion is more significant at higher modulation frequencies and severely limits the fibre transmission distance. In the conventional intensity modulated direct detection (IM-DD) RoF system, the information signal is generated on both sides of the optical carrier which is known as double sideband (DSB) modulation [27]. When the optical carrier and the two sidebands are transmitted over fibre, the chromatic dispersion causes a phase change for each sideband depending on the fibre length, modulation frequency, and chromatic dispersion parameter. This results in the two RF signals generated by the two sidebands beating with the optical carrier, at the receiver, being out of phase, resulting in low RF power.

2.6 Network Architectures for RoF technologies

The integration between broadband wireless and the optical access networks enables a wide range of applications and services for wireless connectivity between the users. RoF networks have different architectures according to the required application. In mobile cellular networks, rural and urban regions are divided into small geographical areas known as cells and connected to the central station through optical fibre as shown in Fig. 2.8. The first cellular system was achieved by using high power base stations inside relatively large cells or macrocells (with a diameter of 16 – 48 km). This was possible only for a small number of users, however to increase system capacity, each large cell is split into several small cells known as microcells (a few hundred meters) where the carrier frequency can be reused [28].

In each microcell radio port, the base station consists of a simple and compact optoelectronic repeater connected by an optical fibre link to the centralized radio and control equipment. This allows the changes of modulation format or system frequency to be done at the central location without the need to update any radio equipment. For in-building coverage, RF signals are very weak and often can not penetrate building walls. Therefore, RoF links were also used for in building coverage for 2G networks such as large office blocks, shopping malls, airports,

stadium, and subways [29].

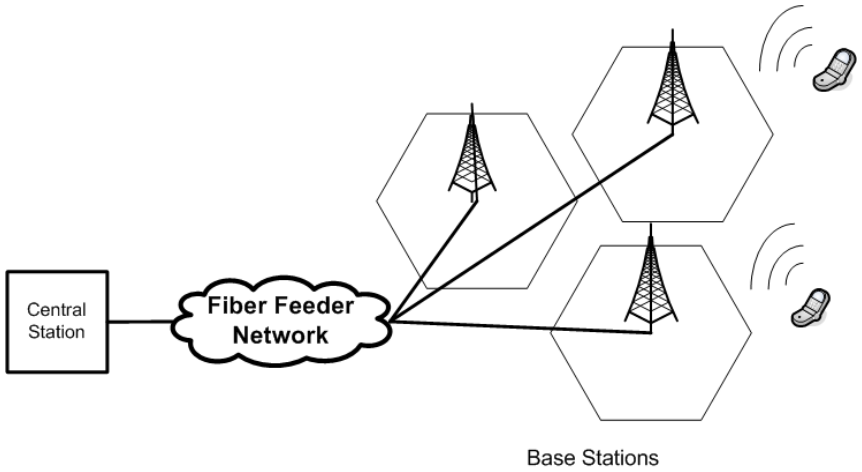

Fig. 2.8. Fiber feeding for mobile cellular communications

The indoor distribution of radio system over fibre, known as fibre distributed antenna system (DAS), is considered as a large mass market for extending the capacity and range of radio signals in a variety of locations [5]. Figure 2.9 shows a commercial RoF system for fibre based on DAS for indoor wireless signal distribution. In this case, the wireless signals are distributed to a large number of remote sites, known as pico-cells, (in a building with a high user density) and each cell is connected to the central station through the fibre infrastructure [30].

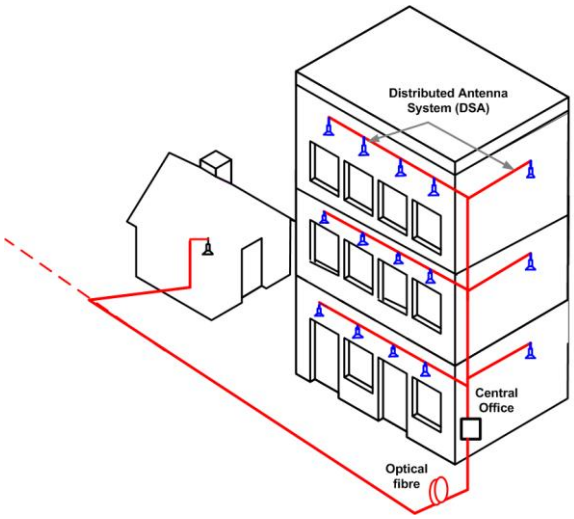

Fig. 2.9. RoF architecture for fibre based distributed antenna system.

Another application for RoF network architectures is shown in Figure 2.9. In this configuration, a large metropolitan area network (MAN) supports multiple optical wavelength division multiplexed (WDM) channels, each carrying data rates up to

10 Gbps. A number of centralized switching nodes are interconnected together via an optical MAN ring. Each switching node provides control, switching, and routing to the remote node (RN) or base stations (BS). As shown in Figure 2.10, the CO can be connected to several RNs using ring or star topology as in CO1 and CO2 respectively. In either arrangement, the optical WDM channels at the CO are de-multiplexed and dropped from the MAN to the remote terminals. Then, each optical channel is directed to the specified BS for signal detection and radio distribution. A full duplex, WDM system, star- tree architecture was demonstrated by Smith et. al for delivering broad band wireless access to the customers [32].

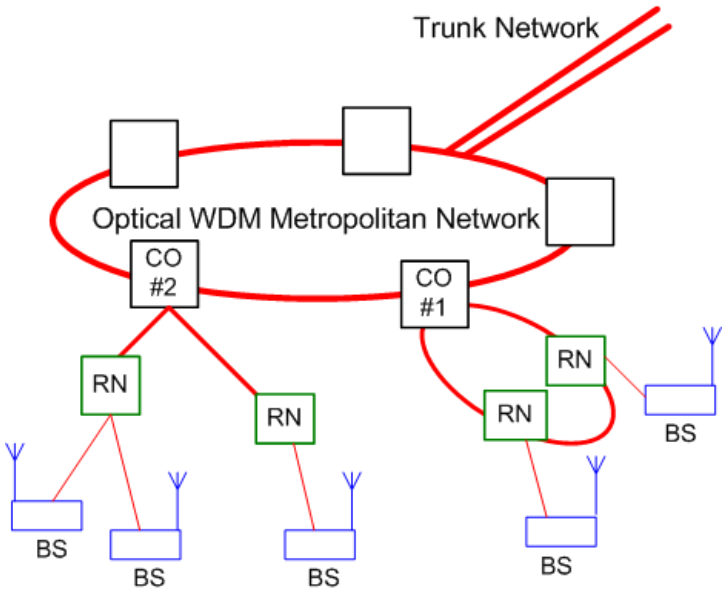

Fig. 2.10. MAN architecture for RoF technology [6].

2.7 Limitation of Radio over Fibre

All optical communication systems suffer from noise and distortions on the optical transmission link. Noise added to the optical signal produces bit errors at the decision gate in the receiver side, while distortion results in inter-symbol interference (ISI) due to the induced changes in the optical pulse shapes which also increases the received bit errors. The system performance is determined by the measurement of bit error rate (BER), usually plotted as a function of received optical power. Therefore, the determination of noise and distortion contribution is vital in digital and analogue optical communication systems and tends to limit the radio system distributions [15,

33]. In this section we describe the main noise sources and the nonlinear distortions in a RoF system.

2.7.1 Noise Sources in the RoF links

The noise sources in optical communication systems include the laser's relative intensity noise (RIN), the laser's phase noise, the photodiode's shot noise, and amplifier's thermal noise [33]. In a semiconductor laser, the output of the laser exhibits intensity fluctuations even when the laser is biased at a constant current with negligible current fluctuations. These intensity fluctuations known as RIN are embedded into the received signal and degrade the signal quality. Another phenomenon called mode partition noise (MPN) can also increase the effect of RIN. In practice, single mode semiconductor lasers oscillate in a single longitudinal mode and are accompanied by one or more side modes. The main and side modes exhibit fluctuations in their intensities, but the total intensity remains relatively constant. These mode fluctuations have no effect in the absence of fibre dispersion, as all modes are received at the same time on the photodiode. However, in the presence of the fibre transmission all modes do not arrive simultaneously at the receiver because they travel at slightly different speeds and cause an amplitude fluctuation of the signal at the decision circuit in the receiver. Therefore, MPN can severely affect the performance of an optical communication system and is dependant on the side mode suppression ratio (SMSR) which is defined as the ratio of the main mode power to the power of the most dominant side mode. In practice, most commercial DFB semiconductor lasers are accompanied by one or more side bands that are suppressed by more than 30 dB [15].

During signal propagation over the fibre, the optical fibre channel does not contribute to noise generation in the optical signal but reduces the signal power through attenuation. However, optical amplifiers are used to increase the signal power but at the same time decrease the SNR by at least 3 dB [33]. All optical amplifiers add noise to the signal due to amplified spontaneous emission (ASE). The effect of the spontaneous emission is to add fluctuations to the amplified power which are converted to current fluctuations during the photodiode detection.

The receiver noise includes shot noise, photodiode dark current noise, and thermal noise from the RF amplifier. In most practical cases for low input power, the dominant noise source is the thermal noise which is due to random thermal motion of electrons and causes current fluctuations at the receiver output. This noise can be reduced by increasing the optical power or the load resistance. Therefore, many attempts were made to reduce this noise contribution by using high impedance or transimpedance front ends. However, if the incident power is large, the receiver performance is dominated by the shot noise where the electric current consists of a stream of electrons that are generated at random times [34]. All these mentioned noise processes tend to limit the noise figure and dynamic range (DR) of RoF links.

2.7.2 Distortions in the RoF systems

The distortions in optical communication systems are produced from the fibre dispersion and nonlinearities in the laser. The effect of fibre dispersion as described previously severely limits the overall transmission distance and the maximum transmission rate [33]. Another important type of distortion is the nonlinearity in the transfer function of the laser or the external modulator. Consider two input signals at f_1 and f_2 which are fed into the link. The output generates spurious signals at the second and third harmonics of the input signals due to nonlinearity. The second harmonic signals can be easily filtered out for narrow band systems, while the most important type of distortion are the third harmonics $2f_1 - f_2$ and $2f_2-f_1$ which are known as the third order inter-modulation products (IM3) [23]. These spurious signals fall in band and cause signal distortions. Fig. 2.11 shows the output power of the fundamental signal and IM3 signal as a function of the input power. The fundamental signal has a slope of one and varies linearly with input power, while the IM3 signal has a slope of three and varies with the cube of the input power. The intersection point between these two lines is an important parameter of optical RoF links. The other important parameter is the spur free dynamic range (SFDR), which can be defined as the range of the input power bounded by the intersection between the fundamental and IM3 with the noise floor. That means that the stronger signal power is limited by a point where the intermodulation products reach the noise floor, whereas the weaker signal is limited by the noise floor. Dynamic range (DR) is an essential parameter for cellular communication systems due to the wide range of the

received power from MUs to the base station. The received input RF power difference between users who are close by and those at the cell edge can be greater than 80 dB. However, this effect of DR can be neglected for in-building coverage systems where the cells are in range of pico and microcells. Many research techniques have been also proposed to combat these nonlinearities and increase the dynamic range in RoF links by using distortion cancellation methods [35-37], or by reducing system's noise floor including the RIN, shot noise, and phase induced intensity noise [38, 39].

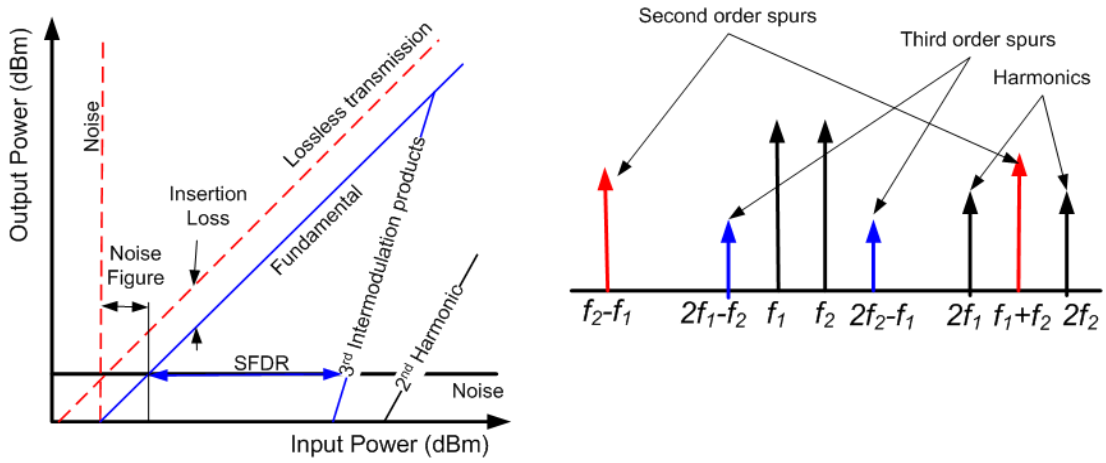

Fig. 2.11. Output power versus input optical power for analogue optical links, illustrating spurious free dynamic range (SFDR) due to third order inter-modulation products.

2.8 Summary

This chapter gave an introduction to RoF technology and discussed basic characterization and operation of the required optical components. It has also shown the distribution of the wireless signal over optical links which are classified into three transmitter configurations depending on the hardware components and cost. This shows that centralization of system complexity and simplification of RAUs can help to reduce installation and maintenance costs especially in large scale coverage areas (i.e. picocell networks) compared to the conventional distributed radio. System impairments such as noise, distortion, and fiber dispersion degrade the signal-to-noise ratio and limit the system transmission lengths. However, these impairments can be reduced with careful management of the optical system. Overall, we can see that RoF systems have a very important role in radio signal distribution for cellular networks, and high speed applications in wireless personal networks. In the next

chapter, we will discuss more about optical generation methods and the distribution of RoF systems for future broadband wireless communication concepts such as ultra-wide band (UWB) and millimeter wave (mm-wave) systems.

References

[1] S. Hunziker and W. Baechtold, "Cellular remote antenna feeding: Optical fibre or coaxial cable?" *Electronic Letters,* vol. 34, no. 11, pp. 1038-1040, 1998.

[2] A. J. Cooper, "'Fibre/radio' for the provision of cordless/mobile telephony services in the access network," *Electronic Letters,* vol. 26, no. 24, pp. 2054, 1990.

[3] M. Sauer, A. Kobyakov, and J. George, "Radio over fiber for picocellular network architectures," *Lightwave Technology, Journal of,* vol. 25, no. 11, pp. 3301-3320, 2007.

[4] J. J. O'Reilly, P. M. Lane, and M. H. Capstick, ,"Optical generation and delivery of modulated mm-waves for mobile communications," in B. Wilson, Z. Ghassemlooy, and I. Darwazeh, *Analogue optical fibre communication,* 1st ed., the institute of Electrical Engineers, London, 1995.

[5] D. Novak, et al.,"Hybrid fiber radio- concepts and prospects," in C. H. Lee, *Microwave photonics,* 1st ed., CRC Press, USA, 2007.

[6] C. Lim, A. Nirmalathas, M. Bakaul, P. Gamage, K. Lee, Y. Yang, D. Novak, and R. Waterhouse, "Fiber-wireless networks and subsystem technologies," *Lightwave Technology, Journal of,* vol. 28, no. 4, pp. 390-405, 2010.

[7] D. Wake,"Radio over fiber systems for mobile application," in H. Al-Raweshidy and S. Komaki, *Radio over fiber technologies for mobile communications networks,* Artech House, Norwood, 2002.

[8] L. D. Westbrook and D. G. Moodie, "Simultaneous bi-directional analogue fibre-optic transmission using an electroabsorption modulator," *Electronic Letters,* vol. 32, no. 19, pp. 1806, 1996.

[9] D. Wake, D. Johansson, and D. G. Moodie, "Passive picocell: A new concept in wireless network infrastructure," *Electronic Letters,* vol. 33, no. 5, pp. 404, 1997.

[10] G. Agrawal and N. K. Dutta, Long-Wavelength Semiconductor Lasers Van

Nostrand Reinhold, 1986.

[11] Y. Matsui, H. Murai, S. Arahira, S. Kutsuzawa, and Y. Ogawa, "30-GHz bandwidth 1.55-μm strain-compensated InGaAlAs-InGaAsP MQW laser," *Photonic Technology Letters,* vol. 9, no. 1, pp. 25-27, 1997.

[12] L. Bach, W. Kaiser, J. P. Reithmaier, A. Forchel, T. W. Berg, and B. Tromborg, "Enhanced direct-modulated bandwidth of 37 GHz by a multi-section laser with a coupled-cavity-injection-grating design," *Electronic Letters,* vol. 39, no. 22, pp. 1592-1593, 2003.

[13] L. Chrostowski, X. Zhao, C. J. Chang-Hasnain, R. Shau, M. Ortsiefer, and M. C. Amann, "50 GHz directly-modulated injection-locked 1.55 μm VCSELs," *Optical Fiber Communication Conference, Technical Digest.(OFC/NFOEC 2005)* , Vol. 4, pp. 3, 6 -11 March, Anaheim, California, USA, 2005.

[14] E. K. Lau, Hyuk-Kee Sung, and M. C. Wu, "Ultra-high, 72 GHz resonance frequency and 44 GHz bandwidth of injection-locked 1.55-/spl mu/m DFB lasers," *Optical Fiber Communication and the National Fiber Optic Engineers Conference (OFC/NFOEC 2006),* pp. 3, 5- 10 March, Anaheim, California, USA, 2006.

[15] G. P. Agrawal, Fiber-Optic Communication Systems, Wiley-Interscience, 2002.

[16] W. K. Marshall, B. Crosignani, and A. Yariv, "Laser phase noise to intensity noise conversion by lowest-order group-velocity dispersion in optical fiber: Exact theory," *Optics Letters,* vol. 25, no. 3, pp. 165-167, 2000.

[17] C. A. Green, N. K. Dutta, and W. Watson, "Linewidth enhancement factor in InGaAsP/InP multiple quantum well lasers," *Applied Physics Letters,* vol. 50, no. 20, pp. 1409, 1987.

[18] H. D. Summers and I. H. White, "Measurement of the static and dynamic linewidth enhancement factor," *Electronic Letters,* vol. 30, no. 14, pp. 1140-1141, 1994.

[19] C. Lin, J. K. Andersen, and F. Mengel, "Frequency chirp reduction in a 2.2 Gbit/s directly modulated InGaAsP semiconductor laser by CW injection,"

Electronic Letters, vol. 21, no. 2, pp. 80-81, 1985.

[20] W. Stephens and T. Joseph, "System characteristics of direct modulated and externally modulated RF fiber-optic links," *Lightwave Technology, Journal of,* vol. 5, no. 3, pp. 380-387, 1987.

[21] R. H. Kingston, "Electroabsorption in GaInAsP," *Applied Physics Letters,* vol. 34, no. 11, pp. 744, 1979.

[22] P. k. L. Yu and M. C. Wu,"Photodiodes for high performance analog links," in William S. C. Chang, *RF photonic technology in optical fiber links,* 1st ed.,Cambridge University Press, United Kingdom, 2002.

[23] R. C. Williamson and R. D. Esman, "RF photonics," *Lightwave Technology, Journal of,* vol. 26, no. 9, pp. 1145-1153, 2008.

[24] B. H. Kolner and D. W. Dolfi, "Intermodulation distortion and compression in an integrated electrooptic modulator," *Applied Optics,* vol. 26, no. 17, pp. 3676-3680, 1987.

[25] G. Keiser and G. Keiser, Optical Fiber Communications, McGraw-Hill, 1999.

[26] J. M. Senior, Optical Fiber Communications: Principles and Practice Prentice Hall, 1992.

[27] U. Gliese, S. Norskov, and T. N. Nielsen, "Chromatic dispersion in fiber-optic microwave and millimeter-wave links," *Microwave Theory and Techniques, IEEE Transaction on,* vol. 44, no. 10, pp. 1716-1724, 1996.

[28] L. J. Greenstein, N. Amitay, Ta-Shing Chu, L. J. Cimini Jr., G. J. Foschini, M. J. Gans, I. Chih-Lin, A. J. Rustako Jr., R. A. Valenzuela, and G. Vannucci, "Microcells in personal communications systems," *Communication Magazine, IEEE,* vol. 30, no. 12, pp. 76-88, 1992.

[29] A. Arredondo, D. M. Cutrer, J. B. Georges, and K. Y. Lau, "Techniques for improving in-building radio coverage using fiber-fed distributed antenna networks," *Vehicular Technology Conference, 'Mobile Technology for the Human Race., IEEE 46th 1996,* vol.3, pp. 1540-1543, 28th April - 1st May,

Atlanta, Georgia, USA.

[30] A. Ng'oma and M. Sauer, "Radio-over-fiber technologies for high data rate wireless applications," *2009 IEEE Sarnoff Symposium*, pp. 1-6, 30th March- 1 April, NJ, USA.

[31] CommScope :Andrew [Online]. Available: http://www.commscope.com/andrew /eng/index.html. [accessed: 10/11/2010]

[32] G. H. Smith, D. Novak, and C. Lim, "A millimeter-wave full-duplex fiber-radio star-tree architecture incorporating WDM and SCM," *Photonics Technology Letters, IEEE,* vol. 10, no. 11, pp. 1650-1652, 1998.

[33] P. A. Davies and N. J. Gomes,"Subcarrier multiplexing in optical communication networks," in B. Wilson, Z. Ghassemlooy, and I. Darwazeh, *Analogue optical fibre communications,* Institution of Electrical Engineers, London, 1995.

[34] J. C. Palais, Fiber Optic Communications (5th Edition) Prentice Hall, 2004.

[35] S. Yaakob, W. R. W. Abdullah, M. N. Osman, A. K. Zamzuri, R. Mohamad, M. R. Yahya, A. F. A. Mat, M. R. Mokhtar, and H. A. A. Rashid, "Effect of laser bias current to the third order intermodulation in the radio over fibre system," *RF and Microwave Conference, 2006. RFM 2006. International*, pp. 444-447.

[36] D. Hassin and R. Vahldieck, "Feedforward linearization of analog modulated laser diodes-theoretical analysis and experimental verification," *Microwave Theory and Techniques, IEEE Transactions on*, vol. 41, no. 12, pp. 2376-2382, 1993.

[37] L. Roselli, V. Borgioni, F. Zepparelli, F. Ambrosi, M. Comez, P. Faccin, and A. Casini, "Analog laser predistortion for multiservice radio-over-fiber systems," *Lightwave Technology, Journal of*, vol. 21, no. 5, pp. 1211-1223, 2003.

[38] R. D. Esman and K. J. Williams, "Wideband efficiency improvement of fiber optic systems by carrier subtraction," *Photonics Technology Letters, IEEE,* vol. 7, no. 2, pp. 218-220, 1995.

[39] S. Mathai, F. Cappelluti, T. Jung, D. Novak, R. B. Waterhouse, D. Sivco, A. Y. Cho, G. Ghione, and M. C. Wu, "Experimental demonstration of a balanced electroabsorption modulated microwave photonic link," *Microwave Theory and Techniques, IEEE Transactions on,* vol. 49, no. 10, pp. 1956-1961, 2001.

Chapter 3 –RoF for Short Range Wireless Communications

The demands for fast, high capacity and more secure wireless connections have attracted much attention from both researchers and industrial developers. In addition, the rapid evolution of wireless technologies facilitates the distribution of high-speed applications to the customers which takes the form of short range wireless communications. Ultra-wideband (UWB) wireless communication is one of the most important candidates for short range wireless signals at high data rates (>1 Gbps). It has been allocated in unlicensed frequency band between 3.1 – 10.6 GHz (7.5 GHz width) by the Federal Communications Commission (FCC) of the United States in February, 2002 [1]. This frequency band is partially occupied with narrowband wireless services. Therefore the average radiated power of the UWB signal was limited to -41.3 dBm/MHz to minimize the effect of interference on the existing signals. Another frequency band has also been located at millimetre-wave (mm-wave) frequencies around 60 GHz to support high-speed data for medium and short range wireless applications [2]. The FCC set aside 7 GHz of spectrum at 57 - 64 GHz for general unlicensed applications with an equivalent isotropic power density (EIRP) of 40 dBm/MHz [3, 4]. The wide bandwidth and high allowable transmit power at 60 GHz enable multi-Gbps wireless transmission over typical indoor distances. However, signals at 60 GHz suffer from high path loss of about 20 – 40 dB compared to the low microwave frequencies [5, 6] and the atmospheric absorption such as gases, rain, scattering, and diffraction loss also increases the power loss by 7- 15.5 dB/km [6]. Despite these disadvantages, the 60 GHz signal is confined within a room in an indoor environment, allowing high frequency reuse and more densely packed communication links [7]. Typically, 60 GHz systems are designed to provide multi-Gigabit rates with operating range below 20 m and to support various applications [8]. Both frequency bands are suitable for numerous applications for high data rate in home area networking (HAN) and wireless personal area networking (WPAN), such as transferring a video stream between a VCR, camcorders, and other consumer electronic devices such as laptop, DVD, digital camera, and HDTV monitors.

In this chapter, we describe the spectral definition and regulations of the UWB and 60 GHz mm-wave technologies in section 3.1. The type of UWB signals and modulation techniques are presented in section 3.2, followed by discussion of several approaches for transmitting UWB over fibre in section 3.3. In section 3.4, the optical methods for generation and distribution of mm-waves are then described in terms of the receiver technology. Finally, the chapter is concluded and summarised in section 3.5.

3.1 Regulations and Spectral Definitions

3.1.1 Conventional UWB Radio Signal

The FCC's First Report and Order (R&O) in 2002 has defined UWB technology as any UWB device emitting a signal with a fractional bandwidth greater than 0.2 or a bandwidth of at least 500 MHz [1]. This fractional bandwidth is defined by:

$$BW_f = \frac{2(f_H - f_L)}{(f_H + f_L)} \geq 20\% \qquad 3.1$$

where f_H and f_L are the upper and lower frequency at -10 dB emission point. The FCC mandated Part 15.209 rules to approve the UWB deployment in the unlicensed frequency band from 3.1 to10.6 GHz for indoor wireless communications, with a power spectral density (PSD) less than -41.3 dBm/MHz as shown in Fig. 3.1. The FCC's spectrum mask for UWB also has additional power limitations for the existing radio systems such as global position system (GPS) at 1.5 GHz and digital cellular network at 1.9 GHz.

In Europe and other countries, the UWB spectrum has different regulations to protect other wireless signals such as WiMax terminals or Radar systems [9-11]. In July, 2007, the electronic communication committee (ECC) of the European conference of posts and telecommunications (CEPT) has defined UWB for short range radio communication with bandwidth more than 50 MHz in the frequency bands 3.1- 4.8 GHz, and 6- 8.5 GHz with emission level less than -41.3 dBm/MHz [9]. The

frequency band over 3.1- 4.8 GHz has a restricted operation with mitigation technique detection and avoidance mechanism (DAA) on UWB devices. The DAA mechanism is used to reduce the emitted power to −70 dBm/MHz level (or completely stop it). In Japan, the ministry of internal affairs and communications (MIC) has approved the frequency bands 3.4 - 4.8 GHz and 7.25- 10.25 GHz with emission limit similar to FCC rule. A DAA mechanism is also required for the emission level of – 41.3 dBm, otherwise -70 dBm is required [10]. While in Korea, the UWB spectrum has been assigned in the frequency band 3.1- 4.2 GHz under DAA control, and 7.2 - 10.6 GHz without DAA requirement [11].

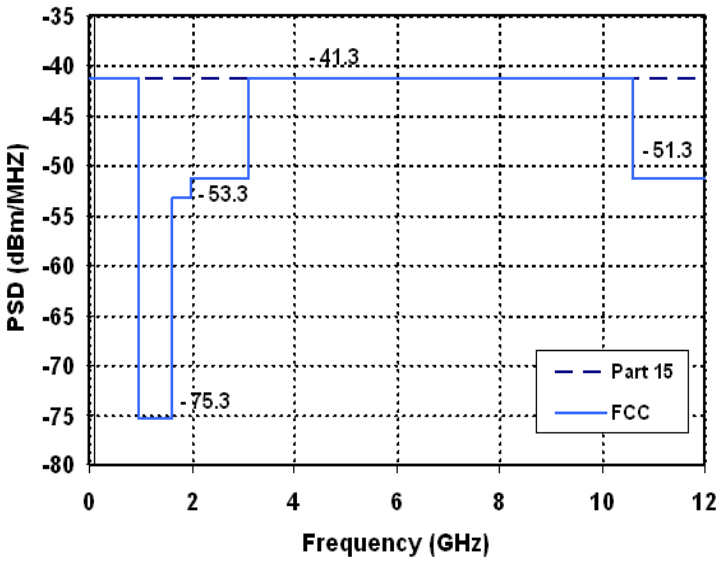

Fig. 3.1. UWB spectral mask for indoor distribution

Generally, UWB communication is allowed with a very low average transmitted power below the noise level, this restricts UWB signals to short range applications in comparison with the conventional narrowband systems.

3.1.2 60 GHz Millimetre Wave Signals

The unlicensed frequency band available around 60 GHz millimetre wave band has been assigned globally for medium and short range wireless communications. The frequency band, maximum transmitted power, and EIRP are listed in table 3.1 for various regulatory regions. The frequency band (57.0 -64.0 GHz) is regulated for unlicensed utilization for indoor application in most of the countries with average transmitted power 10 dBm.

Table 3.1. Frequency band, maximum transmitted power, and EIRP for various countries

Region	Unlicensed Bandwidth (GHz)	Transmitted Power (dBm)	EIRP (dBm)	Ref.
USA/Canada	57-64 GHz (7 GHz)	27	43	[4, 12]
Japan	59- 66 GHz (7 GHz)	10	58	[13]
Australia	59.4-62.9 GHz (3.5 GHz)	10	27	[14]
Korea	57- 64 GHz (7 GHz)	10	51.7	[15]
Europe	57- 66 GHz (9 GHz)	13	57	[16]

3.2 Types of UWB Signals

There are two common types of UWB communications; single band and multiband signals [17, 18]. A single band is usually known as impulse radio UWB (IR-UWB) where the signal consists of very short pulses, while multiband-based is achieved by using orthogonal frequency division multiplexing (OFDM) and dividing the UWB frequency band into multiple smaller bands.

3.2.1 IR-UWB Signals

IR-UWB is based on sending very narrow pulses, typically on the order of nanoseconds, with a very low duty cycle to convey information. This small pulse width covers a large spectral bandwidth [18]. It is a carrier free signal that can be implemented with simple, low cost transceiver circuits and low consumed power. The extremely low power spectral density and short time duration of the pulse makes the transmitted signal difficult to detect and intercept, which is an advantage for ensuring a secure network. However, fast switching times for the transmitter and receiver are needed for highly precise synchronization.

The pulse shape is an important key issue in IR-UWB since the choice of it can affect the UWB performance [19, 20]. Hence, several pulse shapes have been investigated for generating UWB signals. It has been shown that the Gaussian monocycle pulse and its higher derivatives spread its power over a wide range of frequencies and have virtually no DC component which makes it more suitable for

UWB communications [21]. It was also reported that the higher derivatives of the Gaussian pulses meet more to the FCC mask with the decreasing of their bandwidth as the order of the derivation increase [20]. The basic Gaussian pulse equation is expressed as follow;

$$p(t) = \frac{A}{\sqrt{2\pi}\sigma} \exp\left(-\frac{(t-\mu)^2}{2\sigma^2} \right) \tag{3.2}$$

where A is the amplitude of the pulse, μ is the location in the time for the midpoint of the Gaussian pulse in time, and σ is the standard deviation or the pulse shape used as bandwidth decaying parameter. The n^{th} derivative of the Gaussian pulse can be determined from,

$$p_n(t) = -\frac{n-1}{\sigma^2} p_{n-2}(t) - \frac{(t-\mu)}{\sigma^2} p_{n-1}(t) \tag{3.3}$$

The normalized PSD for the n^{th} derivative of the Gaussian pulse is given by,

$$|P(f)| = \frac{(2\pi f\sigma)^{2n} \exp\left(-(2\pi f\sigma)^2\right)}{n^n \exp(-n)} \tag{3.4}$$

The order of derivative and the suitable pulse width are selected in order to get pulses that meet the FCC's mask. Fig 3.2 and 3.3 shows the higher derivatives Gaussian pulses and the normalized PSD for orders (1, 2, 3, and 4). It can be seen that the high order derivatives of the Gaussian pulse satisfies the FCC's mask for UWB indoor communications. These higher derivatives could be implemented easily by using a bandpass filter which acts in a similar manner as frequency derivative.

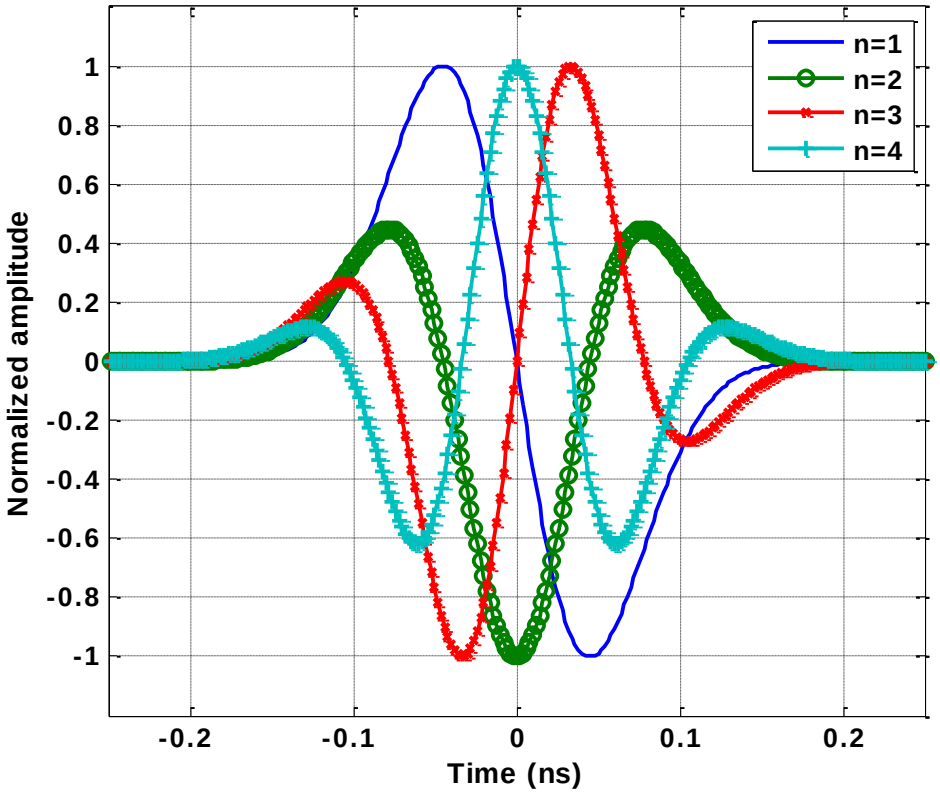

Fig. 3.2. Gaussian pulses for higher order derivatives.

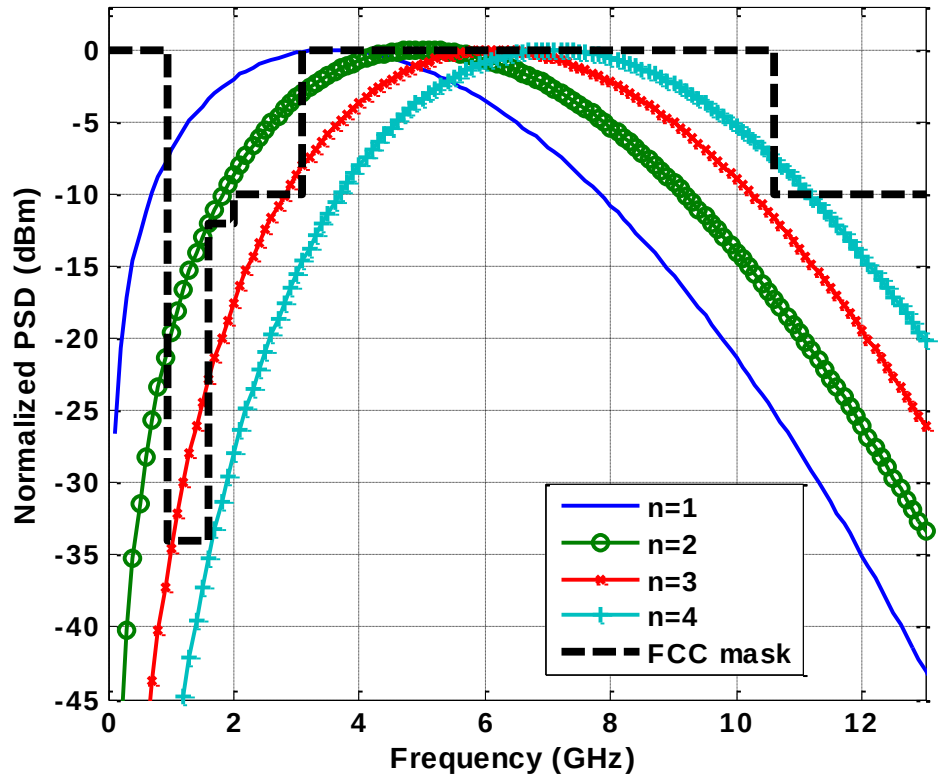

Fig. 3.3. PSD for Gaussian pulses with higher order derivatives.

The pulse modulation scheme is also an important aspect of UWB systems. Several modulation schemes have been widely used in order to satisfy the application and the design parameters as illustrated in Fig. 3.3 [17, 22]. A pulse position modulation (PPM) transmits bit '1' as a pulse without any delay and bit '0' is transmitted with a delay τ relative to window time reference. The delay time is a fraction of a nanosecond and the frame time is typically much longer to avoid interference between pulses. In an on-off keying (OOK) modulation, the information bit '1' is encoded by the presence of a pulse and no pulse is sent for bit '0'. A pulse amplitude modulation (PAM) is based on encoding the information with the amplitude of the impulse as illustrated in Fig. 3.2 (c) such as '0' bit is represented with a lower level of amplitude than bit '1'. For binary phase shift keying (BPSK) scheme, the polarity of the pulses is switched to encode '0' or '1' as shown in Fig. 3.2 (d).

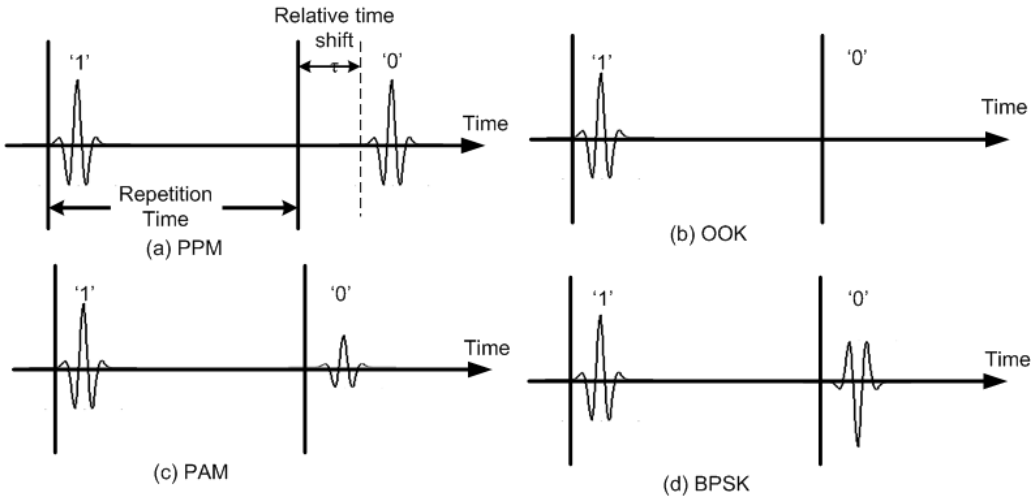

Fig. 3.3. UWB pulses with different modulation schemes.

3.2.2 MB-OFDM UWB Signals

MB-OFDM is a multiband scheme that divides the UWB spectrum into 14 bands called sub-bands each with 528 MHz bandwidth [23]. The first 12 sub-bands are grouped into 4 band groups and the last two sub-bands are grouped into a fifth band group as shown in Fig. 3.4. The sixth band group contains the sub-bands 9, 10, and 11. The MB-OFDM transmits information on 110 subcarriers overlapped in the frequency domain without interference. In addition, 12 pilot subcarriers are used for coherent detection. Each group of OFDM signals are hopped at different frequency

sub-bands with a sequence determined by a time frequency hopping codes (TFC). This technique offers the advantage of coexistence with other narrowband signals and has a more relaxed synchronization requirement than IR-UWB signals. However, this approach needs an inverse fast Fourier transformer (IFFT) at the transmitter and FFT at the receiver side which makes it more complex.

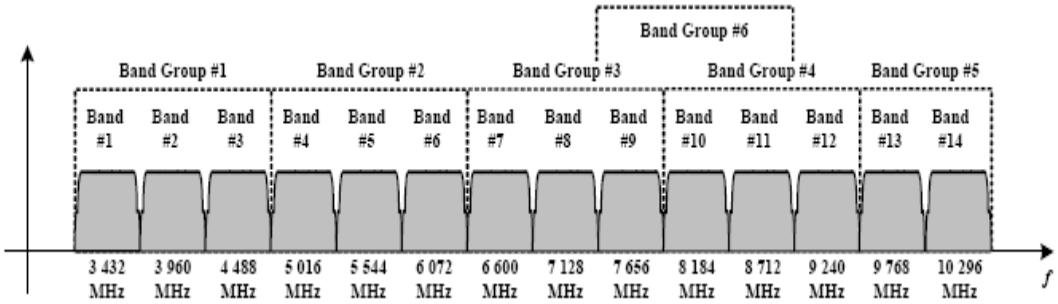

Fig. 3.4. UWB spectrum configurations for MB-OFDM [18].

3.3 Fibre Distribution for Short Range Wireless Signals

As mentioned above, UWB and 60 GHz mm-wave signals are limited to short range distribution distance. In order to overcome this limitation and deploy it for longer transmission distances, RoF systems are considered as a cost effective solution to distribute short range wireless signals over hundreds of metres inside a building or a medium range network in the home or business offices [24, 25]. UWB or mm-wave signals over fibre can be generated first at the central office before being distributed to the remote access points through single mode optical fibre as illustrated in Fig. 3.5. The modulated optical signal will then be recovered at the remote access points for wireless transmission. A RoF network using single mode fibre is an attractive method to distribute UWB radio due to the large bandwidth, low loss and the ability to centralise the operation. This helps to reduce the infrastructure and operational cost.

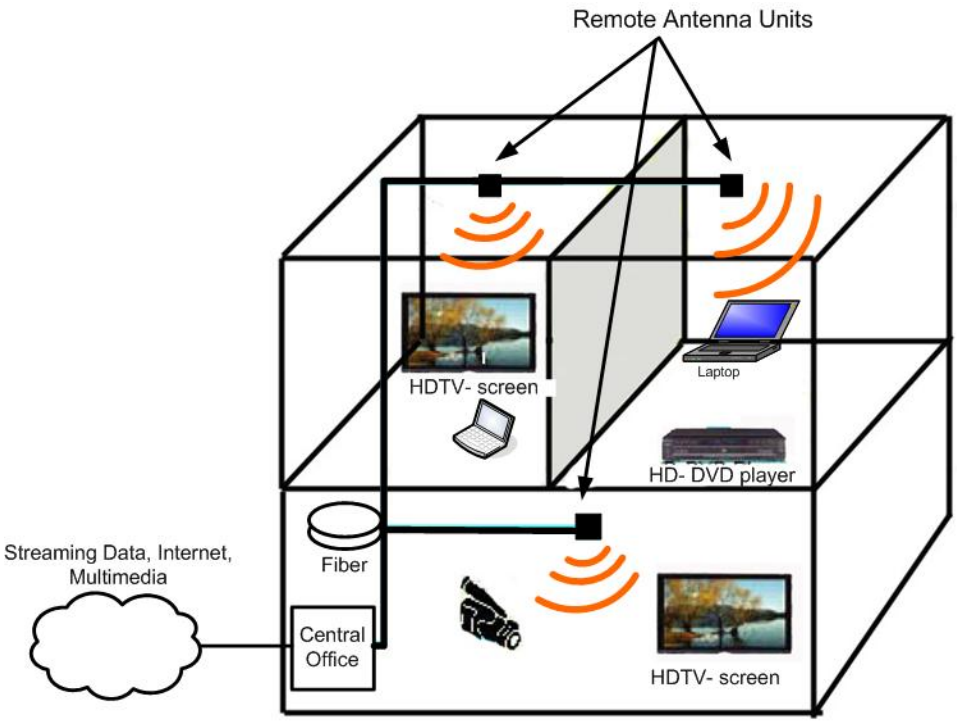

Fig. 3.5. Fibre distribution for short range wireless communication signals.

3.4 Optical Methods for Generation and Distribution of UWB Signals

A basic setup for optical distribution of UWB signals is shown in Fig 3.6 [26]. This setup is a full duplex transmission system and consists of a laser and photodiode at each end. The laser is directly intensity modulated by the input electrical UWB signals. After transmission over optical links, the optical UWB signal is recovered by direct detection at the photodiode and radiated to a wireless UWB device. The transmission of UWB has been investigated for single and multi-mode fibers [26, 27]. SMF systems have a higher cost of optical single mode fibre with the advantage of broadband optical bandwidth, while multi mode fibre (MMF) systems exhibit very low cost transducers and fiber and are suitable for small area coverage.

Since UWB radio signals are distributed over optical fibers, it is preferable to generate UWB signals directly in the optical domain without the need for an extra electrical-to-optical conversion. In addition, the other benefits from using the optical techniques are the light weight and small size of the optical components, and the large bandwidth that is offered by optics enables the easy generation of UWB pulses.

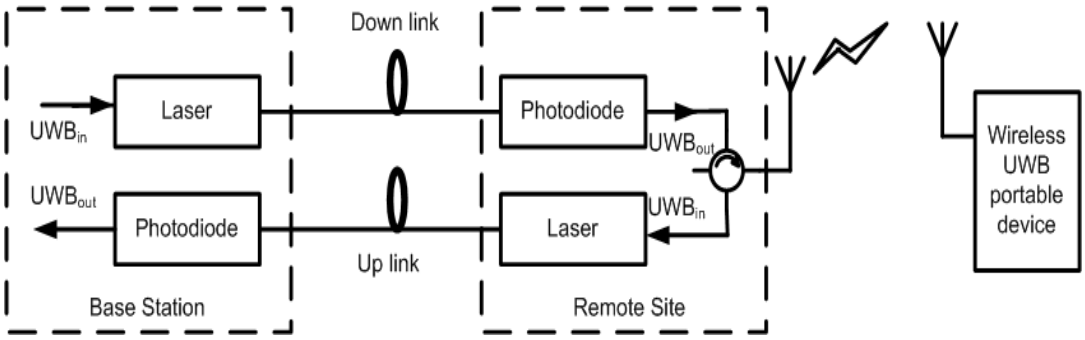

Fig. 3.6. The basic UWB over fibre distribution for up and down link.

In the following subsections, we describe the optical methods for generating and distributing IR-UWB signals over fiber that have been developed over the last few years [26-37]. These approaches will be classified and discussed based on the method of UWB generation.

A. Optical UWB Generation based on PM-IM Conversion

Optical generation of UWB pulses was achieved by using an electro-optic phase modulator (EOPM) and a fixed length of single mode fiber (SMF) as shown in Fig. 3.7 [29]. This combination works as an all-optical microwave bandpass filter which was used to shape the input Gaussian pulse into that of the Gaussian doublet pulse that meets the UWB spectral requirement. In Fig. 3.7, the optical carrier is phase modulated by the Gaussian pulse train representing the data sequence, with the EOPM, and then transmitted through SMF to the photodiode. Due to chromatic dispersion in SMF, the optical phase modulated signal is converted to an intensity modulated (IM) signal. The frequency response is shown as inset in the Fig. 3.6 and forms a passband with a notch at dc value and second notch determined by fibre length. This generates a spectrum corresponding to Gaussian monocycle, or doublet pulses. However, this technique needs a certain fixed fiber length to achieve the desired filtering which limits the distribution distance of UWB signal. This was solved by using a fiber Bragg grating (FBG) and altering the location of the optical carrier at the linear or the quadrature slopes of the FBG frequency response to generate either monocycle or doublet Gaussian pulses [30].

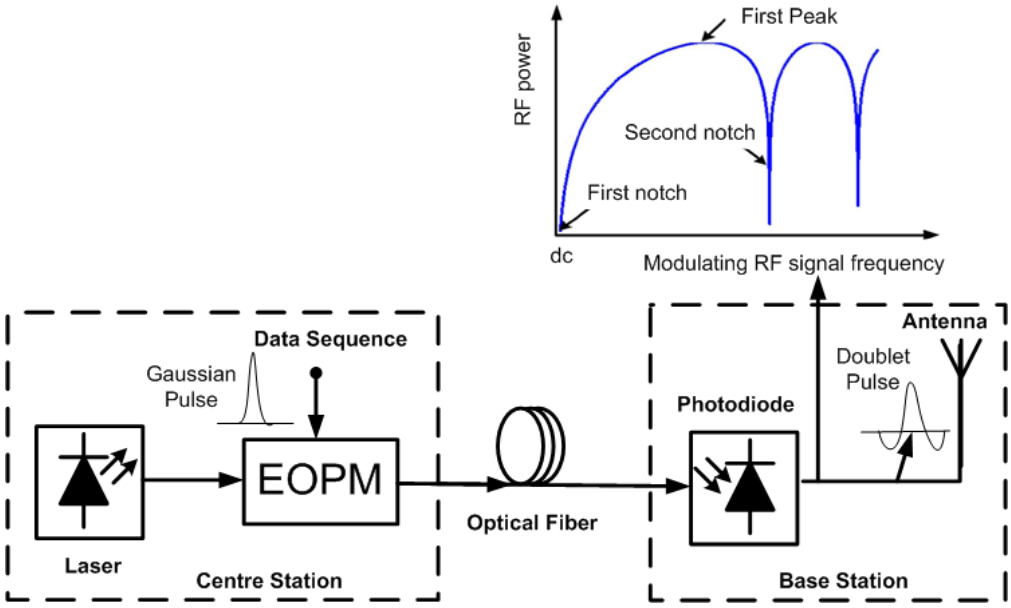

Fig. 3.7. Schematic diagram of optical UWB generation based on PM-IM method.

B. Optical UWB Generation based on Electro-Optic Intensity Modulator (EOM)

Another technique has been used to generate optical UWB Gaussian monocycle and doublet pulses in [32]. Three optical light sources and two external modulators are exploited to generate a UWB pulse from an electrical Gaussian pulse. However, this technique needs to bias the two modulators at different points in their transfer functions, which increases the cost and complexity of the system. Bolea et al. [38] proposed another scheme based on biasing two electro-optic modulators (EOMs) at opposite slopes in the linear region. When an electrical Gaussian pulse is applied to the EOMs, two optical pulses with different polarities are obtained at the output. Then, these pulses are combined to generate a monocycle UWB pulse by using a variable optical delay.

In a different approach, Wang et al. proposed a simple scheme to generate doublet UWB pulses by employing only a single laser diode and an EOM as shown in Fig. 3.8 [34]. A Gaussian pulse is applied to the EOM which is biased at a nonlinear region near the maximum or minimum point in its transfer function, which leads to inversion of the pedestal or the peak of the Gaussian pulse and forms a UWB Gaussian doublet pulse with both polarities. An optical amplifier is used in this technique to compensate the insertion loss in the EOM. In this case, the bias voltage of EOM is high and the output power is not stable.

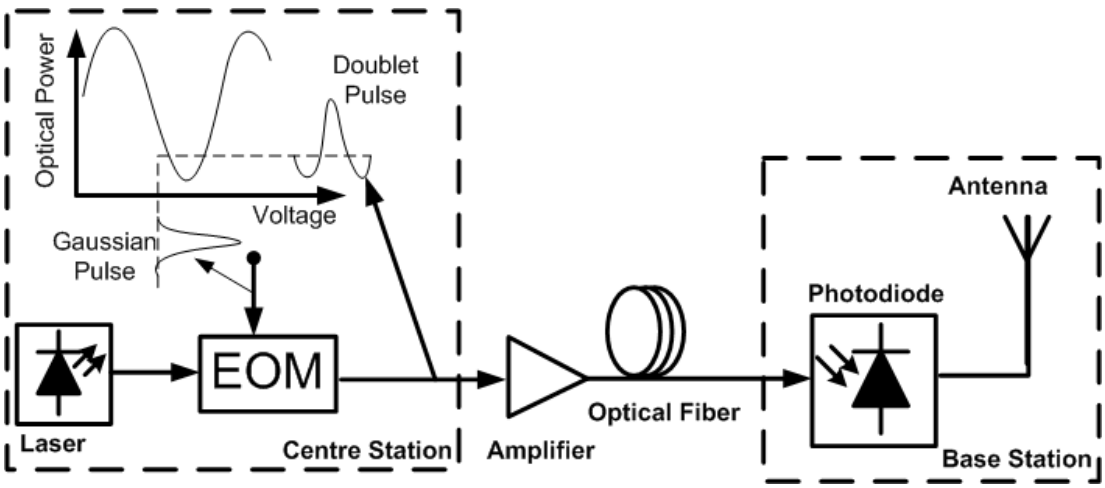

Fig. 3.8. Schematic diagram for optical UWB generation based on EOM

C. Optical UWB Generation based on Cross Gain Modulation (XGM)

In this technique, the cross gain modulation (XGM) effect in a semiconductor optical amplifier (SOA) is employed to generate UWB monocycle pulses [35]. As shown in Fig. 3.9, an optical Gaussian pulse pump and a continuous wave (CW) probe with different optical wavelengths are applied together into the SOA. When a high-power pulsed pump light is injected into the SOA, the variation of the pump power modulates the carrier density of the SOA so that the gain of the SOA varies inversely with the input laser power leading to a variation of the CW probe power. At the output of the SOA, a pair of polarity-reversed pulses is generated, with one pulse at the pump wavelength and the other at the probe wavelength. If a proper time-delay difference is introduced between the two pulses, a new pulse that has a monocycle shape is generated. However, this method needs two optical sources and two FBGs specially designed with accurate delay controlling and wavelength reflection.

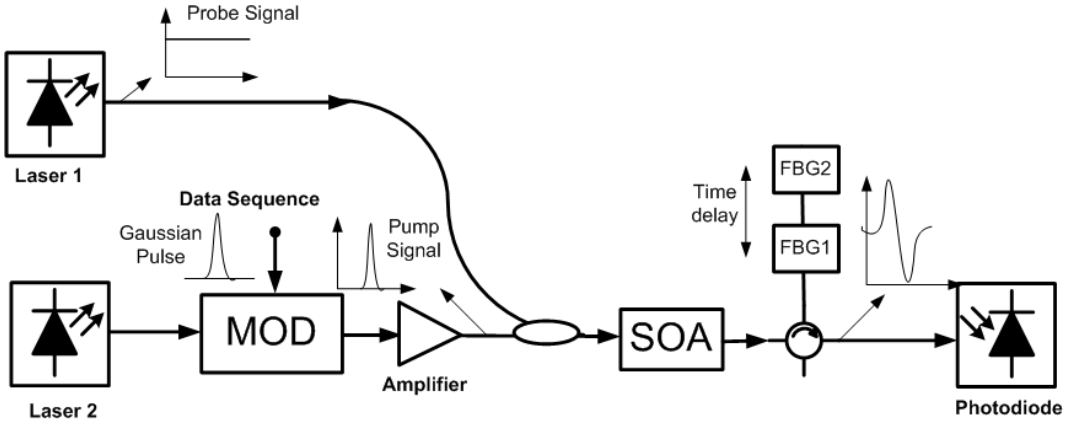

Fig. 3.9. Schematic diagram for optical UWB generation based on XGM

D. Optical UWB Generation based on Balanced Photodetection

Optical UWB Gaussian monocycle pulses can also be generated by using a balanced photo-detection of modulated Gaussian pulses as has been proposed by Beltrán et al [39]. In this technique as shown in Fig. 3.10, a pulsed laser was used to generate optical Gaussian pulses that are then intensity modulated with an electrical data sequence. After that, the optical data pulses are split into two equal parts to drive the two inputs of the balanced photo-detector (BPD). An optical delay line is employed to adjust the relative time delay between the two signals. The pulse width of the Gaussian pulses and the time-delay difference are adjusted so as to generate the desired UWB bandwidth. This approach has been experimentally demonstrated in a system that has Gaussian monocycle UWB pulses with a 10 dB bandwidth of 6 GHz, and can transmit at 1.25 Gbps. Another approach from Beltrán et al. has also been proposed based on differential photoreception of data Gaussian pulses to achieve low cost and less complexity [40]. Instead of using two photo-detectors, the optical data pulses are split after photo-detection and amplified by an electrical amplifier. The two outputs are then combined after adjusting their relative time delay to generate monocycles. This approach shows monocycles pulses with a 10 dB bandwidth of 3.8 GHz for1.244 Gbps data transmission.

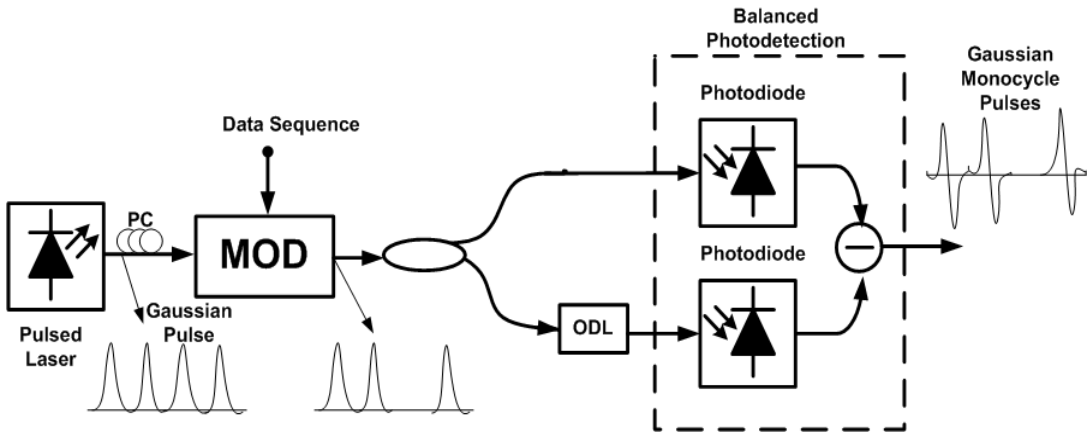

Fig. 3.10. Schematic diagram for optical UWB generation using BPD method.

E. Optical UWB Generation based on Microwave Differentiator

Lin et al. proposed a hybrid system for generating UWB monocycle pulses [36, 37]. A Gaussian pulse train is generated by using a gain switched Fabry–Perot laser diode (FP-LD) and an erbium doped fiber amplifier (EDFA) as an external injection light source. These pulses are recovered by a PIN photodiode, and then filtered by using a

microwave differentiator to generate the first derivative of the Gaussian pulse. Simulated results show that a Gaussian monocycle pulse results with a 10 dB bandwidth of 6.5 GHz centered around 3.2 GHz. In a different approach, Lin et al. proposed the generation of UWB pulses by using a gain switched distributed feedback laser diode (DFB-LD), and a pair of UWB antennas used as bandpass filters to generate UWB pulses that meet FCC regulations. This approach results in UWB pulses with a 10 dB bandwidth of 2.8 GHz for 100 Mbps transmission, and 2 GHz of bandwidth for 500 Mbps transmission

3.5 Optical Methods for Generation and Distribution of Millimetre wave Signals

In this section, we will discuss the methods that are available for optical generation of mm-waves. These methods can be classified into those that are based on intensity modulation and direct detection receivers, and those that are based on remote heterodyning receivers.

3.5.1 Intensity Modulation Direct Detection (IMDD) Receivers

The simplest and easiest way for optical mm-wave generation is to modulate the intensity of the laser output by either directly modulating the laser intensity or using an external modulator as shown in Fig. 3.11. After transmission through the optical fibre, the mm-wave can be recovered by direct detection on a photodiode, amplified and transmitted by the antenna. The main limitation of the direct modulation is its restriction to the modulation bandwidth of the laser. In addition, the laser noise is high due to intensity modulation, and the nonlinearity in the laser leads to inter-modulation products that cause signal distortion. On the other hand, external modulators suffer from high insertion loss and need high driving voltages which in turn increase the cost and complexity of the system [41].

A further limitation of this method is the chromatic dispersion that reduces the transmission distance of the fibre. With this technique, the data signal is carried in side-bands on both sides of the optical carrier which is known as double side band (DSB) operation. Transmission of such a signal through a fibre will cause a phase

shift between the two sidebands due to the chromatic dispersion effect. This can cause fading in the received power as a result of destructive interference as the two side bands add vectorially [42, 43]. However, it is also possible to suppress one sideband to give a single side band (SSB) modulation scheme which reduces the power fading effect. This can be achieved by filtering one of the sidebands [44], or using a dual drive intensity modulator [42]. Nevertheless, this increases the complexity and cost of IMDD and has lower receiver sensitivity than DSB due to the large dc power component at the optical carrier [42, 45-49].

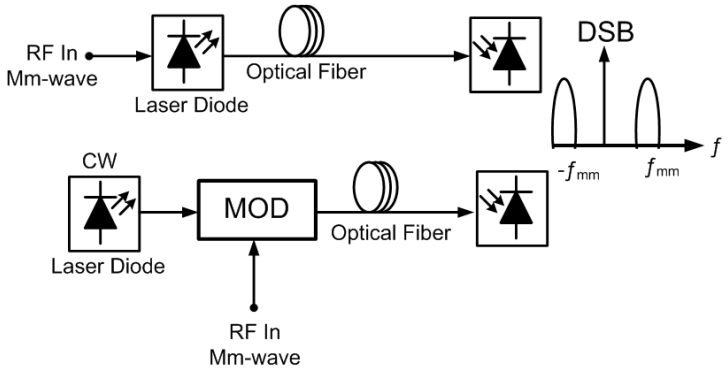

Fig. 3.11. Schematic diagram of optical mm-wave generation using direct modulation of the optical intensity

3.5.2 Remote Heterodyne Receivers

A microwave or mm-wave signal can be generated optically by using a remote heterodyne receiver as illustrated in Fig. 3.12 where two phase correlated optical carriers are generated at the centre station with a frequency offset equal to the desired frequency of the microwave or mm-wave signal. The generated carriers are then transmitted over the fibre and beat together at a high-speed photodetector. This technique can be explained as follows [41, 50, and 51]. Consider two optical fields with angular frequencies ω_1 and ω_2 as shown in Fig. 3.12 and are given by

$$E_1 = E_{01}\cos(\omega_1 t + \phi_1) \qquad 3.2$$

$$E_2 = E_{02}\cos(\omega_2 t + \phi_2) \qquad 3.3$$

where E_{01}, E_{02} are the amplitude terms, and ϕ_1, ϕ_2 are the instantaneous phase terms of the two optical waves. When these fields are combined together and hit on the surface of a photodetector with a limited bandwidth, a photocurrent that is

proportional to the square of the sum of the two fields is generated at the output of the photodetector

$$I_{PD} = A\cos\left[\left(\omega_1 - \omega_2\right)t + \left(\phi_1 - \phi_2\right)\right] + \ other\ terms \qquad 3.4$$

where A is a constant which is determined by E_{01}, E_{02} and the responsivity of the photodetector. The first term is the only term of interest that shows that any frequency of the mm-wave can be generated by controlling the frequency difference between the two optical fields up to THz frequencies, limited only by the bandwidth of the photodiode. The other terms include higher frequency components that are suppressed at the output of photodiode due to its limited bandwidth.

Using this technique can greatly reduce the bandwidth of the optical components required at the centre station, and can also eliminate the power fading effect due to fibre transmission. However, the major problem in this technique is the purity of generated microwave or mm-wave signal. The beating of two optical waves from two free running lasers produces a mm-wave signal with high phase noise if the phases of the two optical waves are not correlated. Therefore, it is necessary to either remove the actual laser signal phase noise or to correlate the phase noise of the two laser signals to generate a highly phase stable microwave or mm-wave signal. Several methods have been proposed to generate low phase noise microwave signals. These methods can be classified into:

1- Optical injection locking (OIL),
2- Optical phase lock loop (OPLL),
3- Optical injection phase locking (OIPL),
4- Microwave generation using external modulator, and
5- Dual wavelength laser source.

In the next subsection, we will give a brief description for each of them and show recent reported examples.

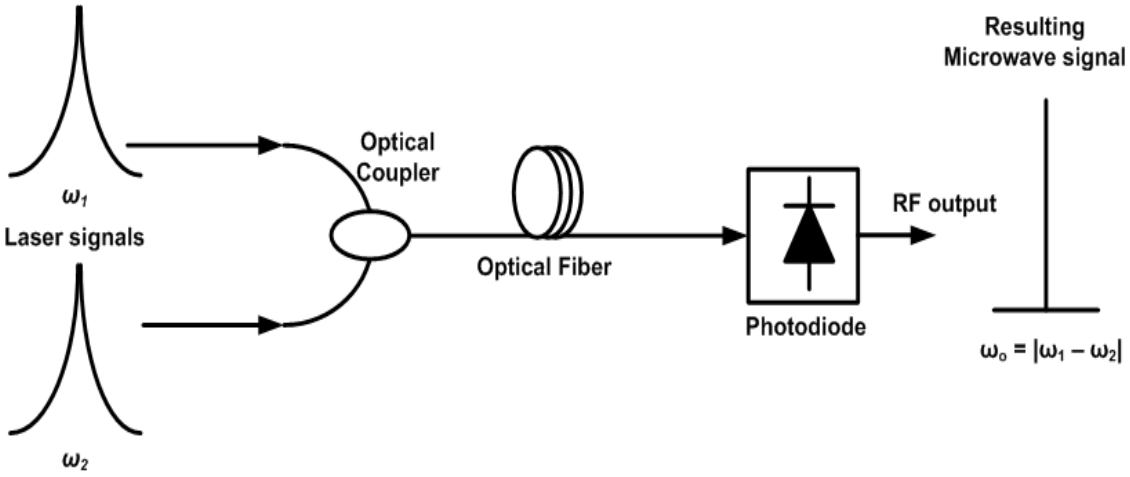

Fig. 3.12. Optical remote heterodyne to generate microwave signal using two optical waves

A. Optical Injection Locking (OIL)

Optical injection locking (OIL) generates high quality microwave or mm-wave signal by injection locking of either two slave laser diodes [52] or a multi-longitudinal mode slave laser [53]. In Fig. 3.13, the master laser is frequency modulated (FM) with an RF reference to generate at the output an optical carrier and different orders of optical sidebands spaced by the modulating frequency. The output signal of the master laser is then injected into the two slave lasers. To achieve optical injection locking, the wavelengths of two slave lasers must be selected close to two sidebands, such as $+2^{nd}$ order and -2^{nd} order sidebands as in Fig. 3.12 [52]. The output of the two slave lasers are phase correlated and would produce a beat note with low phase noise at a photodetector. In another scheme, a single multi-longitudinal-mode slave laser was used as a replacement of the two slave lasers. A beat note at 35 GHz was generated by injection locking from a master laser modulated by an RF frequency of 5.846 GHz [53].

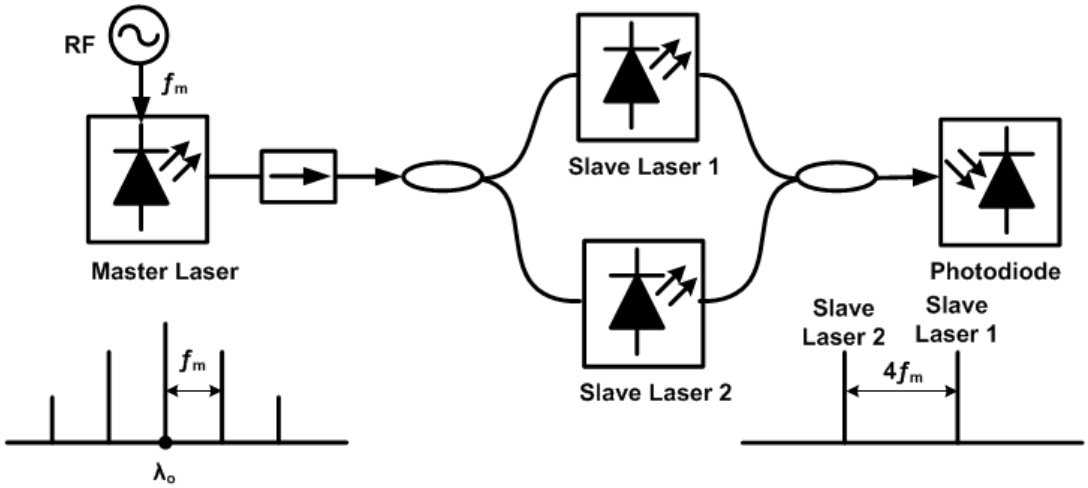

Fig. 3.13. Schematic diagram of the optical injection locking of two slave lasers using a frequency modulated master laser

B. Optical Phase lock loop (OPLL)

This approach represents another way to achieve phase coherence between two optical waves. The phase of one laser is locked to that of a second laser by using an optical phase lock loop (OPLL) as shown in Fig. 3.14. The generated microwave signal at the output of the photodetector is compared with an RF reference at the mixer and then filtered by low pass filter. The output voltage is fed back to control the phase of the locked laser by changing the laser cavity length or the injection current. However, to achieve effective phase locking this method requires two lasers with narrow linewidth and therefore have phase fluctuations only at low frequencies, which eases significantly the requirement for a very short feedback loop. A microwave tuneable signal from 6- 34 GHz with a linewidth less than 1 MHz was obtained by using two Nd: YAG lasers [54] and a package of OPLL system was produced with two semiconductor lasers capable of producing a microwave signal up to 14 GHz [55].

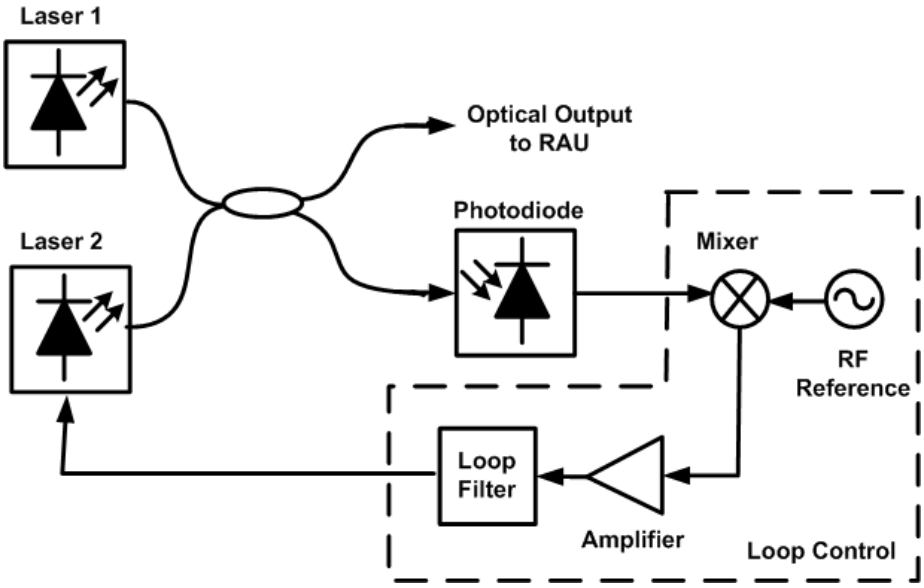

Fig. 3.14. Schematic diagram of optical phase lock loop.

C. Optical Injection Phase Locking (OIPL)

The signal quality can be further improved if the two techniques of OIL and OPLL are combined together. The diagram of an optical injection and phase locking (OIPL) is shown in Fig. 3.15. The master laser is modulated with an RF signal to generate harmonic sidebands. The optical output of the master laser is then divided into two channels before being injected into the slave laser. The slave laser is locked to the n^{th} harmonic sideband of the master laser as in the OIL case. The other channel of the master laser is then combined with the output of the slave laser and beat at the photdetector. After that, the beat signal is mixed with a microwave reference and then filtered to achieve an OPLL. This technique produces a microwave signal with a lower phase noise compared with the other techniques. In addition, it overcomes the drawbacks in the OIL and OPLL, allowing locking with wide linewidth lasers and wide locking range [56]. The generation of a 36 GHz mm-wave was reported with a very narrow linewidth of a few kHz in [57] and a modulated 36 GHz mm-wave was also demonstrated with 140 Mbps data rate [58]. This technique greatly adds cost and complexity to the overall system.

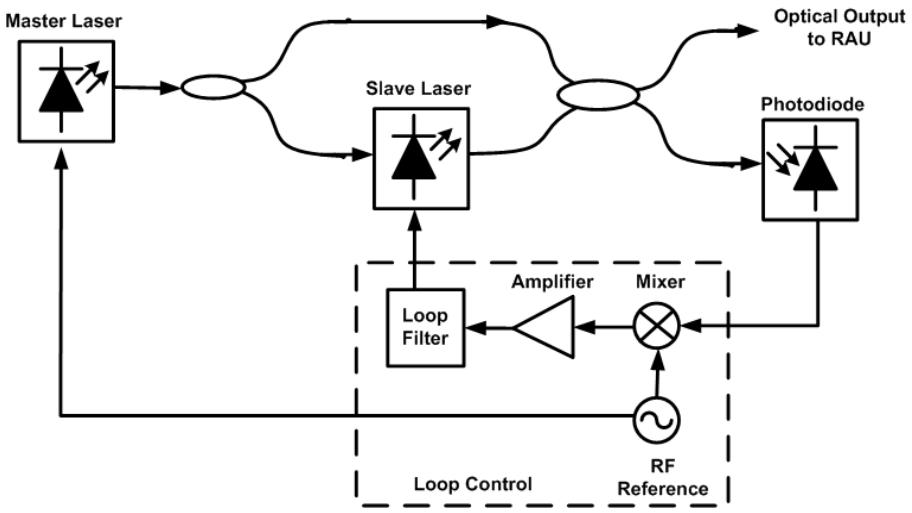

Fig. 3.15. Schematic diagram showing an optical injection locking and phase locking

D. Microwave Generation using External Modulator

Another technique to generate high quality microwave signals can also be achieved by using the non-linearity of external modulators. Here the modulator is driven with an RF signal to produce sidebands spaced by the driving RF frequency and phase correlated since they are derived from the same optical source. The use of external modulators has been widely used for generating frequency doubling and quadrupling of the RF sinusoidal drive signal. A frequency doubled electrical signal can be optically achieved by biasing the Mach-Zehnder modulator (MZM) at the minimum transmission point to suppress the even order optical sidebands. Two strong components therefore result centred at the optical carrier and separated by twice the RF drive frequency. Then, these components are mixed at the photodetector to generate a desired frequency doubled beat signal with a linewidth dependent only on the signal purity of the RF source. This was first proposed to generate a 36 GHz by driving the MZM modulator with an 18 GHz microwave signal in 1992 [59] and then was employed for a remote delivery of video services [60].

A quadrupled frequency signal can be generated if the modulator is biased at the maximum transmission point of the transfer function to suppress the odd order optical sidebands. A 60 GHz millimetre wave signal was generated when a 15 GHz drive signal was applied to the MZM [61]. However, to ensure a clean spectrum at the output of a photodetector, a Mach-Zehnder filter was used to select the two second order sidebands and suppress the unwanted optical spectral components.

Another approach was used to generate a continuously tunable mm-wave signal based on external modulation using a MZM and a wavelength fixed optical filter which is used as a notch filter to remove the optical carrier as shown in Fig. 3.16 [62]. In this approach, a 32-50 GHz mm-wave signal with low phase noise was generated when the electrical drive signal was tuned from 8-12.5 GHz. Both frequency doubling and quadrupling systems can produce a high quality mm-wave. However, these systems are based on biasing the MZM at the minimum or maximum transmission point to suppress the odd or even order optical sidebands, which would suffer from bias drifting, leading to poor system robustness. This can only be reduced by employing a complex bias control circuit.

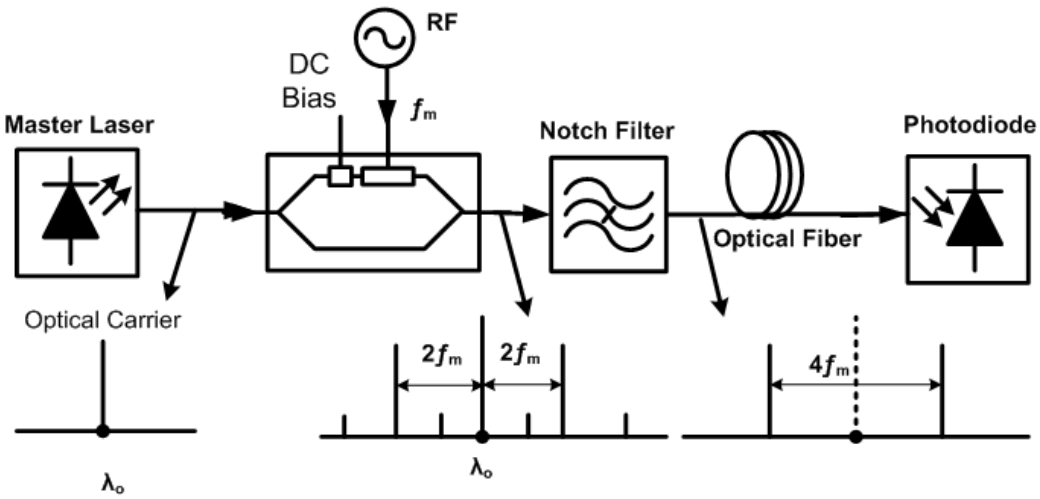

Fig. 3.16. Schematic diagram for generating a continuously tunable microwave signal based on external modulation and notch optical filter.

E. Dual Wavelength Laser Source

A dual wavelength laser source is another approach to ensure that the optical modes become phase correlated so that the beat noise is cancelled. This technique generates two optical modes from the same laser cavity and separated by the desired frequency. The dual wavelength is different than the techniques of OIL and OPLL where the two wavelengths are not phase locked but are phase correlated since they are generated from the same laser cavity. The advantage of using a dual wavelength laser source is the generation of a microwave or mm-wave signal with a simpler system with no need for optical injection or phase locking needed in the other systems and can greatly reduce the system cost. The generation of 57 GHz mm-wave with a

linewidth less than 10 Hz was reported using a dual multi-section semiconductor laser modulated with 6.3 GHz [63, 64].

3.6 Summary

UWB radio signals and 60 GHz mm-waves are short range wireless communication signals due to the power restriction on UWB signals and high path loss around 60 GHz. Therefore, in order to extend their coverage area, RoF is used to distribute these signals within rooms for indoor environment system. By employing optical techniques the flexibility for system deployment is greatly increased, allowing the signal transport over hundreds of meters, and contributing to low construction, installation and maintenance costs. Several optical techniques have been proposed for generating and distributing UWB or mm-wave signal over fiber. These techniques have been classified and reviewed here. In the next two chapters, we propose other methods for distributing UWB and mm-wave signals. Chapter 4 describes two different techniques for generating and distributing UWB over fiber based on a gain switched DFB-LD and UWB bandpass filter, and each method is analyzed for system performance and stability. In Chapter 5, a modulated mm-wave signal is generated by using two approaches based on a gain switched laser and remote heterodyne receivers. Both methods are described clearly and analyzed.

References

[1] Federal Communications Commission (FCC), "Revision of part 15 of the commission's rules regarding ultra-wideband transmission Systems ," First Note and Order, ET Docket 98- 153, FCC 02-8, 2002.

[2] R. C. Daniels and R. W. Heath, "60 GHz wireless communications: Emerging requirements and design recommendations," *Vehicular Technology Magazine, IEEE* , vol. 2, no. 3, pp. 41-50, 2007.

[3] D. Cabric, M. S. W. Chen, D. A. Sobel, J. Yang, and R. W. Brodersen, "Future wireless systems: UWB, 60GHz, and cognitive radios," *in Proc. of the IEEE Custom Integrated Circuits Conference*, pp. 793-796, 2005.

[4] Federal Communications Commission, "Part 15.255 operation within the band 57-64 GHz," *in 47CFR15.255,* title 47, volume 1, pp. 840-842, Oct. 2007,

[5] H. Zhang and T. A. Gulliver, "On the capacity of 60 GHz wireless communications," *in Canadian Conference on Electrical and Computer Engineering (CCECE '09), 2009,* pp. 936-939, 2009.

[6] F. Giannetti, M. Luise, and R. Reggiannini, "Mobile and personal communications in the 60 GHz band: A survey," *Wireless Personal Communication,* vol. 10, no. 2, pp. 207- 243, 1998.

[7] C. Park and T. S. Rappaport, "Short-range wireless communications for next-generation networks: UWB, 60 GHz millimeter-wave WPAN, and ZigBee," *Wireless Communications, IEEE,* vol. 14, no. 4, pp. 70-78, 2007.

[8] S. K. Yong and C. C. Chong, , "An overview of multigigabit wireless through millimeter wave technology: Potentials and technical challenges," *Wireless Communications and Networking, EURASIP Journal on,* vol. 2007, Article ID 78907, 10 pages, pp. 10 pages, 2007.

[9] Electronic Communications Committee, , "ECC decisionof 24 march 2006 amended 6 july 2007 at constanta on the harmonised conditions for devices using ultra-wideband (UWB) technology in bands below 10.6 GHz

(ECC/DEC/(06)04)," 6th July, 2007.

[10] Ministry of internal affairs and communications (MIC), "Regulations for enforcement of radio law," article 4.4, Japan, Aug. 2006.

[11] Chang-joo Kim, Cha-sik Leem, Sung-chul Kang, and Jaiyong Lee, "Policy and technology of dynamic spectrum access in korea," *3rd International Conference on Cognitive Radio Oriented Wireless Networks and Communications (CrownCom 2008),* pp. 1-4, 2008.

[12] Spectrum Management Telecommunications, "Radio standard specification-210, issue 6, low-power licensed-exempt radio communication devices (all frequency bands): Category 1 equipment," September 2005.

[13] Regulations for enforcement of the radio law, 6-4-2 specified low power radio station, (11) 59-66GHz band, Japan, *2000,*

[14] Australian Communications and Media Authority (ACMA), "Radio communications (Low Interference potential devices) class license variation 2005," no. 1, Aug. 2005.

[15] Ministry of Information and Communication of Korea, "Frequency allocation comment of 60GHz band," April 2005.

[16] ETSI DTR/ERM-RM-049, "Electromagnetic compatibility and Radio spectrum Matters (ERM), System Reference Document, and Technical Characteristics of Multiple Gigabit Wireless Systems in the 60 GHz Range," March 2006.

[17] J. G. Reed, An Introduction to Ultra Wideband Communication Systems, Prentice Hall, Upper Saddle River, NJ, 2005.

[18] Xuemin Shen, et al, Ultra-Wideband Wireless Communications and Networks Chichester, Wiley, England, 2006.

[19] Bo Hu and N. C. Beaulieu, "Pulse shapes for ultrawideband communication systems," *Wireless Communications, IEEE Transactions on,* vol. 4, no. 4, pp. 1789-1797, 2005.

[20] P. Orlik, E. M. Haimovich, L. J. Cimini, J. Zhang, H. Sheng, H. Sheng, P. O.

Alex, and J. U. J. Zhang, "On the spectral and power requirements for ultra-wideband transmission," *IEEE International Conference on Communications 2003*, vol. 1,pp. 11-15, 2003.

[21] X. Chen and S. Kiaei, "Monocycle shapes for ultra wideband system," *in Proc. IEEE International Symposium on Circuits and Systems*, pp. I-597-I-600, 2002.

[22] R. C. Qiu, H. Liu, and X. Shen, "Ultra-wideband for multiple access communications," *IEEE Communication Magazine*, vol. 43, no. 2, pp. 80-87, 2005.

[23] ECMA- 368, "High rate ultra wideband PHY and MAC standard," Dec. 2008.

[24] A. Ng'oma and M. Sauer, "Radio-over-fiber technologies for high data rate wireless applications," *2009 IEEE Sarnoff Symposium*, pp. 1-6, 2009.

[25] M. Sauer, A. Kobyakov, and J. George, "Radio over fiber for picocellular network architectures," *Lightwave Technology, Journal of*, vol. 25, no. 11, pp. 3301-3320, 2007.

[26] Y. Le Guennec, M. Lourdiane, B. Cabon, C. Maury, and P. Lombard, "Technologies for UWB-over-fiber," *in 19th Annual Meeting of the IEEE Lasers and Electro-Optics Society (LEOS 2006)*, pp. 518-519, 2006.

[27] L. C. Ong, M. L. Yee, and B. Luo, "Transmission of ultra wideband signals through radio-over-fiber systems," *in 19th Annual Meeting of the IEEE Lasers and Electro-Optics Society, 2006 (LEOS 2006)*, pp. 522-523, 2006.

[28] H. Chen, M. Chen, C. Qiu, J. Zhang, and S. Xie, "UWB monocycle pulse generation by optical polarisation time delay method," *Electronic Letters*, vol. 43, no. 9, pp. 542-543, 2007.

[29] Fei Zeng and Jianping Yao, "An approach to ultrawideband pulse generation and distribution over optical fiber," *Photonics Technology Letters, IEEE*, vol. 18, no. 7, pp. 823-825, 2006.

[30] Fei Zeng and Jianping Yao, "Ultrawideband impulse radio signal generation using a high-speed electrooptic phase modulator and a fiber-bragg-grating-based

frequency discriminator," *Photonics Technology Letters, IEEE,* vol. 18, no. 19, pp. 2062-2064, 2006.

[31] Hongwei Chen, Minghua Chen, Jian Zhang, and Shizhong Xie, "UWB monocycle and doublet pulses generation in optical domain," *in Microwave Photonics, 2007 IEEE International Topical Meeting on,* pp. 145-148, 2007.

[32] J. Li, et al., "Photonic pulse generation and modulation for ultra-wideband-over-fiber applications," *in Conference on Optical Fiber communication/National Fiber Optic Engineers Conference (OFC/NFOEC 2008),* pp. 1-3, 2008.

[33] M. Y. Wah, Chia Yee, and Ming Li Yee, "Wireless ultra wideband communications using radio over fiber," *in Ultra Wideband Systems and Technologies, 2003 IEEE Conference on,* pp. 265-269,

[34] Q. Wang and J. Yao, "UWB doublet generation using nonlinearly-biased electro-optic intensity modulator," *Electronic Letters,* vol. 42, no. 22, pp. 1304-1305, 2006.

[35] Q. Wang, F. Zeng, S. Blais, and J. Yao, "Optical ultrawideband monocycle pulse generation based on cross-gain modulation in a semiconductor optical amplifier," *Optics Letters,* vol. 31, no. 21, pp. 3083-3085, 2006.

[36] Wen-Piao Lin and Jun-Yu Chen, "Implementation of a new ultrawide-band impulse system," *Photonics Technology Letters, IEEE,* vol. 17, no. 11, pp. 2418-2420, 2005.

[37] Wen-Piao Lin and Yuan-Ching Chen, "Design of a new optical impulse radio system for ultra-wideband wireless communications," *Selected Topics in Quantum Electronics, IEEE Journal of,* vol. 12, no. 4, pp. 882-887, 2006.

[38] M. Bolea, J. Mora, B. Ortega, and J. Capmany, "Flexible monocycle UWB generation for reconfigurable access networks," *Photonics Technology Letters, IEEE,* vol. 22, no. 12, pp. 878-880, 2010.

[39] M. Beltran, M. Morant, J. Perez, R. Llorente, and J. Marti, "Photonic generation and frequency up-conversion of impulse-radio UWB signals," *in 21st Annual Meeting of the IEEE Lasers and Electro-Optics Society (LEOS 2008),* pp. 498-

499, 2008.

[40] M. Beltran, R. Llorente, R. Sambaraju, and J. Marti, "60 GHz UWB-over-fiber system for in-flight communications," *in Microwave Symposium Digest (MTT '09), IEEE MTT-S International*, pp. 5-8.

[41] P. A. Davies and N. J. Gomes,"Subcarrier multiplexing in optical communication networks," in B. Wilson, Z. Ghassemlooy, and I. Darwazeh, *Analogue optical fibre communications*, Institution of Electrical Engineers, London, 1995.

[42] G. H. Smith, D. Novak, and Z. Ahmed, "Overcoming chromatic-dispersion effects in fiber-wireless systems incorporating external modulators," *Microwave Theory and Techniques, IEEE Transaction on*, vol. 45, no. 8, pp. 1410-1415, 1997.

[43] C. Lim, K. Lee, A. Nirmalathas, D. Novak, and R. Waterhouse, "Impact of chromatic dispersion on 60 GHz radio-over-fiber transmission," *in 21st Annual Meeting of the IEEE Lasers and Electro-Optics Society (LEOS,2008)*, pp. 89-90, 2008.

[44] J. Capmany, B. Ortega, A. Martinez, D. Pastor, M. Popov, and P.Y. Fonjallaz, "Multiwavelength single sideband modulation for WDM radio-over-fiber systems using a fiber grating array tandem device," *Photonics Technology Letters, IEEE*, vol. 17, no. 2, pp. 471-473, 2005.

[45] H. Schmuck, "Comparison of optical millimetre-wave system concepts with regard to chromatic dispersion," *Electronic Letters*, vol. 31, no. 21, pp. 1848-1849, 1995.

[46] J. Ma, J. Yu, C. Yu, X. Xin, J. Zeng, and L. Chen, "Fiber dispersion influence on transmission of the optical millimeter-waves generated using LN-MZM intensity modulation," *Lightwave Technology, Journal of*, vol. 25, no. 11, pp. 3244-3256, 2007.

[47] U. Gliese, S. Norskov, and T. N. Nielsen, "Chromatic dispersion in fiber-optic microwave and millimeter-wave links," *Microwave Theory and Techniques,*

IEEE Transaction on, vol. 44, no. 10, pp. 1716-1724, 1996.

[48] A. Kaszubowska, P. Anandarajah, and L. P. Barry, "Multifunctional operation of a fiber bragg grating in a WDM/SCM radio over fiber distribution system," *Photonics Technology Letters, IEEE,* vol. 16, no. 2, pp. 605-607, 2004.

[49] J. Yu, Z. Jia, L. Yi, Y. Su, G. K. Chang, and T. Wang, "Optical millimeter-wave generation or up-conversion using external modulators," *Photonics Technology Letters, IEEE,* vol. 18, no. 1, pp. 265-267, 2006.

[50] Jianping Yao, "Microwave photonics," *Lightwave Technology, Journal of,* vol. 27, no. 3, pp. 314-335, 2009.

[51] U. Gliese, T. N. Nielsen, S. Norskov, and K. E. Stubkjaer, "Multifunctional fiber-optic microwave links based on remote heterodyne detection," *Microwave Theory and Techniques, IEEE Transactions on,* vol. 46, no. 5, pp. 458-468, 1998.

[52] L. Goldberg, H. F. Taylor, J. F. Weller, and D. M. Bloom, "Microwave signal generation with injection-locked laser diodes," *Electronic Letters,* vol. 19, no. 13, pp. 491-493, 1983.

[53] L. Goldberg, A. M. Yurek, H. F. Taylor, and J. F. Weller, "35 GHz microwave signal generation with an injection-locked laser diode," *Electronic Letters,* vol. 21, no. 18, pp. 814-815, 1985.

[54] K. J. Williams, L. Goldberg, R. D. Esman, M. Dagenais, and J. F. Weller, "6-34 GHz offset phase-locking of nd:YAG 1319 nm non planar ring lasers," *Electronic Letters,* vol. 25, no. 18, pp. 1242-1243, 1989.

[55] L. N. Langley, M. D. Elkin, C. Edge, M. J. Wale, U. Gliese, X. Huang, and A. J. Seeds, "Packaged semiconductor laser optical phase-locked loop (OPLL) for photonic generation, processing and transmission of microwave signals," *Microwave Theory and Techniques, IEEE Transactions on,* vol. 47, no. 7, pp. 1257-1264, 1999.

[56] C. Walton, A. C. Bordonalli, and A. J. Seeds, "High-performance heterodyne optical injection phase-lock loop using wide linewidth semiconductor lasers,"

Photonics Technology Letters, IEEE, vol. 10, no. 3, pp. 427-429, 1998.

[57] L. A. Johansson and A. J. Seeds, "Millimeter-wave modulated optical signal generation with high spectral purity and wide-locking bandwidth using a fibre-integrated optical injection phase-lock loop," *Photonics Technology Letters, IEEE,* vol. 12, no. 6, pp. 690-692, 2000.

[58] L. A. Johansson and A. J. Seeds, "36-GHz 140-Mb/s radio-over-fiber transmission using an optical injection phase-lock loop source," *Photonics Technology Letters, IEEE,* vol. 13, no. 8, pp. 893-895, 2001.

[59] J.J. O'Reilly, P.M. Lane, R. Heidemann, and R. Hofstetter, "Optical generation of very narrow linewidth millimetre wave signals," *Electronic Letters,* vol. 28, no. 25, pp. 2309-2311, 1992.

[60] J. O'Reilly and P. Lane, "Remote delivery of video services using mm-waves and optics," *Lightwave Technology, Journal of,* vol. 12, no. 2, pp. 369-375, 1994.

[61] J. J. O'Reilly and P. M. Lane, "Fibre-supported optical generation and delivery of 60 GHz signals," *Electronic Letters,* vol. 30, no. 16, pp. 1329-1330, 1994.

[62] Guohua Qi, Jianping Yao, J. Seregelyi, S. Paquet, and C. Belisle, "Generation and distribution of a wide-band continuously tunable millimeter-wave signal with an optical external modulation technique," *Microwave Theory and Techniques, IEEE Transactions on,* vol. 53; 53, no. 10, pp. 3090-3097, 2005.

[63] C. R. Lima, D. Wake, and P. A. Davies, "Compact optical millimetre-wave source using a dual-mode semiconductor laser," *Electronic Letters,* vol. 31, no. 5, pp. 364-366, 1995.

[64] D. Wake, C. R. Lima, and P. A. Davies, "Optical generation of millimeter-wave signals for fiber-radio systems using a dual-mode DFB semiconductor laser," *Microwave Theory and Techniques, IEEE Transactions on,* vol. 43, no. 9, pp. 2270-2276, 1995.

Chapter 4 – Generation and Distribution of IR-UWB Signals

4.1 Introduction

This chapter introduces two different approaches for the generation and distribution of electro-optic impulse radio ultra-wideband (IR-UWB) signals based on a gain switched laser (GSL) and pulse position modulation (PPM) scheme at a bit rate of 1.625 Gbps. The first technique uses one GSL, and two Mach Zehnder Modulators (MZMs) for external data modulation [1], while the second approach is based on two directly modulated (DM) GSLs which is similar to a DM scheme for conversion of an electrical non-return-to-zero (NRZ) data signal to optical return-to-zero (RZ) data [2, 3]. To explore the trade off between cost, performance and reach, the performance of the two system setups has been evaluated using experimental implementations and simulations over different fibre links by using two different configurations of a GSL diode transmitter.

The structure of this chapter is organized as follows. Section 4.2 gives the overview of optical distribution system for electro-optic IR-UWB signals. Section 4.3 describes the gain switching technique and parameters of the optical pulses generated. Section 4.4 outlines the experimental and simulation results using the first transmitter setup for the electro-optic generation of IR-UWB based on a GSL and two external modulators. Section 4.5 then describes the experimental and simulation results of the second approach using two directly modulated GSLs, before section 4.6 presents a summary and conclusion.

4.2 System Overview

The overall architecture of the optical distribution system is shown in Fig. 4.1. It consists of a central node or an optical distribution centre (ODC), which generates a pulse position modulated (PPM) optical signal using a GSL and a pulse pattern generator (PPG) at 1.625 Gbps. These optical signals are then distributed through

fibre links to a number of remote antenna units (RAUs). In the RAU the signals are photodetected, shaped to UWB signals using an electrical bandpass filter (BPF) and radiated through air to the radio terminal (RT). At the user end, the RT, the UWB signals are amplified and demodulated. The system performance has been measured by using a bit error rate tester (BERT) and high speed digital sampling scope. This system allows for the transmission of broadband data over hundreds of metres, with possible application areas of the proposed system involving the distribution of high quality video stream content from DVDs and personal video recorder to high definition television (HDTV) displays.

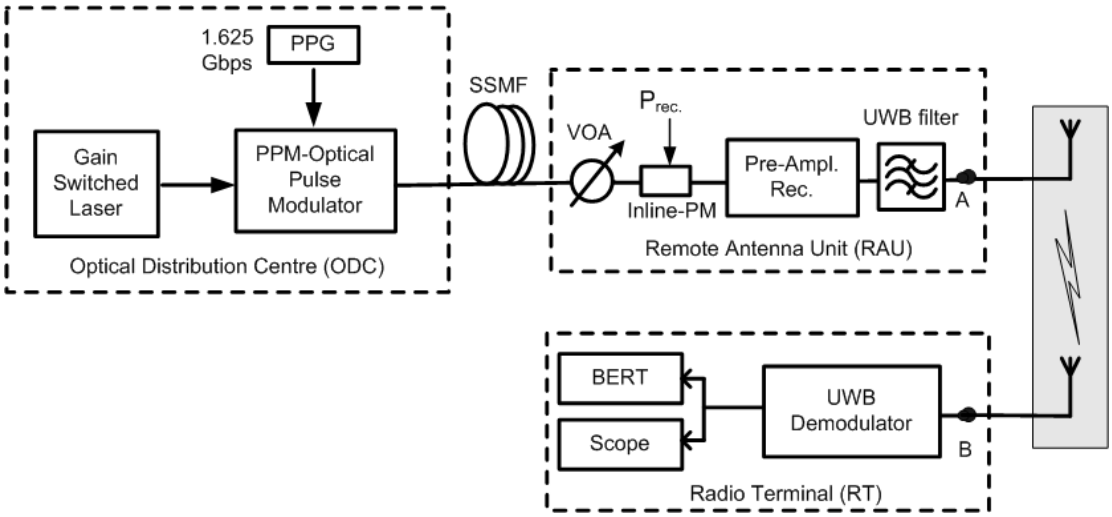

Fig. 4.1. Block diagram of our proposed optical distribution system.

4.3 Gain Switching Technique

Gain switching is one of the simplest and most popular techniques for producing short optical pulses with high repetition rates and high peak power. This technique can be realized in any laser diode structure that has no external cavity or sophisticated fabrication technologies. The gain switching method is simply achieved by biasing the laser diode below the threshold and driving it with an electrical comb generator or a large electrical sinusoidal signal at sub-GigaHertz or GigaHertz frequency. The idea of gain switching originated from the observation of relaxation oscillations when turning on a diode laser from below threshold using electrical pulses with a fast leading edge. The idea of gain switching is to excite the first spike of relaxation oscillation and terminate it before the onset of the second

optical spike. This mechanism of generating short optical pulses is represented in Fig. 4.2. The figure shows a typical evolution in the electron and photon densities during a gain switched cycle. When the laser diode is biased below the threshold the photon density is negligible and the electron density is below the lasing threshold density. By applying a large sinusoidal signal, the carrier density increases above threshold until it reaches peak inversion density. At the same time, the photon density also increases slowly to such a level that stimulated emission begins to consume injected carriers significantly at the peak inversion point, and suppresses any further increase in carrier density.

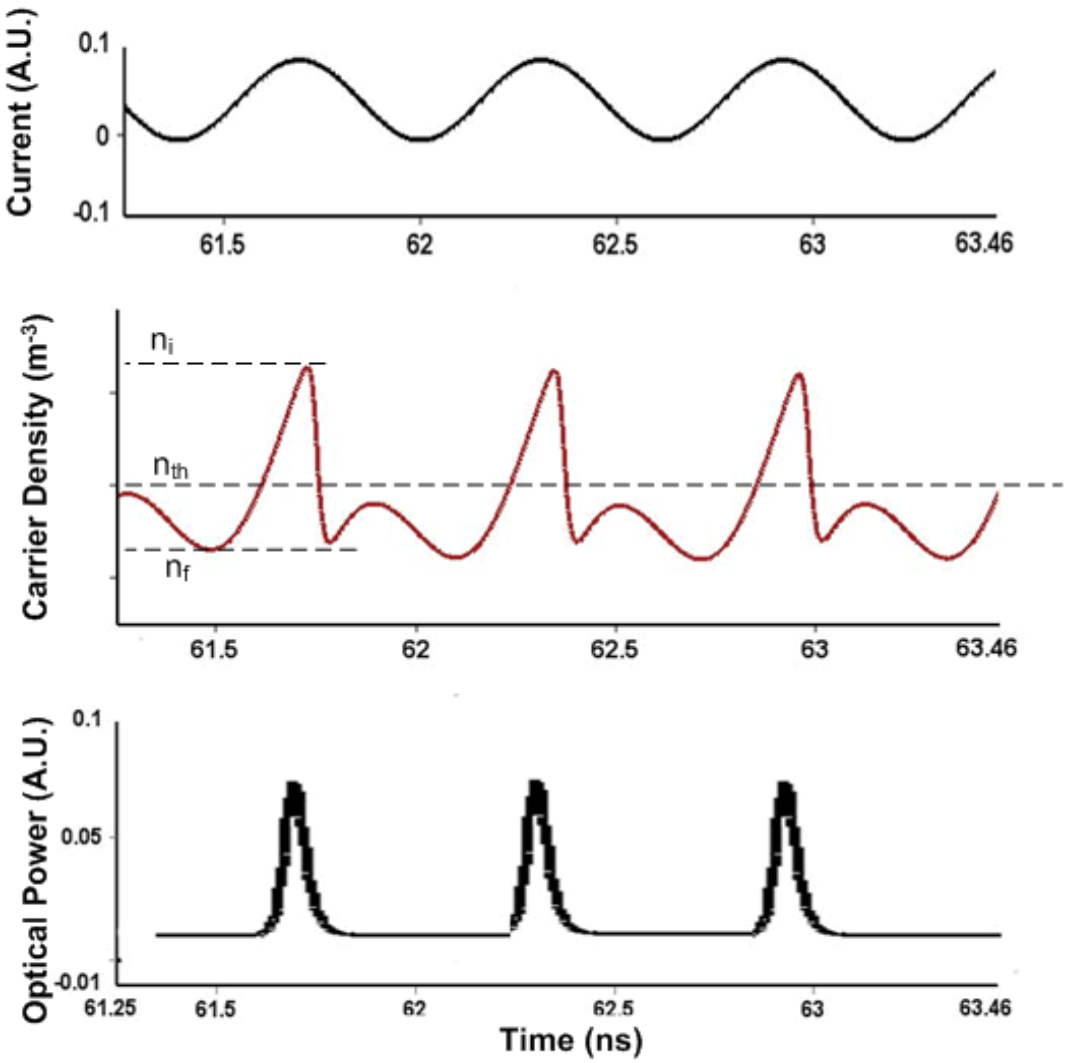

Fig. 4.2. Waveforms for: (a) the applied current, (b) the carrier density, and (c) the output pulses.

Gain switched pulse widths are generally of the order of 10 to 30 ps depending on the laser parameters and driving conditions. However, it is difficult to reduce the pulse width further due to the difficulty in obtaining a large initial population inversion at the beginning of each pulse cycle [4]. The large variation in carrier density also creates a number of optical pulse characteristics that are inherent to this technique, such as frequency chirp, timing jitter, and side mode suppression ratio (SMSR).

- The frequency chirp is a key parameter that limits the system performance due to the significant dispersion penalty from the excessive emission bandwidth. This results from the carrier density variations due to the on-off nature of the applied electrical signal causing a variation in the refractive index.
- The timing jitter is another important parameter that also affects the system performance of gain switched pulses. The timing jitter or pulse-to- pulse jitter is mainly originated from random fluctuations of the photon density in the laser cavity. The start up of each pulse in a gain switched laser relies upon the generation of random spontaneous photons. Typically, the timing jitter values are around 1- 10 ps and can be reduced by optimizing the driving current [5].
- Gain switching also exhibits performance degradation due to a poor SMSR. Normally, distributed feedback (DFB) lasers have a SMSR of more than 30 dB under continuous operation. However, under gain switching conditions the large fluctuations of photon density lead to strongly excite the side modes of the laser, and thus significant degradation of SMSR [6]. This then results in an increase in the noise of the pulses due to mode partition effect. As explained in Chapter (2) (see section 2.7.1), the random fluctuations between the propagated modes, combined with optical filtration and/or dispersion will manifest itself as intensity noise in the transmitted pulses [7, 8].

Several methods have been proposed to mitigate these impairments in the gain switched pulses [6, 9]. It has been shown that external injection with a narrow linewidth continuous wave (CW) laser into the gain switched laser is a simple and cost efficient technique. By controlling the seeding power and aligning the seeding wavelength to the centre of the chirped spectrum, the lowest timing jitter and largest

SMSR can be observed with a slight increase in pulse width [10, 11].

4.4 Generation of IR-UWB Using External Modulators

4.4.1 Experimental Setup

The schematic diagram of the first proposed system is shown in Fig. 4.3. In the ODC section, the optical pulses are generated using the technique of gain switching. Three different laser configurations, operating at 1550 nm, were used for the gain switching: a Fabry Perot laser diode (FP-LD), a DFB-LD and an externally injected DFB-LD (EI DFB-LD). The FP-LD used was a commercially available InGaAsP device with a threshold current of 9 mA. The DFB-LD was a commercial NEL laser within a 14 pin butterfly package. The EI DFB-LD comprises of a modulated DFB laser and a continuous wave (CW) DFB-LD in a master-slave configuration [9]. The optical spectra for the three GSLs are shown in Fig. 4.4 (a), (b), and (c), respectively.

The gain switching of the lasers is achieved by applying a bias below threshold in conjunction with an amplified sinewave at a repetition rate of 1.625 GHz. The gain-switched (GS) pulses, which are of the order of 20 ps width, are shown in Fig. 4.5 (a). These optical pulses are divided into two equal paths by using a 50:50 coupler. A pseudo random bit sequence (PRBS) of length 2^7-1 at a bit rate 1.625 Gbps, from a PPG, is applied to the MZMs (as shown in Fig. 4.3).

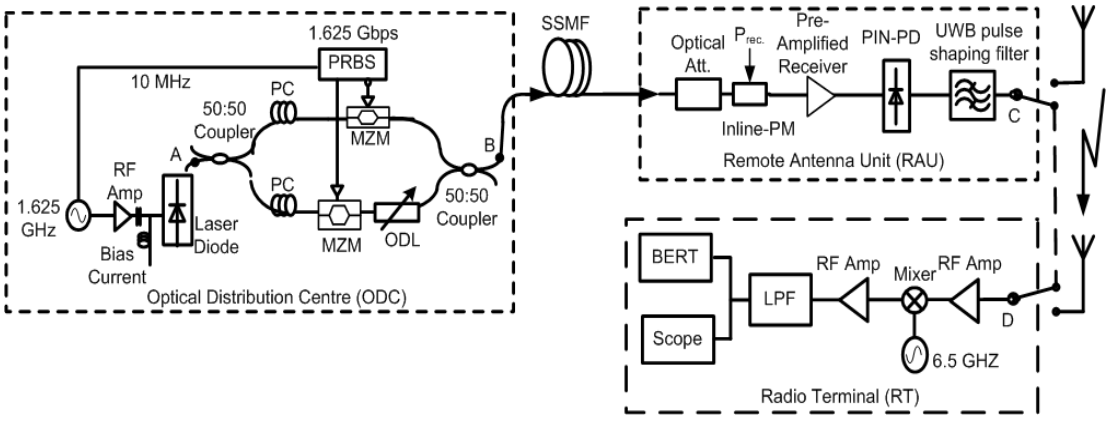

Fig. 4.3. Experimental setup for generating and distributing UWB PPM pulses by using two external modulators.

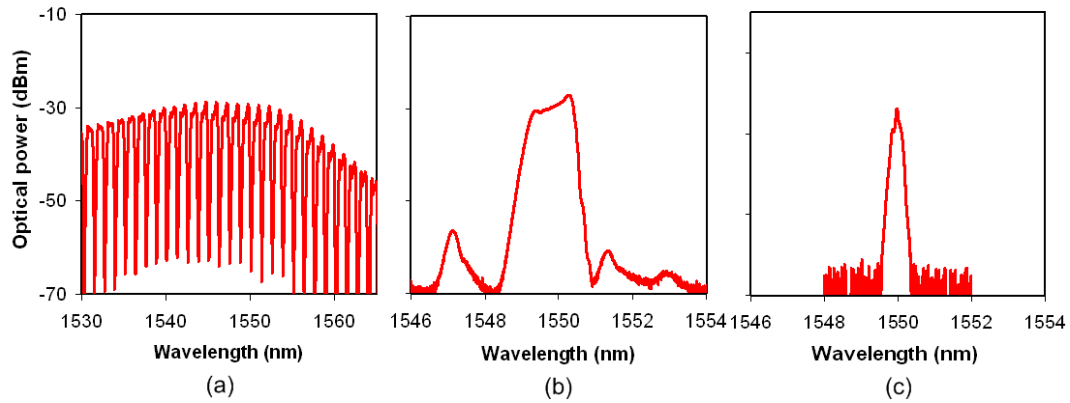

Fig.4.4. Optical spectra for gain switched: (a) FP-LD, (b) DFB-LD, and EI DFB-LD.

The data output (D) of the PPG is used to drive the upper MZM (passing pulses for all logical '1'), while the complementary output ($\overline{D}$) of the PPG is used to drive the lower MZM (passing pulses for all logical '0'). The output pulses from the lower MZM are then delayed using an optical delay line (ODL), before being combined with the output of the upper MZM. This composite waveform represents a PPM signal as shown in Fig. 4.5 (b) for the DFB-LD case for a sequence of '0010110100', which is then transmitted along a length of standard single mode fibre (SSMF) to the RAU. At the RAU, an optically pre-amplified receiver consisting of an erbium doped fibre amplifier (EDFA), an optical bandpass filter (OBPF) and a pin-photodetector (PIN-PD) is used to convert the optical pulses into electrical pulses.

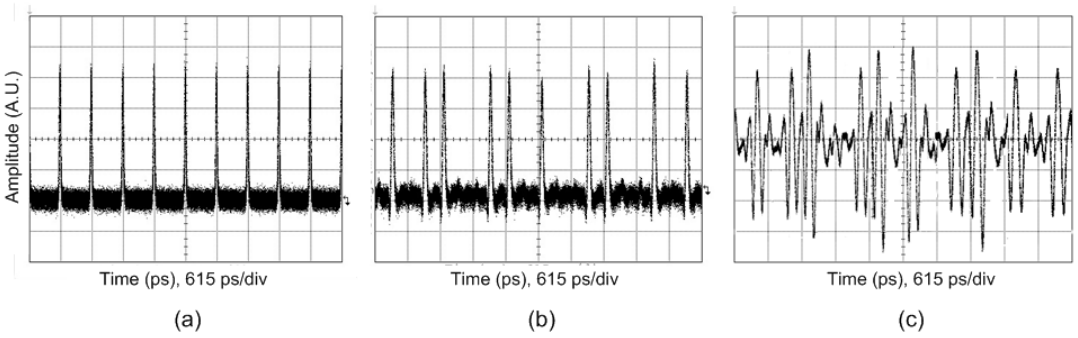

Fig. 4.5. Waveform for gain switched pulses; (a) at the laser output (point A), (b) after coupling (point B), and (c) at the output of UWB filter (point C).

These electrical pulses are amplified and shaped to a UWB signal by using an electrical UWB filter (bandpass 3.1- 10.6 GHz), which acts as a differentiator and converts these Gaussian pulses into doublet Gaussian pulses. These pulses are shown in Fig. 4.5 (c) for the DFB-LD case and are broadly similar for the other lasers

tested. The electrical RF spectrum before and after the UWB filter are shown in Fig. 4.6 (a) and (b). The measured RF spectrum at point A is adjusted to meet the stringent FCC's mask by setting the optical received power using a variable optical attenuator and the square dotted line represents the S21 of the UWB filter [12]. The output of the filter is then connected directly to point D in the RT using 1 m electrical cable. The system is evaluated without antenna transmission to isolate the effect of the fiber distribution system from the radio propagation and focus only on the UWB signal degradation over the fibre transmission link. At the RT, the signal is amplified and mixed with a 6.5 GHz signal (the 4th harmonic of 1.625 GHz) from the local oscillator (LO) to down-convert the UWB signal to baseband.

The output from the mixer is then amplified and filtered with a low pass filter (LPF) to remove the unwanted frequency components yielding a demodulated data signal. Bit error rate (BER) measurements are then performed for a back-to-back (BTB) case as well as for different fibre lengths placed between the ODC and RAU. A variable optical attenuator (VOA) is used with an inline power meter to enable the monitoring of the optical received power (P_{rec}) before the pre-amplified receiver during the measurements of the BER. Eye diagrams are also recorded at the output of the RT by using a high speed digital sampling oscilloscope.

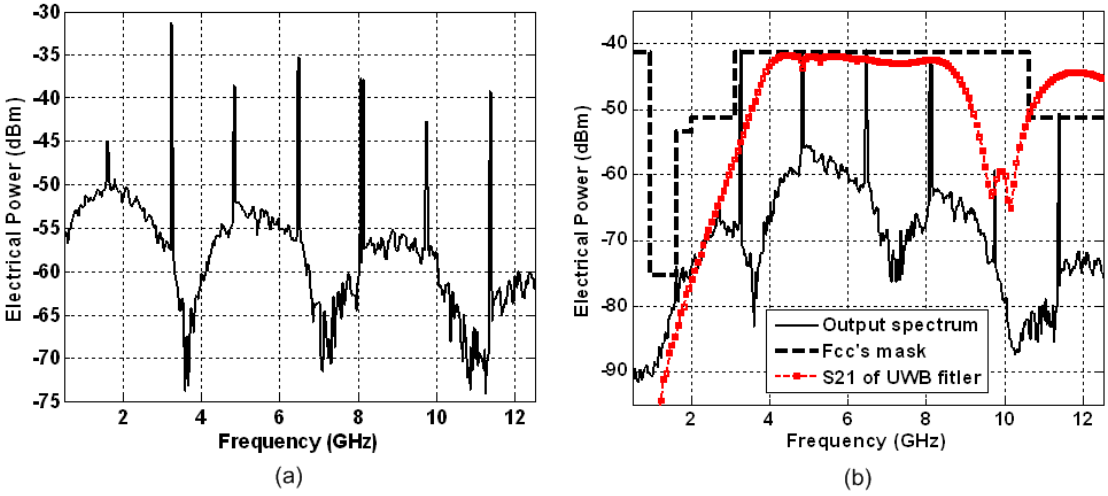

Fig. 4.6. Electrical spectra for; (a) the electrical PPM pulses before and (b) after the UWB filter.

4.4.2 Results and Discussions

In this section, two versions of the RT are considered; the first one uses the LO signal that is generated by a separate signal generator to down covert UWB signal and the second RT retrieves the LO signal from the received UWB signal (carrier recovery).

A. Using Local Oscillator

In this case, the local oscillator signal is generated from a signal generator locked by a 10 MHz reference signal to the signal generator at the transmitter. In Fig. 4.7, the BER is plotted versus received optical power (ROP) at the RAU for the three different optical transmitters. The eye diagrams corresponding to each of the transmitter configurations are shown as insets in each of the figures.

- Fig. 4.7 (a) shows that the GS FP-LD can be used to achieve error free performance (BER<10^{-9}) while transmitting over fibre lengths more than 450 m. The degraded performance over 650 m is mainly due to mode partition noise (MPN). Dispersion in the fibre causes the fluctuations of the energy between the longitudinal modes of the FP-LD to be translated into intensity fluctuations on the transmitted optical signal, thus reducing its signal to noise ratio [13]. Another contributory factor to the performance degradation is the amplified spontaneous emission (ASE) from the EDFA (as no ASE removal filter is used). Optical filtering cannot be employed with this multi-mode transmitter scenario, as it would worsen the effect of MPN [13].
- In the case of the DFB laser (Fig. 4.7 (b)), near error-free transmission whilst transmitting over 1 km of SSMF, can be achieved. In this case the system transmission reach is limited by noise resulting from the degradation in SMSR of the laser (~10 dB for gain-switched DFB), which causes MPN problems as outlined above for the FP laser, as well as a relatively large temporal jitter (5 ps) in the generated optical pulses.

By employing external light injection, the performance of the DFB-LD can be greatly improved as shown in Fig. 4.7 (c) [14]. This improvement is achieved as a result of the enhancement of the pulse SMSR (>30 dB) which eliminates MPN, and a reduction of the temporal jitter (<1 ps). Hence, with this transmitter configuration error-free transmission over 37 km of SSMF has been achieved.

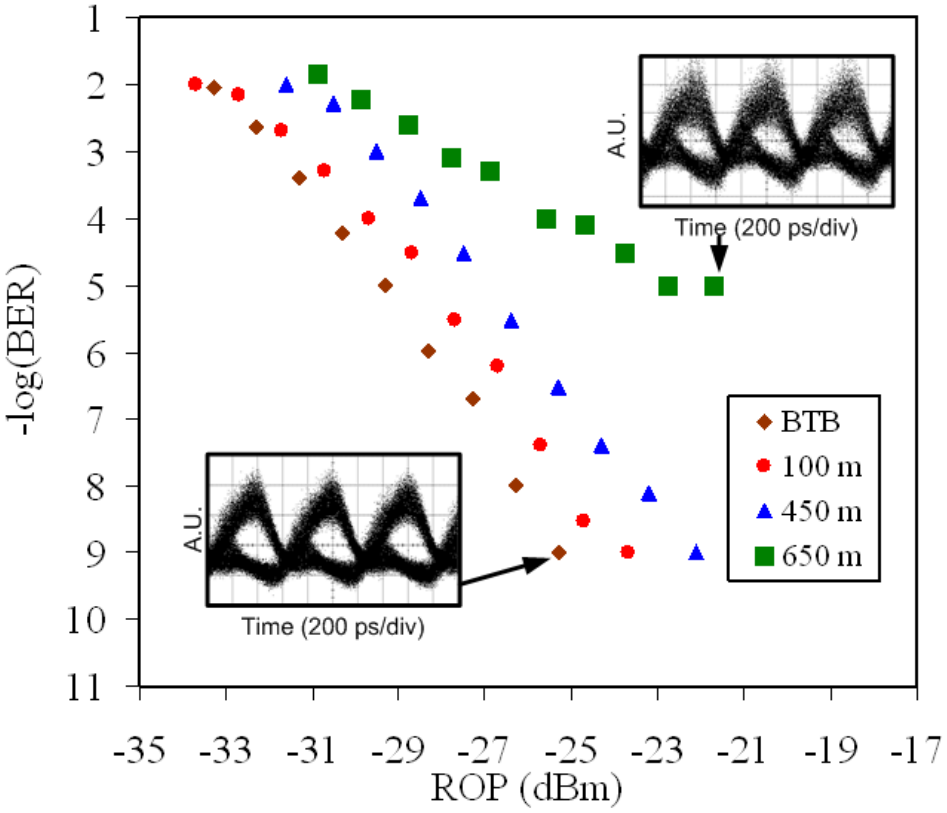
-log(BER)
ROP (dBm)
BTB
100 m
450 m
650 m
A.U.
Time (200 ps/div)
A.U.
Time (200 ps/div)

(a)

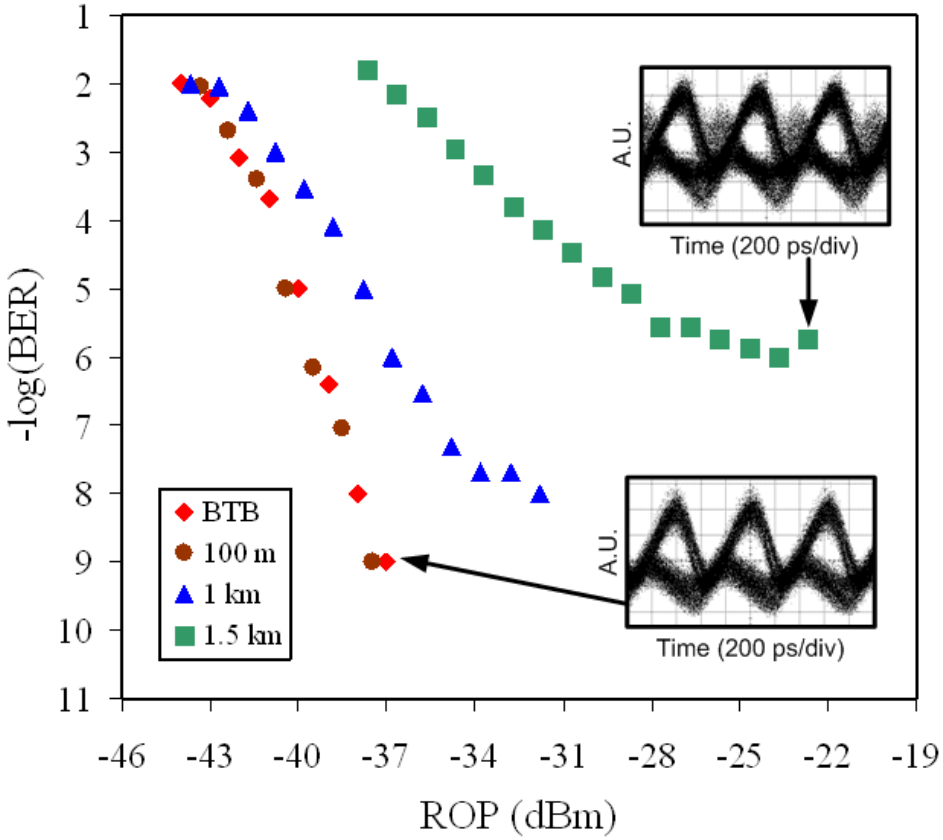
-log(BER)
ROP (dBm)
BTB
100 m
1 km
1.5 km
A.U.
Time (200 ps/div)
A.U.
Time (200 ps/div)

(b)

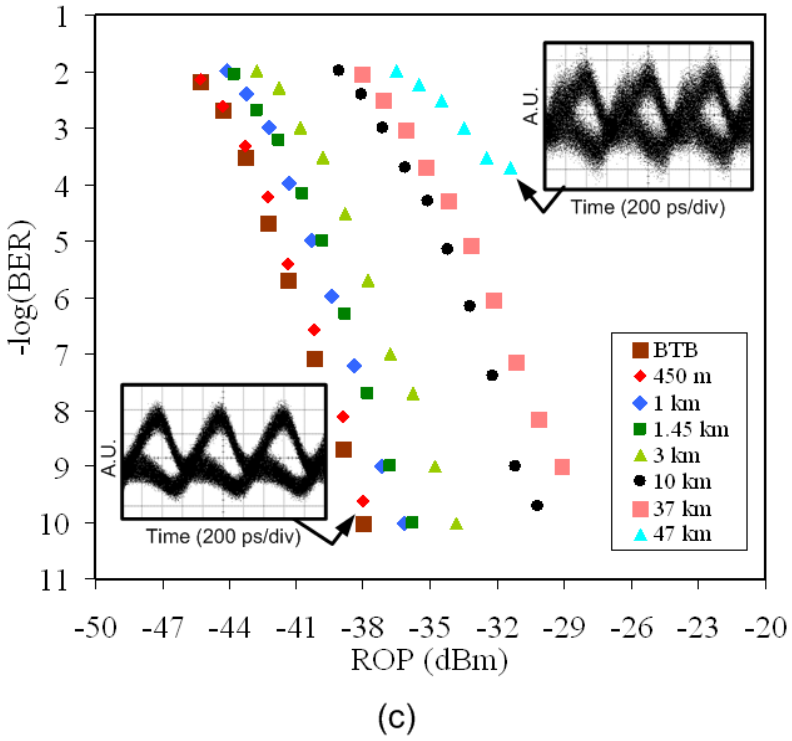

Fig. 4.7. Measured BER versus received optical power and eye diagrams for three different transmitter configurations; (a) FP-LD, (b) DFB-LD, and (c) EI DFB-LD.

B. Using Carrier Recovery

In the second RT configuration, the carrier recovery is realized by splitting the received UWB signal using a 90:10 directional coupler and passing the 10% output of the coupler through a BPF as illustrated in Fig. 4.8. This filter has a bandwidth of 300 MHz and is centred at the 4th harmonic. The S21 transmission of the carrier recovery filter is presented in Fig. 4.9. The recovered carrier is then amplified and used to downconvert the UWB signal. A manual phase shifter was use to eliminate the phase difference between the carrier and the UWB signal.

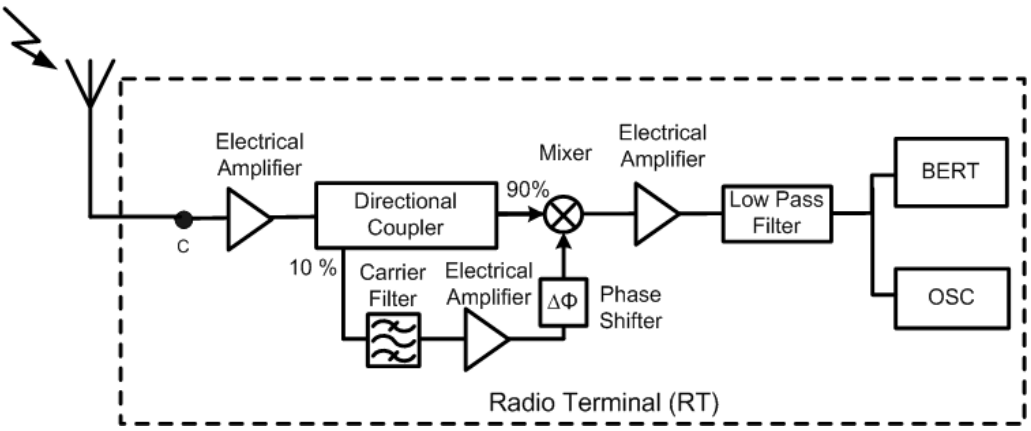

Fig. 4.8. UWB radio terminal using a carrier recovery circuit.

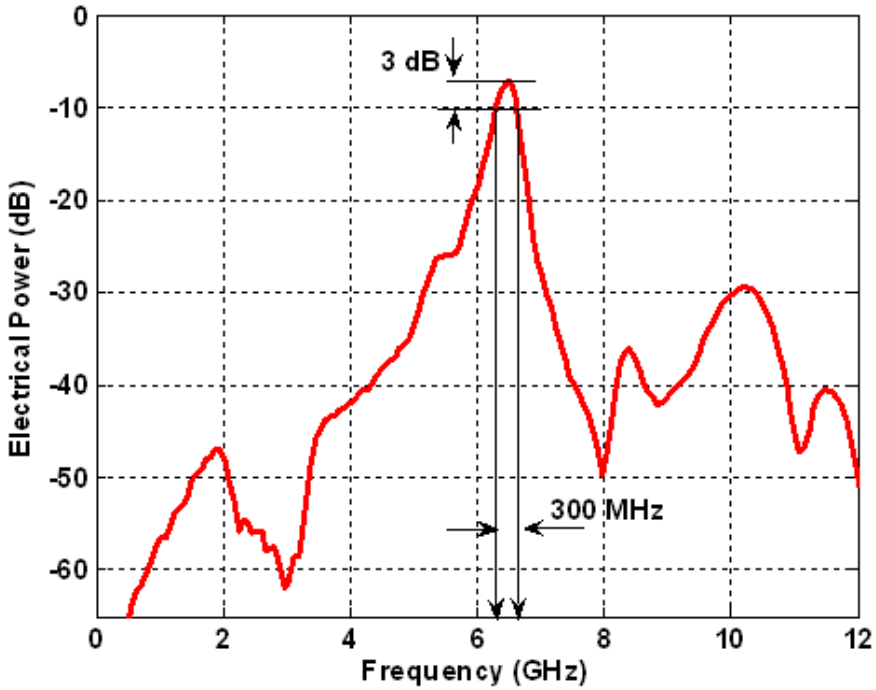

Fig. 4.9. S21 transmission of the carrier recovery filter

In this section we will show that by varying the PPM delay in a signal, one can significantly change the spectrum of the PPM signal and system performance. Since in our system the pulses representing "0" are delayed, the PPM delay is defined as the time between the beginning of the bit period and the centre point of the "0" pulse and is expressed as a fraction of the bit period, e.g. if the 0's are delayed by a half of the bit slot in comparison to 1's the PPM delay equals 50%. Fig. 4.10 shows the received BER as a function of the PPM delay for both RT configurations; the diamonds represent the case when a separate LO is employed at the RT and the triangles represent the case when carrier recovery is used. It can be seen that in the first case the BER remains lower than 10^{-8} for a wide range of PPM delay values (20%-65%), while in the case of the carrier recovery there are two regions of PPM delay for which the BER is low: 23% - 30% and 43% - 55%. This difference in performance is due to the fact that the power of the fourth harmonic component fluctuates as the PPM delay is changed. Since, in the case of carrier recovery, it is this component that is used for signal down-conversion, any reduction in its power will have an adverse effect on the quality of the received signal. Fig. 4.10 shows also the plot of the total RF power in the PPM UWB signal as a function of the PPM delay. The total power in the radio signal was calculated by integration between 3.1

GHz and 10.6 GHz for the two cases. From the plot it can be seen that the total power of the UWB signal varies significantly depending on the PPM delay and that, by correct adjustment of this parameter, the total power can be maximized, and lowest BER can be obtained.

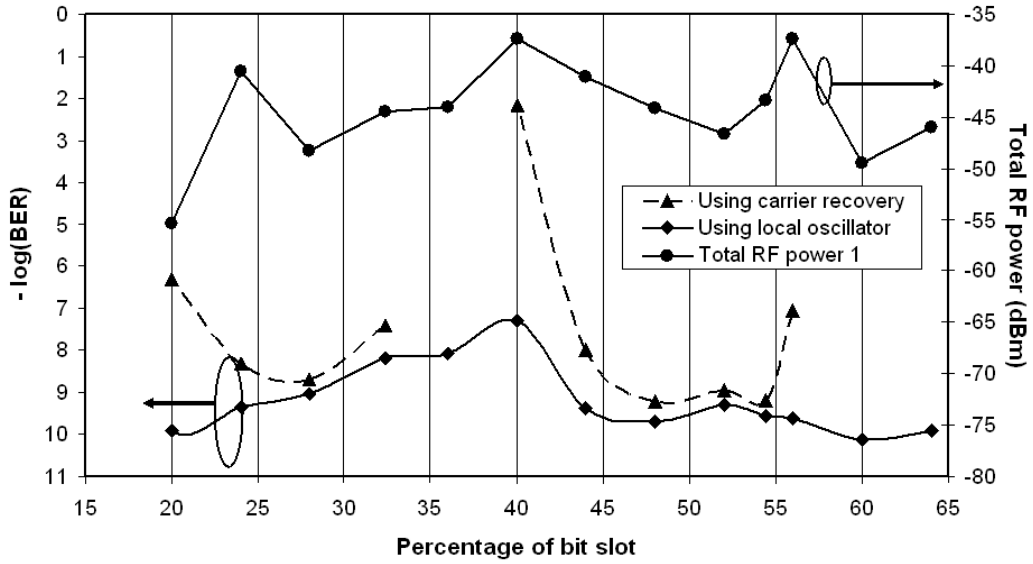

Fig. 4.10. Measured BER and total electrical power versus the percentage of bit slot

The plots in Fig. 4.11 (a) and (b) present the RF spectrum of the UWB signal for PPM delays of 56% and 60% respectively. From the plots it can be seen that increasing the PPM delay from 56% to 60% affects the spectrum shape and reduces the power in the 4^{th} harmonic by around 10 dB. Fig. 4.12 (a) shows the received eye diagrams for the PPM delay of 56% with carrier recovery employed at the receiver. Even though the noise and the ringing on the eye (due to the interference from "0" pulse) are clearly visible, the eye is open and we can achieve a BER of 10^{-9}. The plots in Fig. 4.12 (b) and (c) on the other hand, show the eye diagrams received for PPM delay of 60% for carrier recovery and separate LO respectively. It can be seen that the reduction in the power level in the 4^{th} harmonic component causes a complete eye closure for the carrier recovery case; however, when the separate LO is used the eye opening is very clear and we obtain a BER 10^{-10}. It is envisioned that the regions of good performance while using carrier recovery could be extended to a certain degree, by using a higher gain amplifier and narrower filtering to reduce the noise and interference. These results show how PPM delay can be optimized to improve system performance in this receiver configuration which could be used to

minimize the cost and complexity of a UWB receiver.

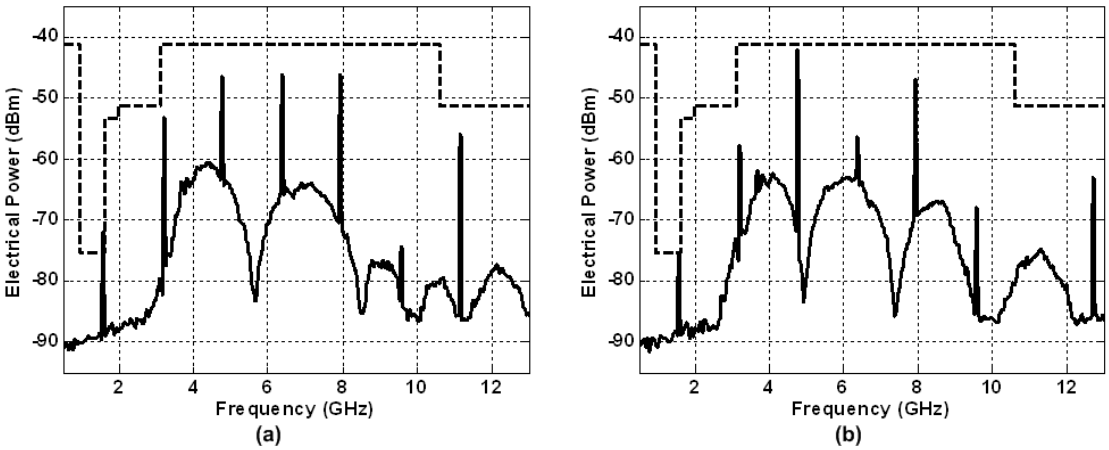

Fig. 4.11. Electrical RF spectrum of the UWB signal for PPM delay of (a) 56% and (b) 60%.

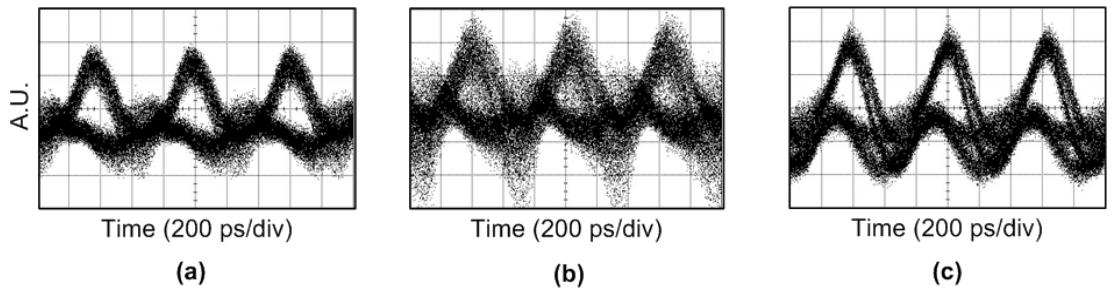

Fig. 4.12. Eye diagrams for PPM delay of (a) 56%, (b) 60% using carrier recovery, and (c) 60% using separate LO.

4.4.3 Simulation Results

Simulations have also been carried out by using VPItransmissionMaker simulation platform to model the proposed setup and verify our experimental results. Fig. 4.13 shows the schematic diagram for our simulation setup. The key parameters of the devices have been chosen to meet the real experimental parameters. The GSL was simulated by using a semiconductor laser module, in the VPI software, at a wavelength of 1550 nm and the output pulses were optimized by adjusting the bias and amplitude of the RF drive. In the case of the EI DFB-LD, a CW module laser was used to realize the external injection. The wavelength and power of the CW module laser were optimized to obtain pulses exhibiting the low jitter and narrow optical spectrum. We also used SSMF with group velocity dispersion (GVD) of 16 ps/nm.km and loss of 0.2 dB/km. The optical receiver has a thermal noise current of 10^{-11} A/Hz$^{1/2}$ and a responsivity of 1 A/W. In the down-conversion block

at the RT, the local oscillator phase was adjusted to give the lowest BER and an open eye diagram for each transmission distance. The simulation results for BER versus ROP for the three configurations are shown together in Fig. 4.14 and the simulated eye diagrams are also shown in Fig. 4.15. These results show the system performance for each of the three transmitter configurations for BTB and different fibre transmission lengths. For the FP-LD, the simulation illustrates that ASE noise causes the FP-LD to portray the worst receiver sensitivity in the BTB case and an error floor could be seen at a BER of 10^{-06}. The error floor at 650 m is primarily caused by the multimode spectrum which when transmitted results in MPN as discussed in section 4.4.2. The simulated eye diagram for BTB and after transmission over 650 m are shown in Fig. 4.15 (a) and (b).

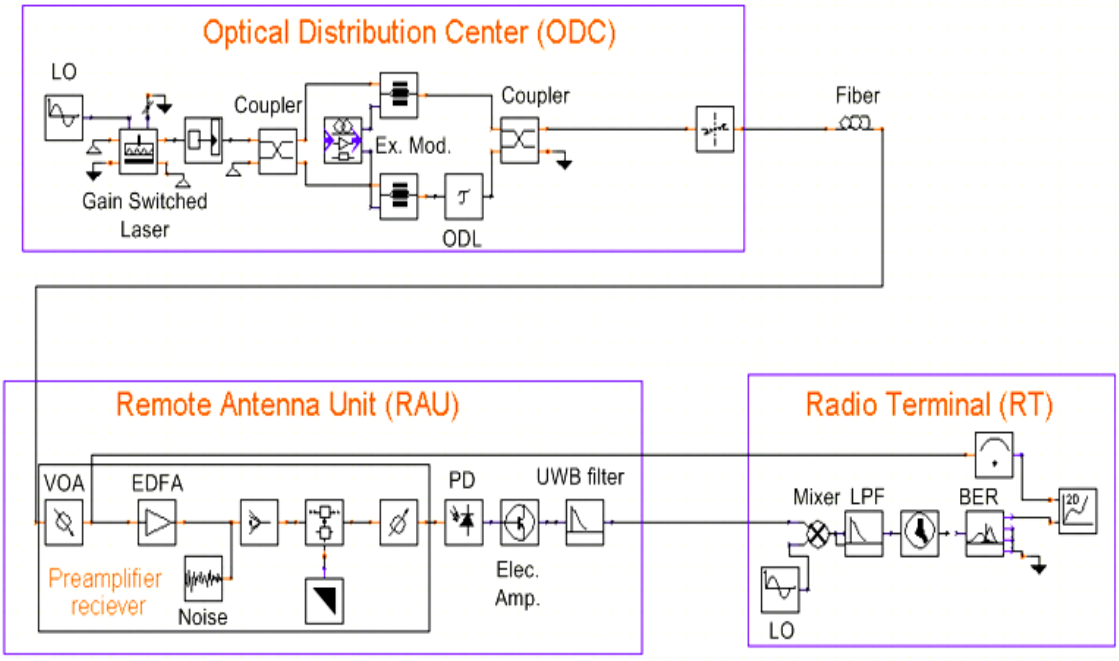

Fig. 4.13. Simulated setup diagram using two external modulators.

In the case of the DFB-LD an improvement in the BTB receiver sensitivity is achieved mainly due to the removal of ASE with the use of an OBPF. However, the transmission distance can only be doubled due to the degraded SMSR of the GS-DFB, which results in MPN. Fig. 4.15 (c) and (d) show the simulated eye diagram for the BTB and after transmission over 1500 m.

The EI DFB-LD exhibits the best BTB receiver sensitivity as a result of the reduced pulse to pulse jitter. Moreover, it also achieves the error free transmission, which can be attributed to the enhanced SMSR, reduced jitter and reduced chirp. This can be seen also in the simulated eye diagram for BTB case in Fig. 4.15 (e). The traces in Fig. 4.15 (f) show that after transmission over a fibre link of 47 km, the eye diagram is degraded due to the combined effect of the fibre's attenuation and dispersion. However it is clear that we are able to achieve significant increase in performance and reach with the EI-DFB.

The experimental and simulated results are also summarized in table 4.1 to show the performance for the three transmitter configurations. The table demonstrates that there are small differences between the simulated and experimental measurements in the receiver sensitivities for BTB, and the power penalty needed for BER $<10^{-9}$. Power penalty defines as the required optical power to account for degradations due to attenuation, inter symbol interference, and MPN.

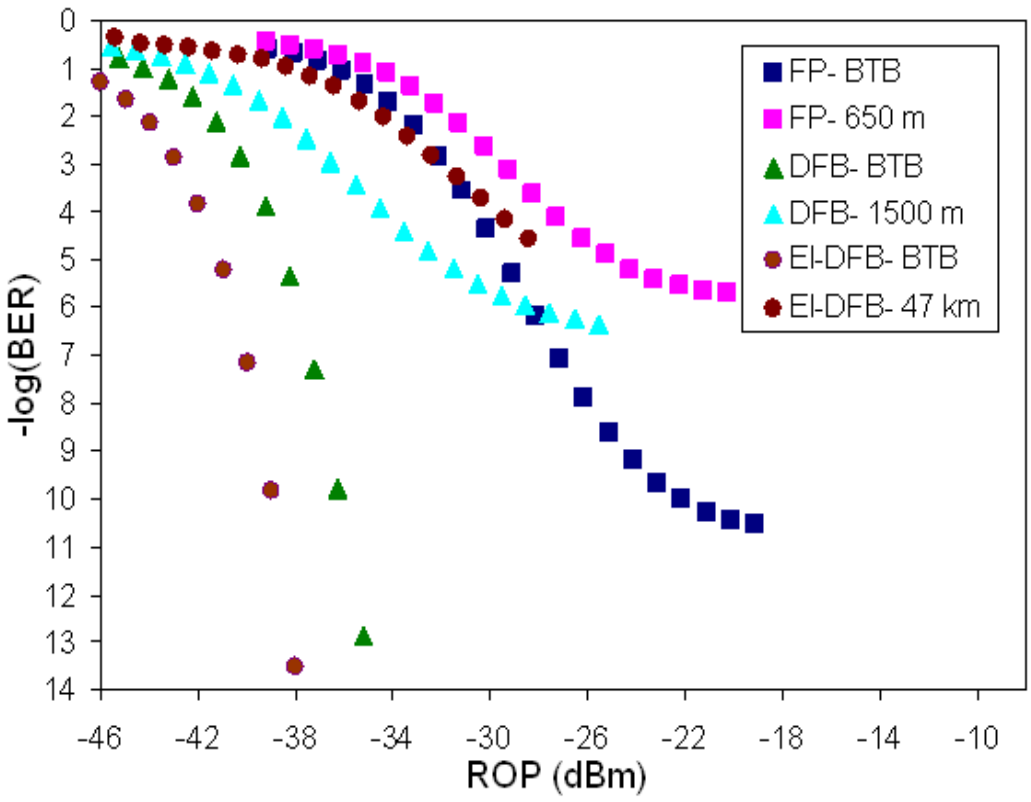

Fig. 4.14. Simulated BER versus received optical power for the three different GSLs.

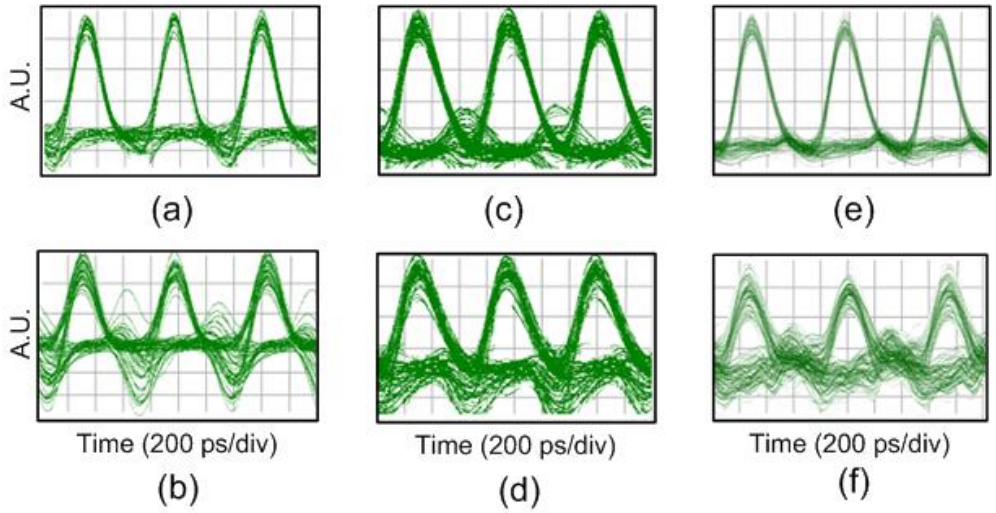

Fig. 4.15. Simulated eye diagrams for FP- lasers at (a) BTB and (b) 650 m, DFB-laser at (c) BTB and (d) 1500 m, and EI-DFB laser at (e) BTB and (f) 47 km.

Table 4.1. Results summary for IR-UWB generation by using two external modulators

Transmitter configuration		BTB threshold at 10^{-9} (dBm)	Power penalty for BER at 10^{-9} (dB)	Fibre length at 10^{-9}	Error floor value	Fibre length at error floor
FP-LD	meas.	-25.3	3.2	450 m	10^{-5}	650 m
	simul.	-25.1	3.5		10^{-6}	
DFB-LD	meas.	-37.5	5.7	1 km	10^{-6}	1.5 km
	simul.	-38.2	4.7		10^{-6}	
EI DFB-LD	meas.	-38.9	9.9	37 km	10^{-4}	47 km
	simul.	-39.9	10.2		10^{-4}	

4.5 Generation of IR-UWB Using Direct Modulation

4.5.1 Experimental Setup

The schematic diagram for the second approach for UWB over fibre (UWBoF) distribution system is shown in Fig. 4.16. The ODC uses the simpler direct modulation of a GSL for data transmission at a rate of 1.625 Gbps. The ODC setup

consists of two DFB-LDs biased below the threshold current value via a bias tee. These two DFB-LDs are modulated using a combination of a 1.625 GHz sinusoidal signal generator and a synchronous 1.625 Gbps pattern generator (2^7-1 PRBS). The output from the signal generator is amplified and then divided into two equal paths before it is combined with the NRZ data pattern for both data and inverted data. The resultant output waveforms are applied to both DFB-LDs to generate Gaussian pulses through the GS process only when the data signal applied to the laser is a bit '1'. The output pulses are tuned by inspection of the eye diagrams to achieve the best extinction ratio and minimum pattern-dependent-effect by adjusting the bias level and the amplitude of the electrical data. The DFB-LD 1 generates a GS Gaussian pulse for each logical bit '1', while the DFB-LD 2 generates a GS Gaussian pulse for each logical bit '0'.

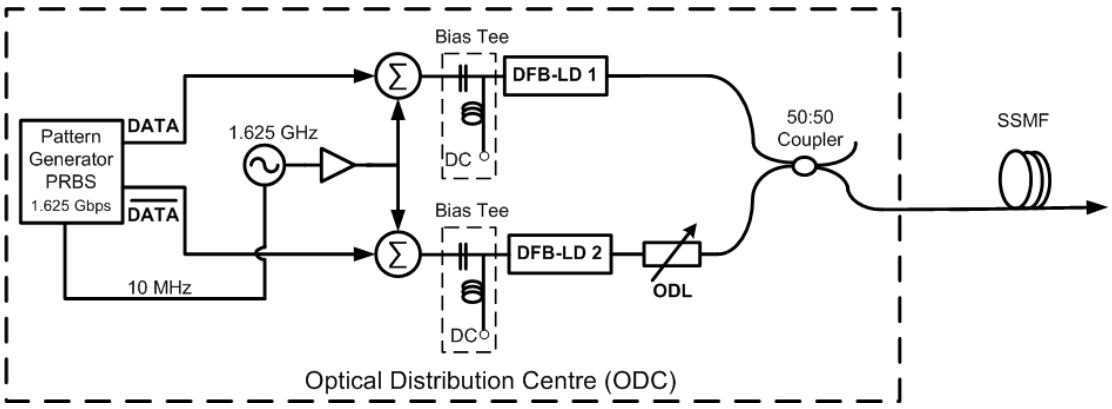

Fig. 4.16. Schematic diagram for generating PPM pulses using two direct modulated GSLs.

The output from both lasers are then delayed relative to one another by using the optical delay line (ODL) before the data and inverted data pulses are combined using a 50:50 coupler, and then transmitted directly as a PPM signal over different lengths of SSMF. After fiber transmission, the signal is received by the same RAU, and RT (shown in Fig. 4.3) which amplifies the received PPM signal and transforms it to electrical UWB pulses. Then, the UWB signal is transmitted directly to the RT at point D to be demodulated using a separate LO and amplified. BER measurements and eye diagrams are recorded for the received signal over different fibre lengths.

4.5.2 Results and Discussion

The system performance is measured using two different configurations of our DM GS laser transmitters. In the first configuration two GS DFB laser diodes (DFB-LD) operating at approximately the same wavelength were used, and their optical spectrum is shown in Fig. 4.17 (a). While in the second configuration, an externally injected light from a third laser in a CW mode was launched into the two GS DFB lasers to give a pair of externally injected GS DFB (EI DFB-LD) lasers that have the optical spectrum shown in Fig. 4.17 (b). Due to the limited availability of practical components, the DFB-LDs and EI DFB-LDs were chosen with different operating wavelengths.

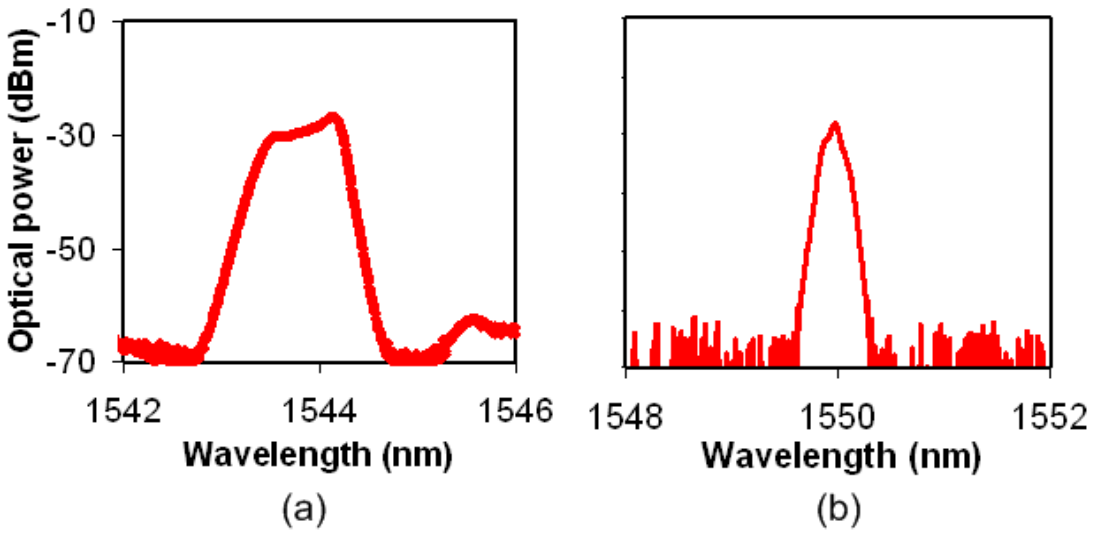

Fig. 4.17. (a), and (b) are optical spectra for direct modulated GS DFB and EI DFB-LD.

The oscilloscope traces in Fig. 4.18 show the NRZ data, the laser drive signal consisting of the data combined with the RF sinusoid and the resulting optical pulses. It is interesting to note that the data needs only to create a small offset to generate narrow pulses with a good extinction ratio. The two optical outputs, which have pulse durations of around 20 ps, are combined together after delaying the lower branch by 285 ps relative to the beginning of a bit period.

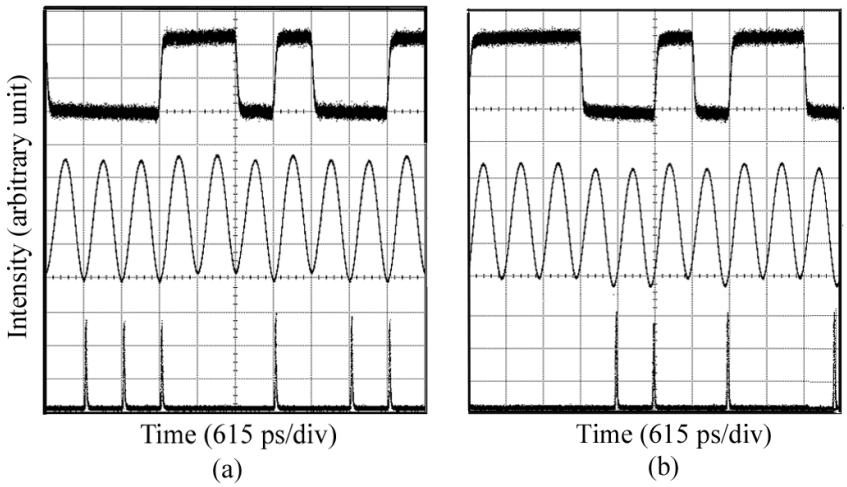

Fig. 4.18. Data, combined data and an RF sinusoid, and output pulses from lasers for (a) data, (b) inverted data at 1.625 Gbit/s.

The BER measurements for the different fibre spans versus the ROP at the RAU (P_{rec}) are shown in Fig. 4.19. The results in Fig. 4.19 (a) show an error floor at 10^{-8} due to significant levels of amplitude noise and temporal jitter on the GS pulses. This limits the performance, but is acceptable for a radio based system which includes a high level of forward error correction. The results also show a penalty of 0.7 dB between BTB and 1 km transmission at BER of 10^{-8}. However, the system reaches an error floor at around 10^{-5} on transmission over 10 km fibre due to the large frequency chirp on the GSL which broadens the spectrum to approximately 1 nm. The fibre dispersion results in the chirped pulses being significantly broadened such that the '1' and '0' data pulses overlap causing intersymbol interference (ISI). The eye diagrams are also shown in Fig. 4.19 (a) as insets for the lowest bit error rate at 1 km, and after transmission over 10 km.

When the EI GS-DFB laser diodes are employed, the performance of the system transmission is greatly improved. The result shown in Fig. 4.19 (b) reveals the transmission length is extended up to 10 km with error free (BER = 10^{-9}) performance. It should be noted that the receiver sensitivity in the BTB case, has been improved by 3 dB compared to the non-injected case due to the reduction of timing jitter (from ~4 ps to <1 ps) and the enhancement in SMSR (from ~10 dB to >30 dB) of the GS-DFB lasers which reduce MPN cause by optical filtering in the experiment [13].

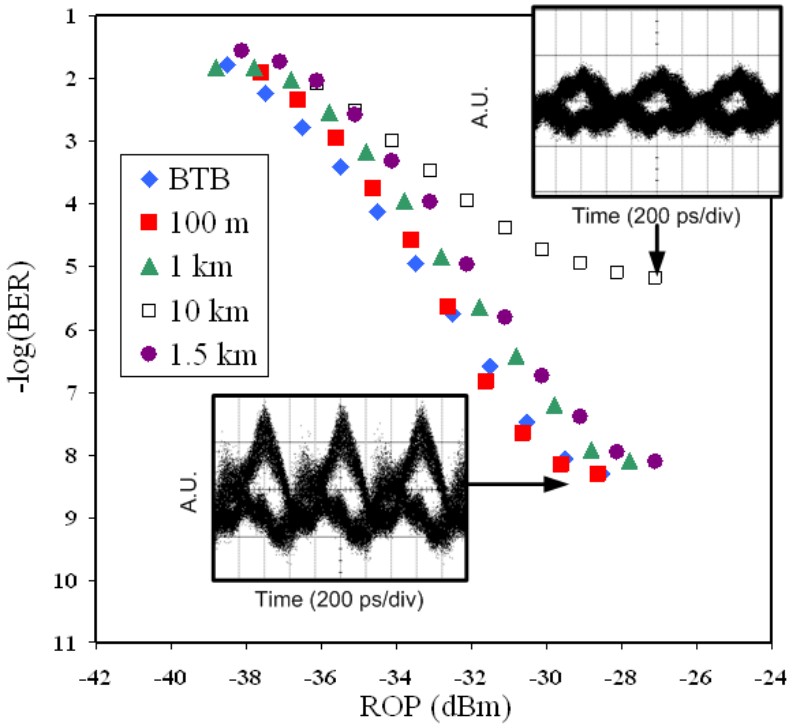

(a)

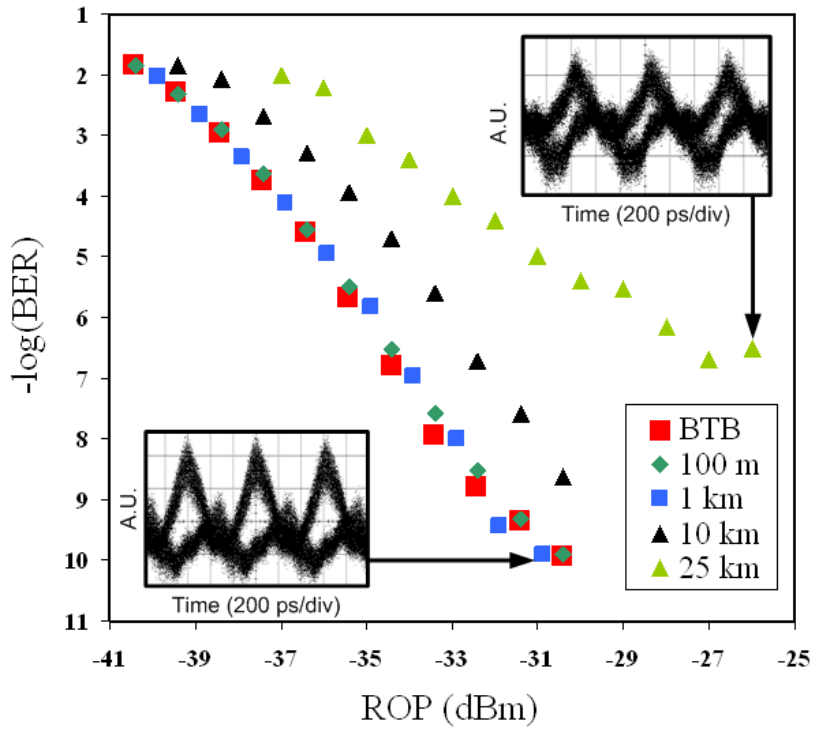

(b)

Fig. 4.19. Measured BER versus received optical power and eye diagrams for two different transmitter configurations; (a) two GS-DFBs, (b) two EI GS-DFBs.

In the EI GS-DFB case, the system displays an error floor around 10^{-7} for a distance of 25 km. As for the non-injected case, this error floor is a result of ISI between the '1' and '0' data pulses. The significantly extended reach in the EI GS-DFB case is due to the chirp reduction caused by the external injection (spectral width reduced from ~1 nm to ~0.3 nm) [15].

4.5.3 Simulation Results

The simulated model for the generation and distribution of UWB signals using directly modulated lasers has been carried out for the non-injected and injected case. As shown in Fig. 4.20, the simulation used two semiconductor laser modules from the VPI software kit with the same bias and RF drive power combined with both data and inverted data to achieve the DM GS DFB-LD.

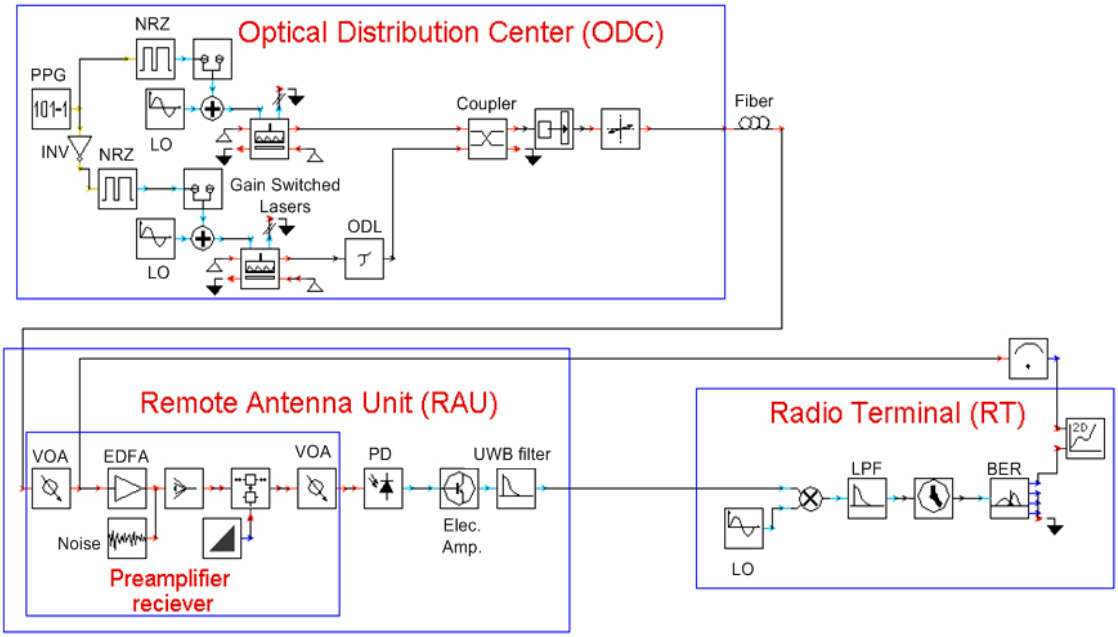

Fig. 4.20. Simulation setup for direct modulated GSL.

The BER versus ROP is shown in Fig. 4.21 and the simulated eye diagrams are also shown in Fig. 4.22 for the direct modulated GS-DFB and EI GS-DFB. Fig. 4.22 (a) and (b) illustrate the simulated eye diagrams for DFB-LD and demonstrate the timing jitter and MPN effect in the downconverted pulse between BTB and 10 km transmission over fibre. These detrimental effects are eliminated in the injected case

as shown by the eye diagrams Fig. 4.22 (c) and (d) for BTB and transmission over 25 km. However, this transmitter configuration shows a maximum reach only to 25 km in EI GS-DFB which is significantly different from the externally modulated configuration that could achieve 37 km error free. This is mainly due to the poor extinction ratio (< 10 dB) in the direct modulation case compared to that with the external modulators.

The important results from the direct modulated GS laser are summarized in table 4.2. The table clearly shows that there is a close match between experimental and simulation results. The simulated and experimental BER shows a 1 dB difference in BTB performance. The power penalty is about 2 dB for both cases at 10^{-9}. While the error floor is nearly the same for the longest transmission distance for DFB and EI DFB at 10 km, and 25 km, respectively.

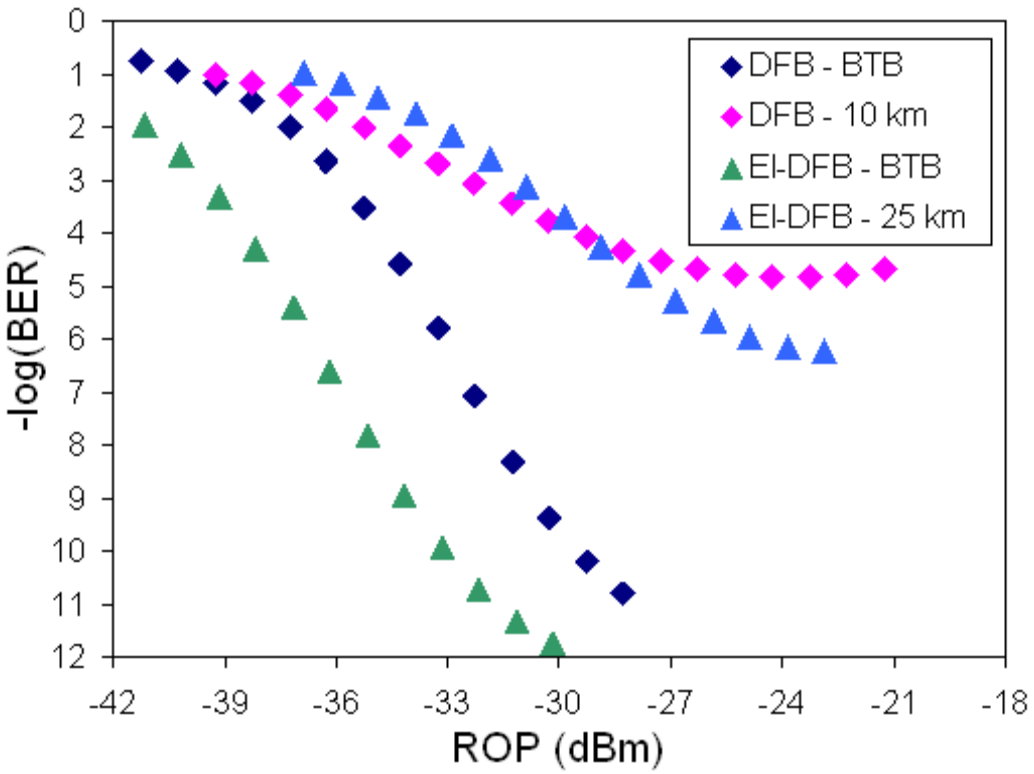

Fig. 4.21. Simulated BER versus received optical power for two transmitter configurations of the two direct modulated GSLs.

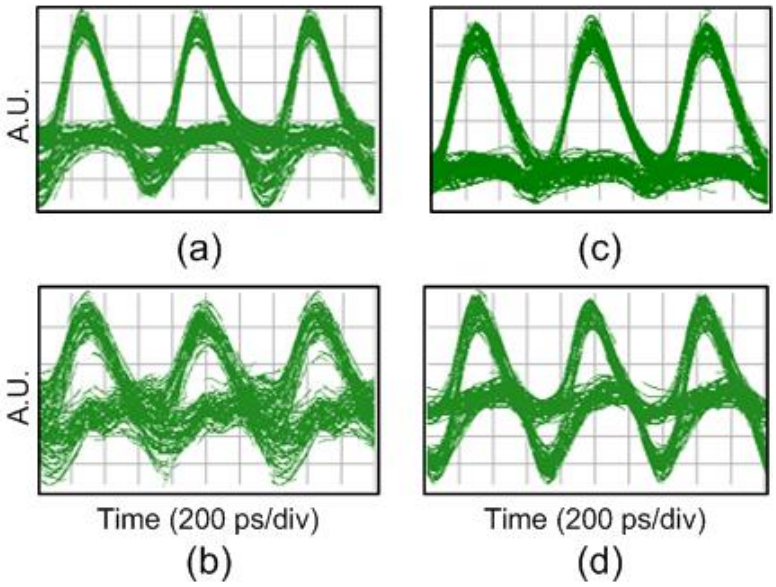

Fig. 4.22. Simulated eye diagrams for DM DFB-LD at (a) BTB and (b) 10 km and DM EI DFB-LD at (c) BTB and (d) 25 km.

Table 4.2. Results summary for IR-UWB generation by using two directly modulated GSLs.

Transmitter configuration		BTB threshold at 10^{-9} (dBm)	Power penalty for BER at 10^{-9} (dB)	Fiber length at 10^{-9}	Error floor value	Fibre length at error floor
DM DFB-LD	meas.	-29.5	2.4	1.5 km	10^{-6}	10 km
	simul.	-31.2	3.1		10^{-5}	
DM EI DFB-LD	meas.	-33.4	2	10 km	10^{-7}	25 km
	simul.	-34.1	2.3		10^{-7}	

The advantage of the direct modulation scheme over the previous setup is its simplicity as it does not require external modulators, and hence there is no additional insertion loss. Such a reduction in cost is vital for the development of a low cost solution for distribution of UWB signals. In table 4.3, the comparison between the two distribution setups is presented in terms of the limiting factors that affect the system distribution and the required costs. In systems that need the distribution for a small residential network or office building, the FP-LD or DM DFB-LD can be the best choice for a low cost and easily integrated system. However for a large distribution system, the EI DFB-LD scheme with two external modulators allows a more reliable and stable system for many end users with maximum reach.

Table 4.3. Comparison between the two approach setups in terms of their limiting factors.

Approach setup	Laser configuration	Costs	Limiting factors
External modulators	FP-LD	$	• MPN resulting from the energy fluctuations in the longitudinal modes due to dispersive transmission.
	DFB-LD	$$$	• SMSR degradation causes MPN problems. • Large inherent timing jitter in the generated gain switching pulses.
	EI DFB-LD	$$$$	• Attenuation and dispersion effect.
Direct modulation	DFB-LD	$$	• Timing jitter in GS pulses. • SMSR degradation causes MPN problems.
	EI DFB-LD	$$$	• Degraded extinction ratio.

4.6 Summary and Conclusions

UWB-over-fibre (UWBoF) is an attractive and cost effective solution for increasing the reach of UWB systems. The work presented in this chapter has successfully demonstrated the generation and distribution of 1.625 Gbps UWB signals modulated in PPM format by using two optical distribution setups. Both setups have been studied over different fibre links with using different GS laser configurations. The first approach uses one GS laser and two external modulators. The results show that error free transmission can be achieved for the GS FP, DFB, and EI DFB laser transmitters over 450 m, 1 km, and 37 km respectively. A simple receiver configuration that utilizes carrier recovery has also been presented in this context. Such an approach could be used to minimize the cost and complexity of a UWB receiver.

An alternative approach for the generation and distribution of UWB signals has also been presented which is based on the direct modulation of a GSL. The method uses two lasers driven with a signal composed of an NRZ data signal and an RF sinusoid. The generated PPM pulses were transmitted over different fibre links by using GS-DFBs and EI GS-DFBs. The obtained results show that the system can provide error free performance over 10 km with an EI GS-DFB. A somewhat degraded

performance is also achievable with an un-injected GS-DFB at 10 km. Since these radio systems typically operate with BER of worse than 10^{-3}, this performance may also be acceptable and offers a simpler transmitter design. There is thus a trade off between the cost/complexity of the transmitter configuration in a UWBoF system, and the required reach and performance of the distribution network. The noise effects caused by pulse propagation from the different sources means that one must choose the transmitter based on the required reach of the network.

References

[1] A. Kaszubowska-Anandarajah, P. Perry, L. P. Barry, and H. Shams, "An IR-UWB photonic distribution system," *Photonic Technology Letters, IEEE*, vol. 20, no. 22, pp. 1884-1886, 2008.

[2] M. J. L. Cahill, G. J. Pendock, and D. D. Sampson, "Low error rate return-to-zero direct modulation of gain-switched lasers," *Optical and Quantum Electronics,* vol. 28, no. 9, pp. 1181-1185, 1996.

[3] Seung-Il Myong, Dong-Sun Seo, Jae-Dong Park, and Moo-Jung Chu, "Pattern independent direct pulse modulation of a gain-switched distributed-feedback laser at 2.5 Gbit/s," *in The Pacific Rim Conference on Lasers and Electro-Optics CLEO/Pacific Rim '99,* pp. 489-490 vol.2, *, 1999.*

[4] K. Y. Lau, "Gain switching of semiconductor injection lasers," *Applied Physics Letters,* vol. 52, no. 4, pp. 257-259, 1988.

[5] P. Vasilev, Ultrafast Diode Lasers: Fundamentals and Applications, Artech House, Boston, 1995.

[6] L. P. Barry, J. Debeau, and R. Boittin, "Simple technique to improve the spectral quality of gain-switched pulses from a DFB laser," *Electronic Letters,* vol. 30, no. 25, pp. 2143-2145, 1994.

[7] N. Jensen, H. Olesen, and K. Stubkjaer, "Partition noise in semiconductor lasers under CW and pulsed operation," *Quantum Electronics, IEEE Journal of* ,vol. 23, no. 1, pp. 71-80, 1987.

[8] P. Anandarajah, M. Rensing, and L. P. Barry, "Signal degradation due to output filtering of self-seeded gain-switched pulses exhibiting weak inherent side-mode-suppression ratios," *Applied Optics,* vol. 44, no. 36, pp. 7867-7871, 2005.

[9] P. M. Anandarajah, C. Guignard, A. Clarke, D. Reid, M. Rensing, L. P. Barry, G. Edvell, and J. D. Harvey, "Optimized pulse source employing an externally injected gain-switched laser diode in conjunction with a nonlinearly chirped

grating," *Selected Topics in Quantum Electronics, IEEE Journal of* , vol. 12, no. 2, pp. 255-264, 2006.

[10] K. Iwashita and K. Nakagawa, "Suppression of mode partition noise by laser diode light injection," *Quantum Electronic, IEEE Journal of,* vol. 18, no. 10, pp. 1669-1674, 1982.

[11] D. Seo, H. Liu, D. Y. Kim, and D. D. Sampson, "Injection power and wavelength dependence of an external-seeded gain-switched Fabry–Perot laser," *Applied Physics Letters,* vol. 67, no. 11, pp. 1503, 1995.

[12] Federal Communications Commission, "Revision of part 15 of the commission's rules regarding ultra-Wideband transmission Systems," First Note and Order, ET Docket 98- 153, FCC 02-8, 2002.

[13] L. P. Barry and P. Anandarajah, "Effect of side-mode suppression ratio on the performance of self-seeded gain-switched optical pulses in lightwave communications systems," *Photonic Technology Letters, IEEE*, vol. 11, no. 11, pp. 1360 - 1362, 1999.

[14] A.M. Clarke, P.M. Anandarajah, and L.P. Barry, "Generation of widely tunable picosecond pulses with large SMSR by externally injecting a gain-switched dual laser source," *Photonic Technology Letters, IEEE,* vol. 16, no. 10, pp. 2344-2346, 2004.

[15] C. Lin, J. K. Andersen, and F. Mengel, "Frequency chirp reduction in a 2.2 Gbit/s directly modulated InGaAsP semiconductor laser by CW injection," *Electronic Letters,* vol. 21, no. 2, pp. 80-81, 1985.

Chapter 5 – Optical Generation of Modulated Millimetre-Wave Signals

5.1 Introduction

In this chapter, the optical generation and distribution of modulated millimeter wave signals (mm-waves) based on a gain switched laser (GSL) is demonstrated and experimentally investigated in two different transmitter configurations. In these configurations the GSL generates a comb of frequencies by driving the semiconductor laser with a large electrical sinusoidal signal which switches the laser on and off. By using appropriate optical filters two of these comb lines can be selected so that a high quality mm-wave can be produced at the photodetector [1, 2].

- The first setup uses an external intensity modulator to modulate the optical tones with non-return to zero (NRZ) data at rates up to 3 Gbps.
- The second setup produces optical OOK modulated tones by directly driving the laser with a combination of a sinusoidal signal and NRZ data up to 3 Gbps [3, 4].

The performance of both systems was experimentally investigated and simulated by using bit error rate (BER) tests. The comparison between both systems was also carried out to show the trade off between system complexity and cost. The external modulation setup increases the system cost and loss, while the direct modulation technique shows a simple and lower cost system solution for generating modulated mm-wave signals. Such a cost reduction will be an important parameter for the commercial deployment of such systems.

This chapter is organized as follows. The principle of the optical mm-wave generation based on the gain switching technique, and the two proposed modulation schemes are described in section 5.2. Section 5.3 demonstrates the experimental setup for the first transmitter configuration, and this is then followed by the directly

modulated GSL setup in section 5.4. Finally, the comparison between theses two configurations and conclusions are outlined in section 5.5 and 5.6.

5.2 Optical Mm-Wave Generation using GSL

The principle of comb generation using a GSL is shown in Fig. 5.1. An electrical local oscillator (LO) signal at frequency f_0 (15 GHz) is amplified with the aid of a high power RF amplifier. A bias tee is then used to combine the electrical RF signal with a DC bias to enable gain-switching of a commercially available NEL[1] distributed feedback (DFB) laser contained within a hermetically sealed high-speed package. The laser used has a 3 dB bandwidth of 18 GHz, and an output power of 4.7 dBm, both measured at a bias current of three times the threshold current (3 I_{th}). In this set up the bias point is selected to be 51 mA. The RF signal is sufficiently large to switch the LD from below to above the lasing threshold (chapter 4, section 4.3) and produces a stream of optical pulses with 15 – 20 ps pulse widths with a repetition frequency of f_0. The generated gain switched spectrum was captured by a high resolution optical spectrum analyzer (OSA) and is shown in Fig. 5.2 (a). The spectrum shows the generated comb of multiple optical phase correlated tones equally spaced by f_0 (15 GHz).

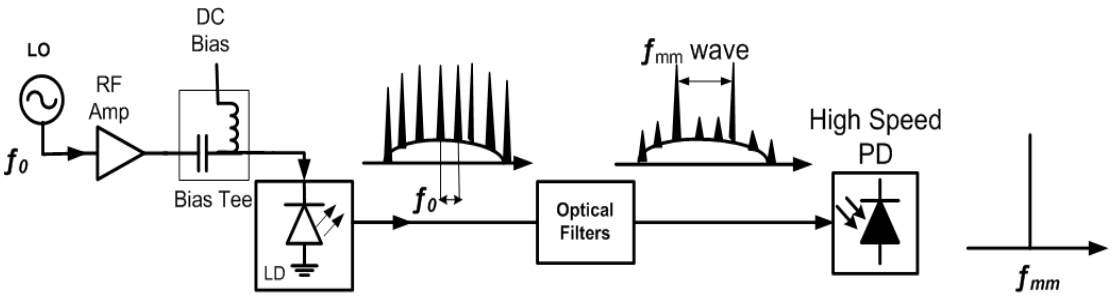

Fig.5.1. Principle of comb generation using a GSL.

Two optical tones, separated by the desired mm-wave frequency, can be selected by using optical filtering methods. The 60 GHz optical mm-wave was generated by using two optical filters; an optical bandstop filter (OBSF) with 3 dB bandwidth of 0.28 nm is to suppress three middle frequency components and an optical bandpass

[1] NTT Electronics corporation

filter (OBPF) with bandwidth 0.485 nm is to reject the outer sidebands. The resultant output optical spectrum is illustrated in Fig. 5.2 (b). The suppressed tones are shown around 17 dB less than the main tones. These unwanted tones could be suppressed more by employing a specially designed Bragg filter to select these two optical carriers spaced by 60 GHz. These optical carriers generate a high stability mm-wave signal when detected at the high speed photo-detector.

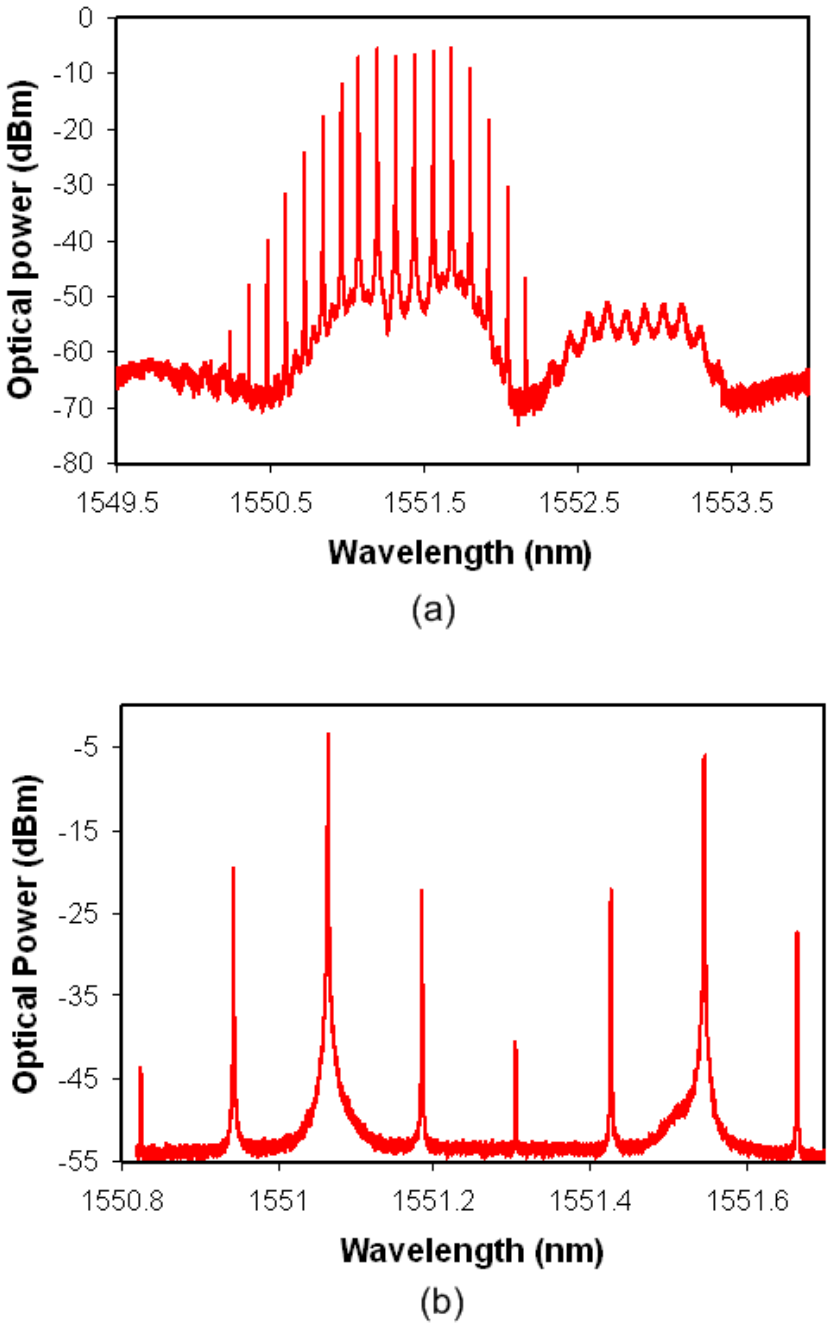

Fig. 5.2. Optical spectra of a GSL: (a) before and (b) after optical filters.

The electrical RF spectrum for the generated 60 GHz was measured by electrical spectrum analyzer (ESA) and is shown in Fig. 5.3. The resolution and video bandwidth for ESA were both adjusted at 1 kHz and the averaging set to 64. The spurs on the sides of the generated tone appear about at 183 kHz with -53 dBc and are caused by the power supply to the laser diode. The phase noise was measured to be -68 dBc/Hz at 10 kHz offset and -80 dBc/Hz at 100 kHz offset. It has been shown that the spectral linewidth of the beat signal does not depend on the laser linewidth and is only affected by the phase noise of the RF drive source [5, 6].

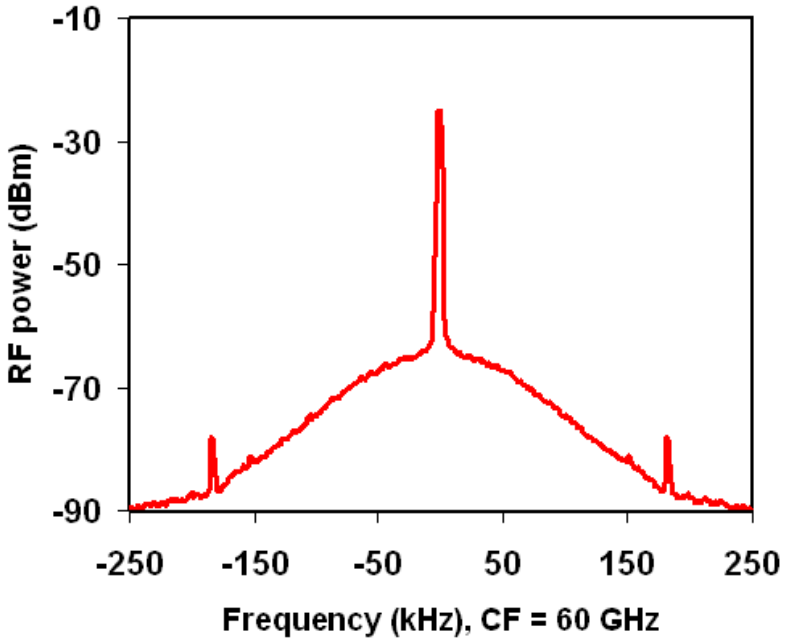

Fig. 5.3. Electric RF spectrum at centre frequency (CF) = 60 GHz.

In the following sections, two different schemes for generation and transmission of optical modulated mm-waves based on the gain switching technique are demonstrated as shown in Fig. 5.4.

- In scheme A, the selected sidebands are on-off keyed (OOK) modulated with a non-return to zero (NRZ) data stream using an external modulator and then transmitted over fiber. At the remote antenna unit (RAU), these components beat together at the photodiode to yield an amplitude modulated mm-wave signal at the frequency corresponding to the difference between the two

filtered lines (60 GHz in our experiment). This signal is then amplified and transmitted to the mobile units (MU).

- In scheme B, gain switching is achieved by driving the laser with a combination of a sinusoid signal and the NRZ data. The GSL generates multiple phase correlated sidebands spaced by the driving RF frequency and modulated with NRZ data. This technique simplifies the transmitter setup as it does not require an external modulator. Hence, there is lower insertion loss and reduced cost.

These two schemes are described in more detail and their performance investigated in the following sections.

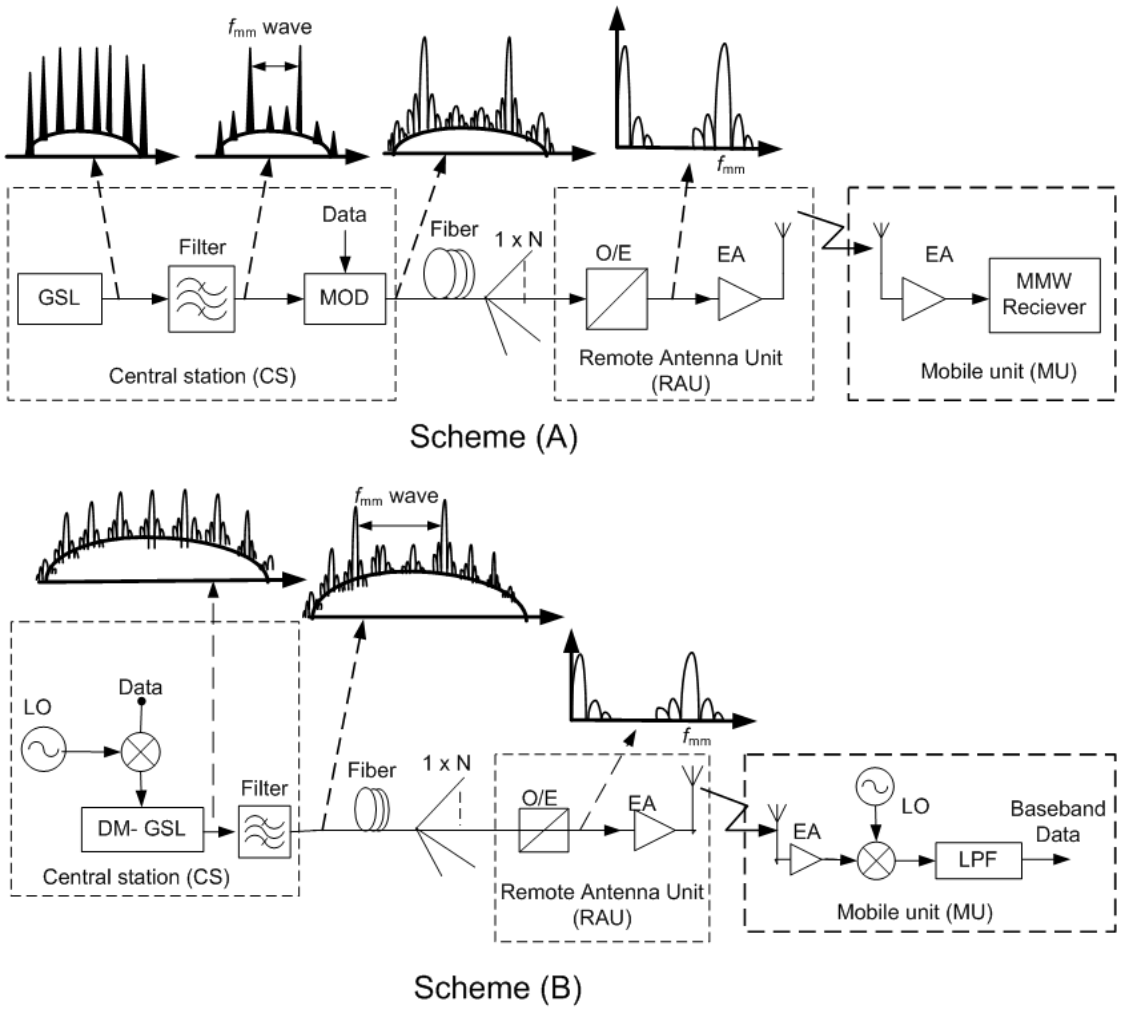

Fig. 5.4. Block diagrams for proposed schemes.

5.3 Externally modulated GSL

5.3.1 Experimental Setup

The proposed experimental setup for scheme A is shown in Fig. 5.5. The front end of the optical transmitter consists of a commercial DFB laser diode (DFB-LD) with an emission wavelength of 1551 nm at room temperature and a threshold current of 15 mA. The DFB-LD was gain switched by biasing it with a DC current of 51 mA and driving with an amplified 15 GHz RF sinusoidal signal at 24 dBm. The optical signal was amplified by an erbium doped fiber amplifier (EDFA) and then filtered by using the same optical filters described in the previous section. After filtering, the optical signal was modulated using a Mach-Zehnder modulator (MZM) with a data stream generated from a pseudo-random bit sequence (PRBS). The polarization controller (PC) is used to change the polarization state of the optical signal before being fed into the MZM.

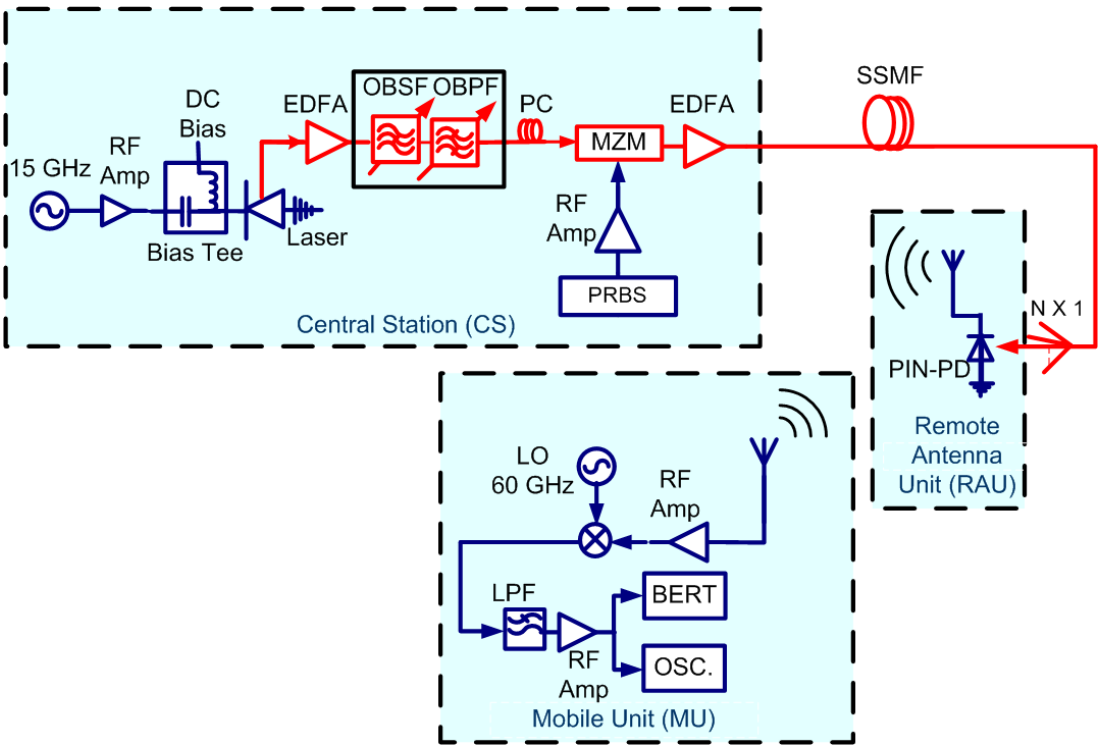

Fig. 5.5. Experimental setup for mm-wave generation and transmission for data downstream link using an external modulator.

The modulated optical signal after amplification is shown in Fig. 5.6 (a) and (b) for 1.25 and 3 Gbps, respectively. It can be seen that the modulation is clearly visible on both of the main tones. This signal was then transmitted through standard single mode fiber (SSMF) to the RAU, where it was photodetected by a high speed photodiode with a 3 dB bandwidth of 70 GHz. The two sidebands beat together in the photo-detector and generate a modulated 60 GHz mm-wave. The generated electrical signal was subsequently amplified and radiated over the air through a horn antenna with 20 dBi gain.

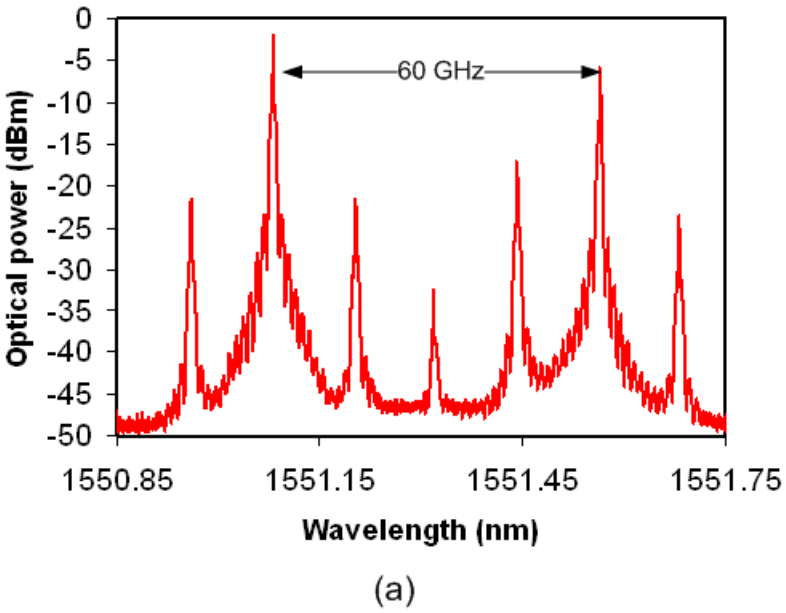

(a)

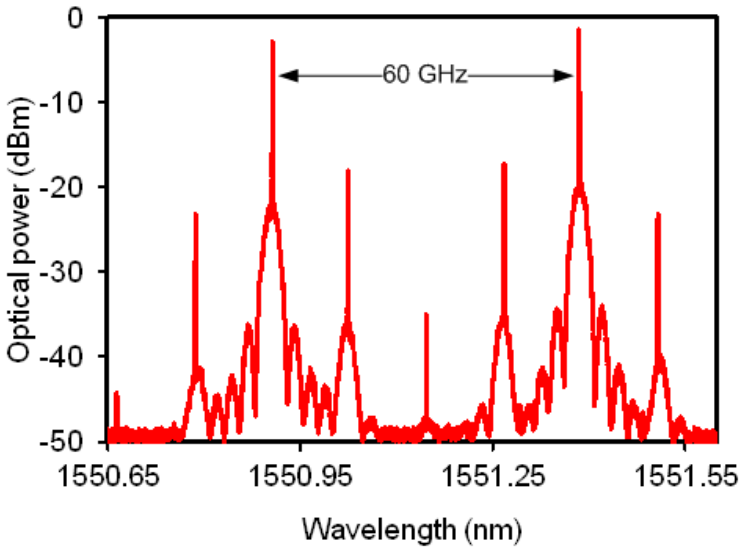

(b)

Fig. 5.6. Optical spectra for a modulated optical 60 GHz with (a) 1.25 Gbps and (b) 3 Gbps.

In the mobile unit (MU), the mm-wave signal was received using another identical 20 dBi horn antenna and amplified. The received signal was demodulated by mixing it with a 60 GHz LO signal. Then, the data was filtered out by using a low pass filter (LPF) and amplified. The received data stream was analyzed by using a bit error rate test set (BERT) and the eye diagrams were recorded by using high speed sampling digital oscilloscope for 1.25 and 3 Gbps data streams as shown in Fig. 5.7 (a) and (b), respectively.

In Fig. 5.7 (a), the measured BER is plotted versus the received optical power (ROP) at the photodetector for back-to-back (BTB), 37 km, and 62 km at 1.25 Gbps data stream without wireless transmission. The eye diagrams of the recovered baseband signals are also shown as insets in the same figure for BTB and 62 km. As can be seen from the figure, for BER of 10^{-9}, the BTB receiver sensitivity is -33 dBm. The power penalty after transmission over 37 km is only 2 dB. However, the system performance degrades after transmission over 40 km and reaches an error floor around 10^{-8} after 62 km transmission. This is due to the impact of chromatic dispersion, where the two optical carriers travel along the fibre with different speeds and are received at the photodetector with a time shift. This is called "bit walk off", and it decreases the duration of the single bit '1' and limits the transmission distance [15, 16], as can be seen in the eye diagram in the inset (ii) in Fig. 5.7 (a). The captured optical pulses for various fibre propagation distances are shown in Fig. 5.8.

To verify that this degradation is caused by dispersion, a dispersion compensating fibre (DCF) was inserted after transmission through 62 km of standard fibre. In this experiment, DCF with a dispersion parameter of -681 ps/nm was used to partially compensate for the dispersion incurred in the 62 km of SSMF. The BER vs. received power for this case is shown in Fig. 5.7 (a), and indicates that the performance is almost as good as that achieved for the BTB case. Unlike normal double side band radio-over-fibre (RoF) systems, this technique does not suffer from dispersive fading problems as there is no carrier signal between the data carrying side-bands.

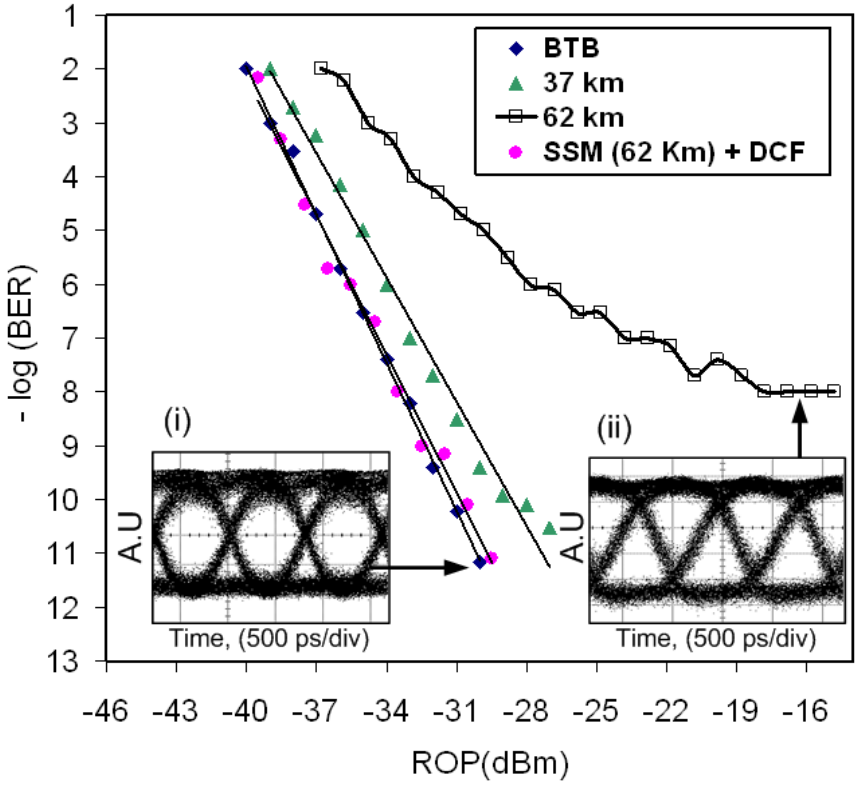

(a)

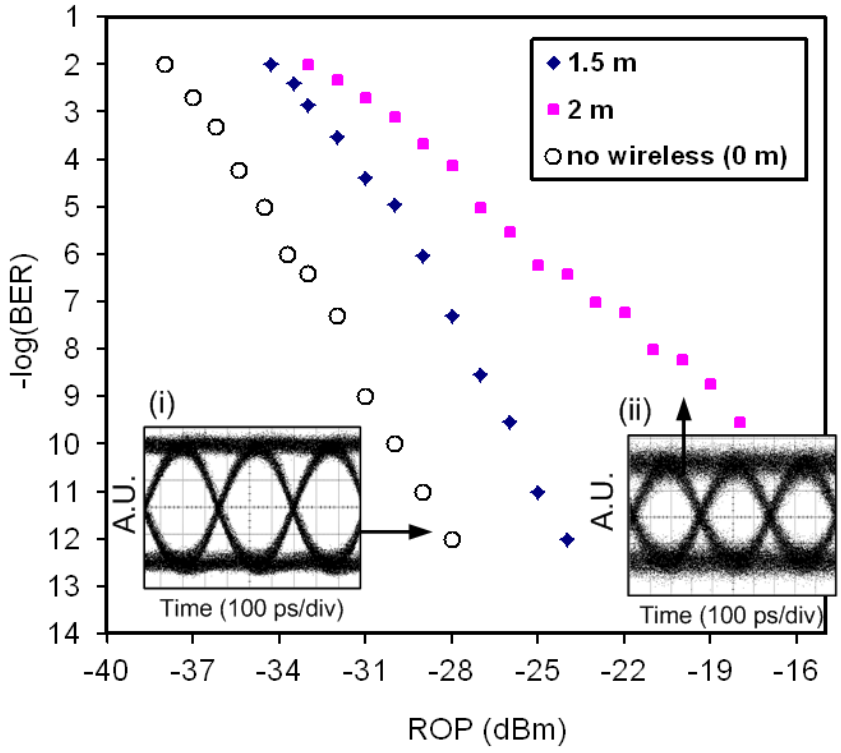

(b)

Fig. 5.7. Measured BER for received baseband signal versus the received optical power.at: (a) 1.25 Gbps and (b) 3 Gbps. Insets: the eye diagrams for lowest BER.

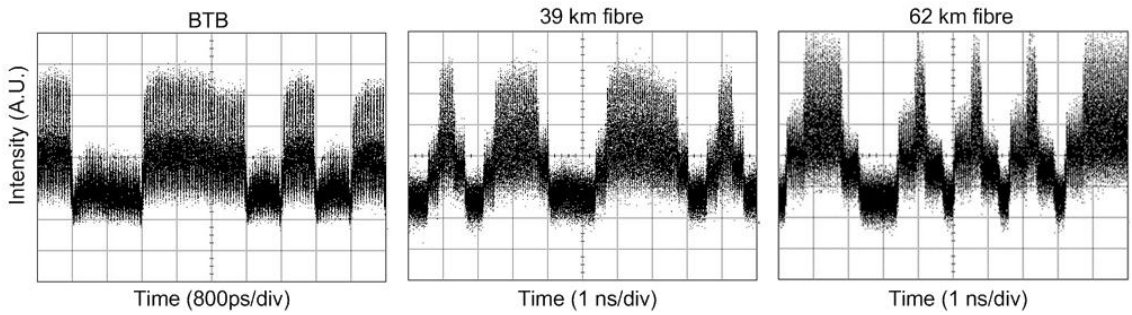

Fig. 5.8. Captured optical pulses at various fibre propagation distances.

In Fig. 5.7 (b), the measured BER is plotted versus the ROP at photodetector after 3 km fiber for no wireless transmission and also for 1.5 m and 2 m wireless transmission distances for a 3 Gbps data stream. The wireless transmission was carried out in the photonic lab using two 20dBi horn antennas within height 100 cm above the ground level and in the line of sight (LoS) position. As can be seen from the figure, for BER of 10^{-9}, the receiver sensitivity for 3 km fiber transmission and direct cable connection from photodetector to the MU, is -31 dBm and the inset (i) shows a clear and open eye diagram. After transmission over 3 km of fibre and 1.5 m wireless propagation, the BER curve shows about 4 dB power penalty due to the reduction of signal to noise ratio at the MU. The measurements were also done for 2 m wireless transmission and the eye diagram for a ROP of -18.5 dBm is shown as inset (ii) in Fig. 5.7 (b). It can be clearly seen from the BER curve that there are two different BER slopes. This appears to be due to an increased level of multipath interference for this wireless transmission distance. It was believed that theses measurements can be improved if the link is located at a better position.

5.3.2 Simulation Results

The system was also simulated using the VPI TransmissionMaker simulation platform as shown in Fig. 5.9. The simulation parameters were chosen to emulate the real experimental parameters. The fiber link was a 3 km SSMF with a group velocity dispersion (GVD) of 16 ps/nm.km and loss of 0.2 dB/km. The optical spectrum was filtered to give the same sideband suppression values as the experimental case. A noise module was added after an optical amplifier to add amplified spontaneous emission (ASE) noise, and a self mixing demodulator was used at the MU. The BER was simulated for 3 km fiber and different bitrates as shown in Fig. 5.10. The BER

curve at 3 Gbps coincides with our experimental measurements with no wireless transmission. The system performance degrades with higher bit rates and shows an error floor at (BER~10^{-7}) for 10 Gbps data rate due to the interference from the suppressed optical sidebands.

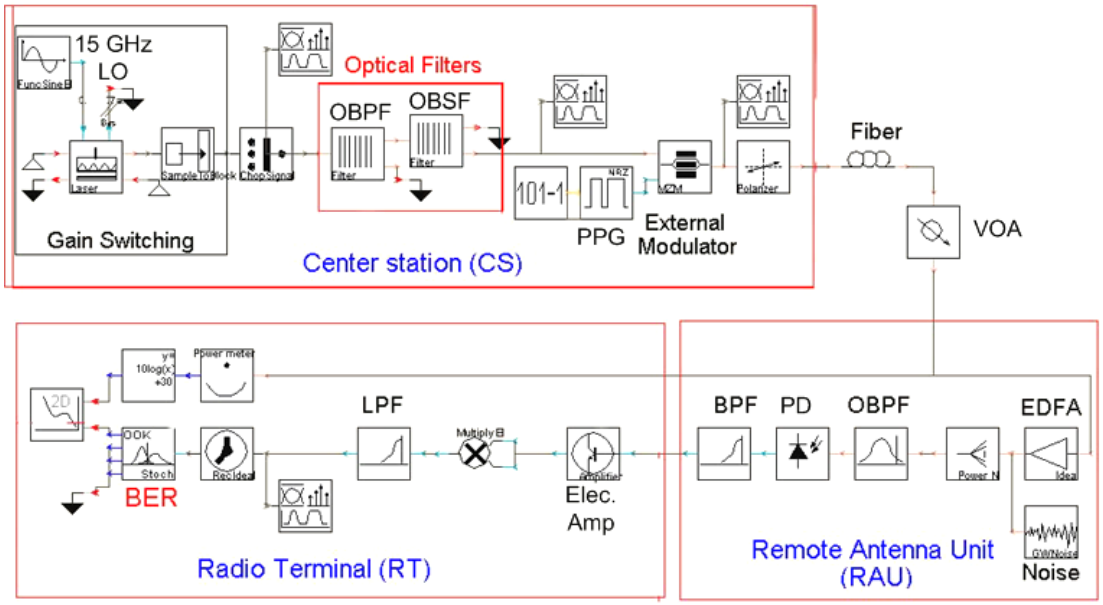

Fig. 5.9. Simulation model for externally modulated GSL.

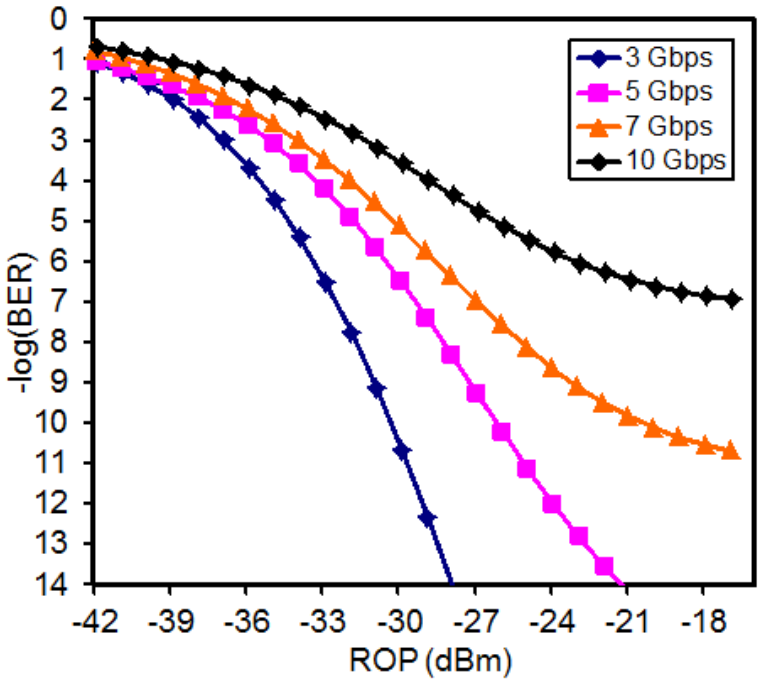

Fig. 5.10. Simulated BER versus received optical power for 3 km fibre transmission and higher bit rates.

5.4 Directly Modulated GSL

5.4.1 Experimental Setup and Results

The proposed experimental setup for optical modulated mm-wave generation and transmission over the fibre using a directly modulated gain switched laser (DM-GSL) is shown in Fig. 5.11. In this case, one DFB-LD with an emission wavelength of 1551 nm at room temperature and a threshold current of 15 mA was biased at 43 mA. The RF drive signal applied to the laser consisted of a 15 GHz sinusoidal signal and a PRBS 3 Gbps data signal combined together with the aid of a passive resistive combiner. The data generator and sine wave generator were locked together using the 10 MHz reference signal from the sine wave generator. The resultant RF signal comprised of a 19 dBm sinusoidal signal and a 10 dBm data signal as depicted in Fig. 5.12 (a), and it can be seen that there are five cycles of the 15 GHz sine wave per temporal bit slot.

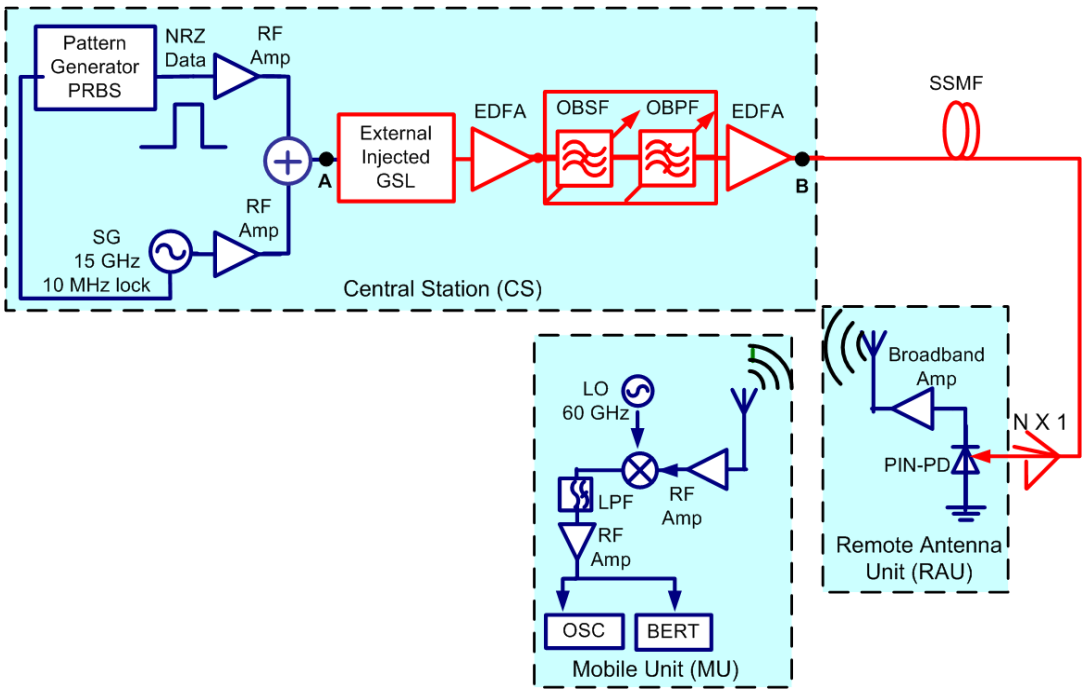

Fig. 5.11. Experimental setup for mm-wave generation using DM-GSL.

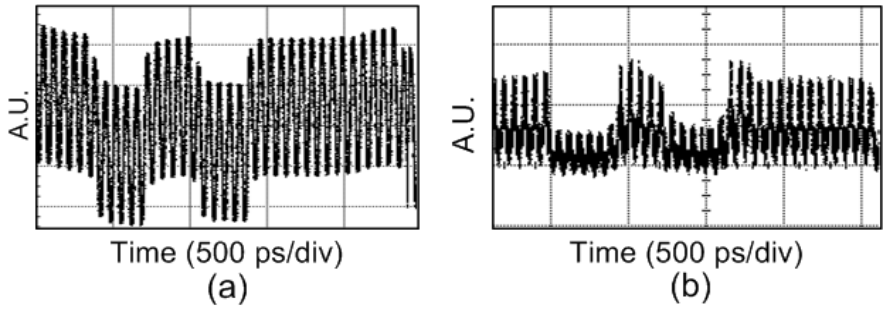

Fig. 5.12. (a) the resultant RF signal at point A, and (b) the filtered optical signal at point B.

The DFB-LD was externally injected with another DFB-LD to decrease chirping and reduce the timing jitter of the gain switched pulses [7]. This was realised using a master-slave configuration with low level injection, with an injected power of ~ -10 dBm (measured at the output of the master laser) and at the same wavelength as that of the slave. In this experiment, the external injection reduced the jitter from ~3 ps to less than 1 ps.

The generated spectrum was captured by a high resolution OSA after an optical amplifier and displayed in Fig. 5.13. The gain switching spectrum with the composite signal (sinewave and data) but without optical injection has a degraded comb as shown in Fig. 5.13 (a). With the external injection, however, the comb has more discernible tones as shown in Fig. 5.13 (b). Each optical tone is modulated by 3 Gbps OOK data and spaced by 15 GHz. This optical spectrum was filtered by using the same optical filtering schemes used in scheme A. The resultant output spectrum is illustrated in Fig. 5.13 (c) and it shows the two main optical tones spaced by 60 GHz which are clearly modulated with the data signal. The suppressed sidebands are 18 dB lower than the main sidebands, with this level of suppression being limited by the optical filters available. The filtered optical temporal signal was captured and shown in Fig. 5.12 (b).

It was noticed that when the extinction ratio of the optical pulses was increased the timing jitter and noise on the optical pulses also increased, resulting in a broadened spectrum with no discernible tones thereby degrading the overall system performance. Hence, to improve this performance, the dc bias can be increased or modulation level reduced to not switch the pulses off completely thereby decreasing the extinction ratio between 1 and 0 bits.

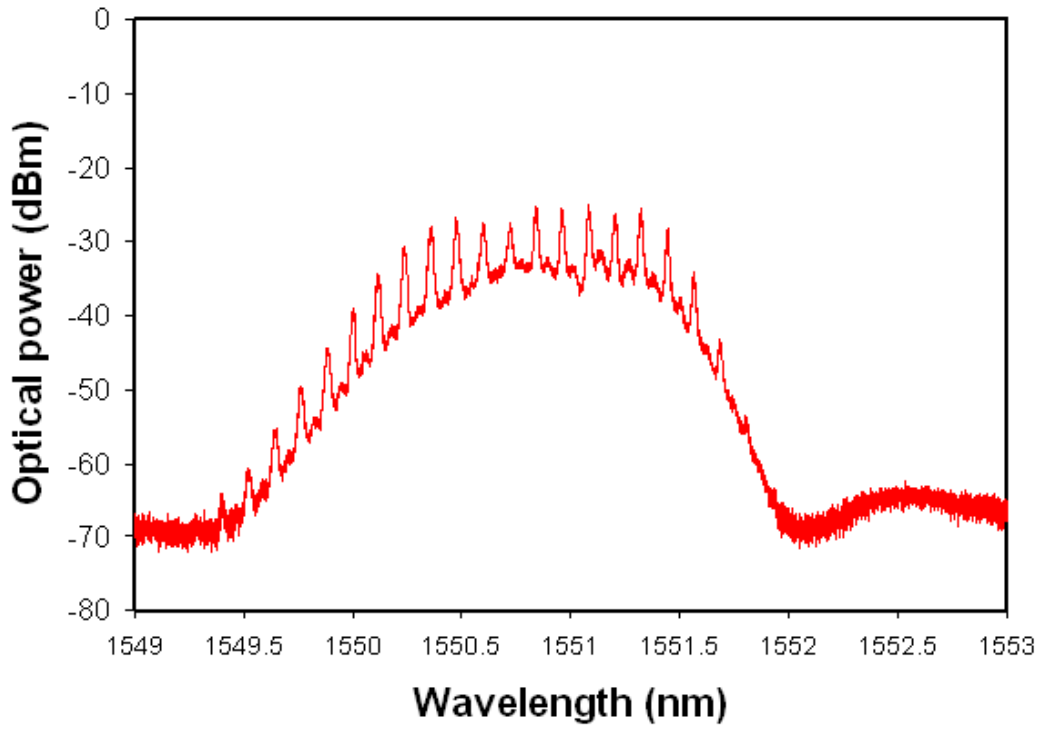
0
-10
-20
-30
-40
-50
-60
-70
-80
Optical power (dBm)
1549
1549.5
1550
1550.5
1551
1551.5
1552
1552.5
1553
Wavelength (nm)

(a)

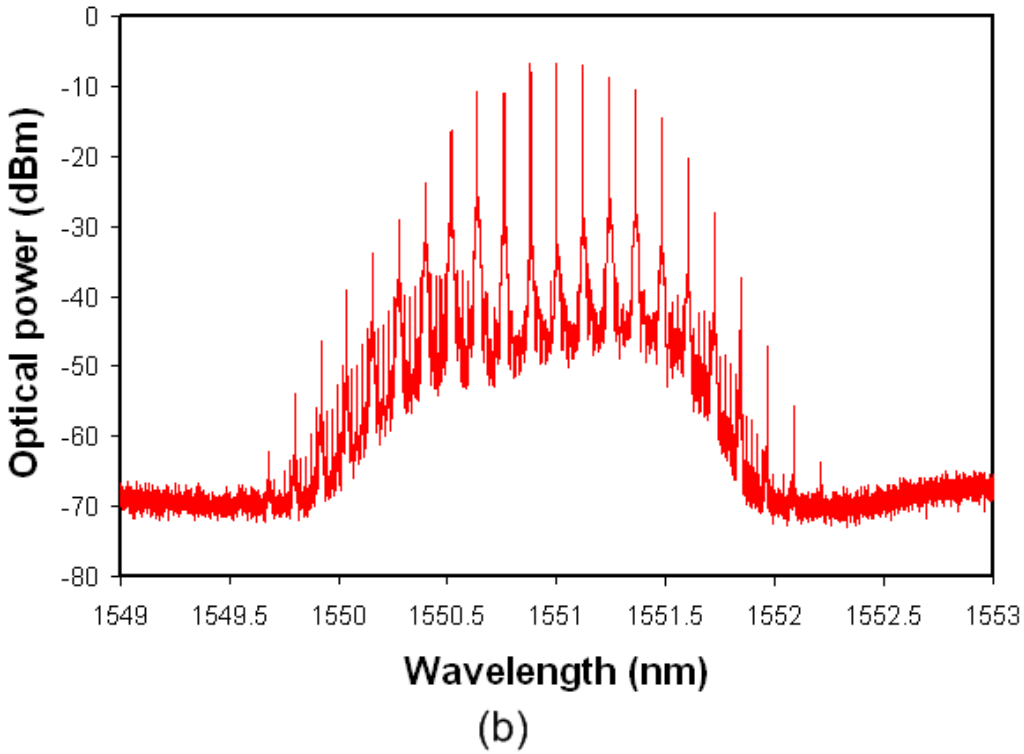
0
-10
-20
-30
-40
-50
-60
-70
-80
Optical power (dBm)
1549
1549.5
1550
1550.5
1551
1551.5
1552
1552.5
1553
Wavelength (nm)

(b)

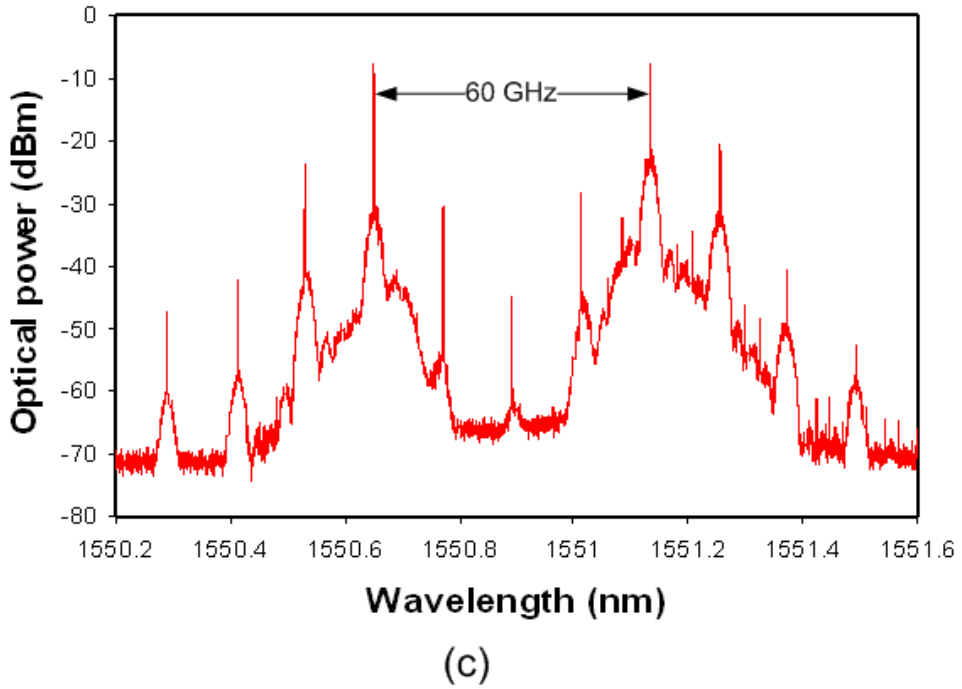

Fig. 5.13. Optical spectra for DM-GSL: (a) without external injection, (b) without external injection, and (c) after optical filters.

When these levels are optimized, subsequent pulses portray improved pulse to pulse phase coherence (reduced timing jitter) and an enhanced spectrum with clearly distinguishable tones [8]. After filtering, the optical signal was amplified again by using an EDFA and then transmitted over 3 km of single mode fiber to the RAUs. At the RAU, the optical signal was photodetected by a high speed photodiode with a 3 dB bandwidth of 50 GHz. The generated electrical mm-wave signal was boosted by a broadband amplifier to compensate for the limited bandwidth of this detector (since the 70 GHz photo-detector was not available at that time). Afterwards, the mm-wave signals were transmitted to a MU via 20 dBi horn antenna. At the MU, the mm-wave signal was received by the same receiver configuration as used in Fig. 5.4. The demodulated signal was then evaluated by a BERT and the eye diagrams were monitored by a high speed scope.

The measured BER is plotted versus ROP for 1.25 and 3 Gbps data stream in Fig. 5.14 (a) and (b), respectively. In Fig. 5.14 (a), the BER was measured for BTB, and 3 km fiber transmission with and without wireless transmission. The eye diagrams of the recovered baseband signals are also shown as insets in Fig. 5.14 (a).

The inset (i) exhibits the eye diagram for BTB without wireless transmission at received power of -30.9 dBm. As can be seen from the figure, the BTB receiver sensitivity for BER of 10^{-9} is -31.9 dBm and there is 0.7 dB power penalty after 3 km fiber transmission without wireless transmission. For BTB optical connection and 2 m wireless transmission, the receiver sensitivity was degraded by 4.4 dB to -26.5 dBm due to the signal to noise ratio degradation in the radio system. For a combined 3 km fiber and 2 m wireless scenario, the receiver sensitivity is further degraded to about -25.2 dBm, and the eye-diagram in this case is shown as inset (ii) in Fig. 5.14 (a) for a received power -24.4 dBm.

The graph in Fig. 5.14 (b) shows the measured BER at 3 Gbps after 3 km transmission through fiber for no wireless transmission and for 2 m wireless transmission. As can be seen from the figure, the receiver sensitivity for BER of 10^{-9} is -30.3.dBm when there is a direct cable connection between RAU and MU, and its eye diagram is shown as inset (i) in Fig. 5.14 (b). For 2 m wireless transmission, the receiver sensitivity was degraded by 9.8 dB to -20.5 dBm due to degraded performance in the radio system which is caused by (i) a reduction in the signal to noise ratio at the MU, and (ii) multipath interference in the wireless transmission. The received eye diagram after 2 m wireless distance is shown as inset (ii) in Fig. 5.14 (b) at ROP of -18.5 dBm.

This system is also suitable for achieving higher data rate transmission on a 60 GHz RF carrier. In Fig. 5.15, the eye diagrams for BTB operation were also captured for downstream data rates of 5, 7.5, and 10 Gbps. The eye diagrams for 5 and 7.5 Gbps were taken when the modulating signal included a 15 GHz sinusoidal signal so that there are three or two cycles of 15 GHz per bit. To achieve 10 Gbps, the DFB-LD was directly modulated with 20 GHz sinusoidal signal and 10 Gbps downstream data. Even though the eye diagram shown in Fig. 5.15 (c) has more noise than those at 5 and 7.5 Gbps, a BER of around 10^{-5} was still achieved. The degradation in the signal to noise ratio is due to the reduced performance of the DFB-LD being driven at the edge of its modulation bandwidth (20 GHz), yielding less optical power.

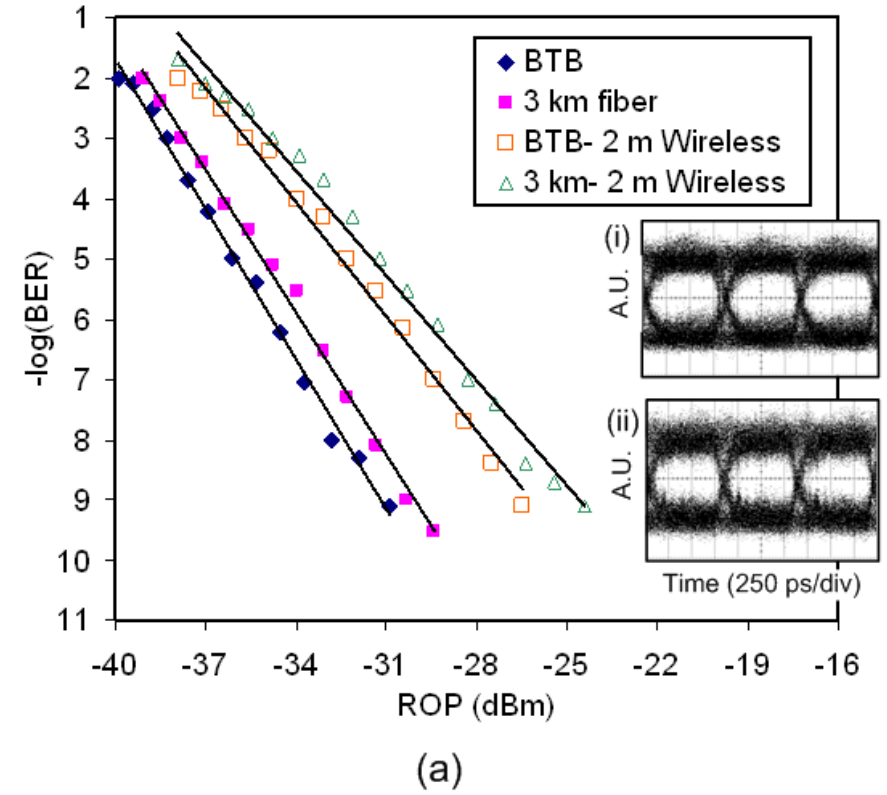

(a)

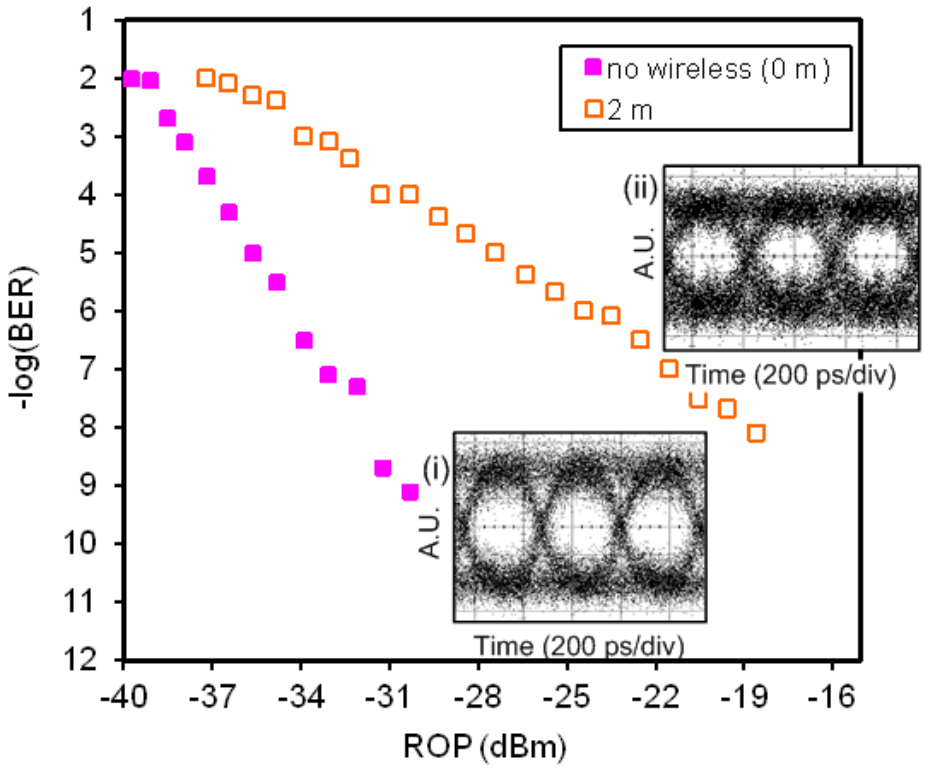

(b)

Fig. 5.14. Measured BER versus ROP for: (a) 1.25 and (b) 3 Gbps baseband signals.

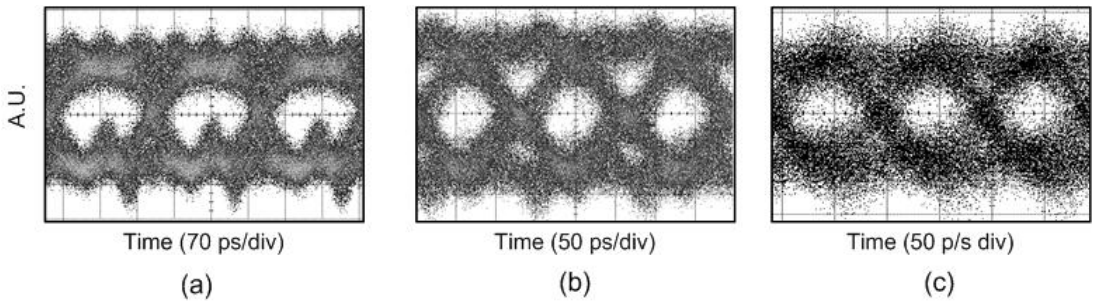

Fig. 5.15. Eye diagrams for base band signal at different bit rates: (a) 5, (b) 7.5, and (c) 10 Gbps.

5.4.2 Simulation Results

The simulation model shown in Fig. 5.16 was also developed for direct modulation of GSL at higher bit rates. The simulation parameters were chosen as in the previous simulation model and the simulated BER versus ROP is shown in Fig. 5.17 (a). The degradation of BER at higher bit rates is evident and shows an error floor at 7.5 and 10 Gbps. These error floors are a little higher than the simulated externally modulated case due to the bandwidth limitations of the laser at higher bit rates. This system shows the possibility to achieve high data rate transmission with a reduced optical component cost and this could be suitable for short range transmission of high data rate mm-wave signals.

The system performance was also investigated with the influence of the optical sideband suppression ratio (OSSR). The OSSR is defined as the optical power of one of the desired comb signals divided by the optical power of the middle suppressed optical sideband. The optical carrier suppression was achieved by controlling the rejection parameter in the optical fibre Bragg grating filter module. The simulated BER was plotted for various optical sideband suppression ratios and is shown in Fig. 5.17 (b). It can clearly be seen that, as the optical suppression for the sidebands increases, the system performance is improved and the lowest BER curve is obtained.

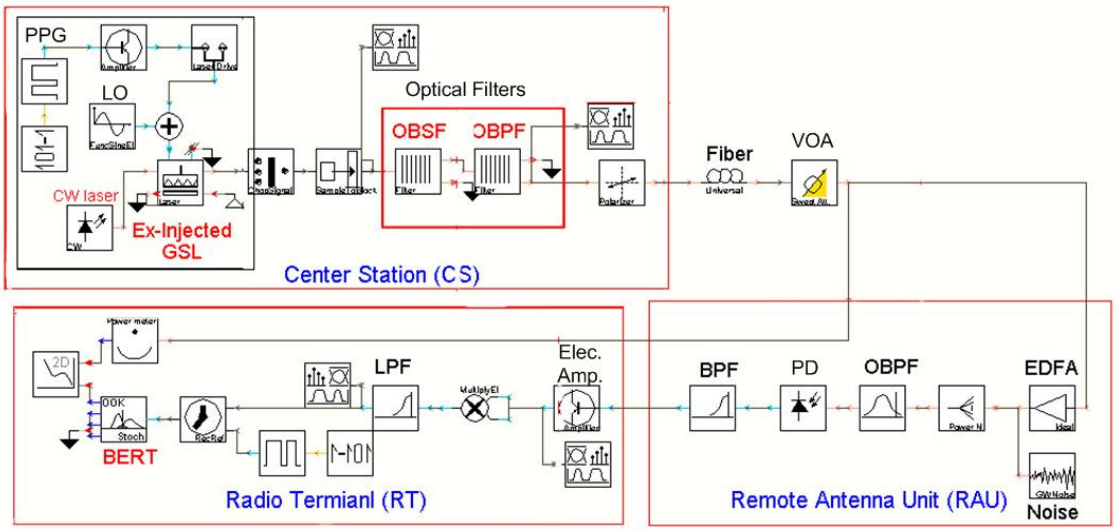

Fig. 5.16. Simulation model for DM-GSL.

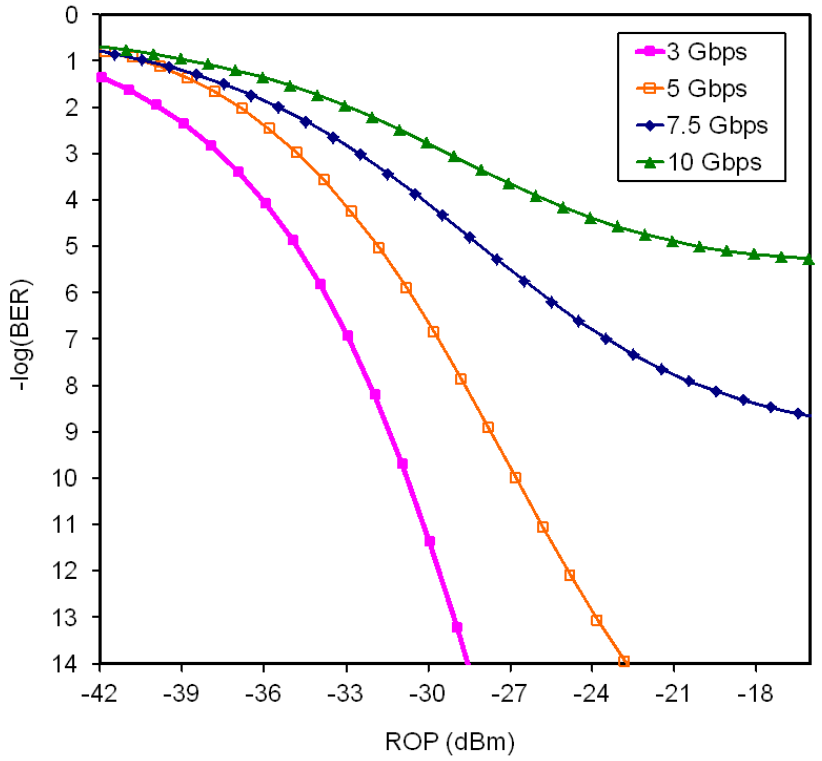

(a)

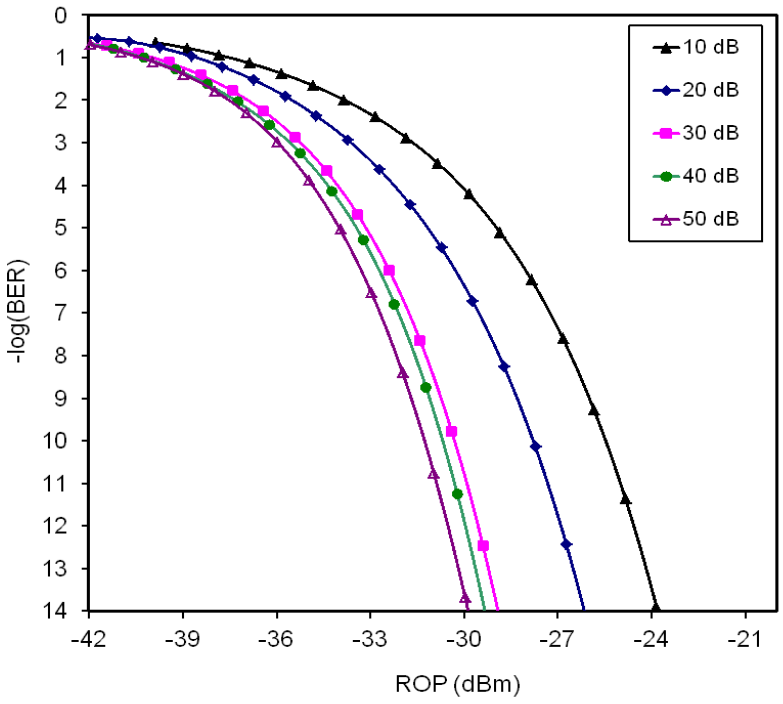

(b)

Fig. 5.17. Simulated BER for direct modulated GSL for (a) higher bit rates and (b) different sideband suppression ratios.

5.5 Comparison of Direct and External Modulation

Gain switching of a DFB laser is known to generate pulses with some level of amplitude and un-correlated temporal jitter, both of which result in noise in the demodulated data signal. It is important to note that both the amplitude and temporal jitter are worse when the DFB laser is directly modulated with a composite of sine wave and data signal than when an external modulator is used. In the externally modulated case, the laser is biased above the threshold and driven with a high power RF signal of 24 dBm, which generates pulses with a duration around 15 ps and a jitter less than 1 ps [9] (which is within the measurement accuracy of our oscilloscope). However, the timing jitter in the directly modulated case can be attributed to the random and longer switching (on and off) of the laser due to the PRBS data. This results in a larger pulse-to-pulse variation in turn on time delay and pulse amplitude. Hence, the intensity noise and temporal jitter on these pulses can be reduced by using external seeding of the gain switched laser to achieve optimal system performance [10, 11].

The conventional technique of using an external modulator, to impose the modulation, yields better performance; however, it results in an increased insertion loss, polarization dependency, bias drifting and cost of the optical system. The directly modulated GSL technique is a simple, robust and low cost solution for generating modulated mm-waves, with the main limitation of requiring external injection to decrease the jitter. However, the advantages of using direct modulation can outweigh the above-mentioned shortcoming, by using two integrated lasers, one for gain switching and the other for injection, thereby maintaining the cost efficiency of this solution.

5.6 Summary and Conclusion

In this chapter, two transmitter configurations were proposed and demonstrated for the optical generation and transmission of optical modulated mm-waves based on GSL. The proposed methods show the simplicity and low cost that can be obtained in comparison with other reported techniques for the generation of modulated optical mm-waves. The GSL generates a frequency comb with a spectrum which has a relatively flat power profile over eight phase correlated sideband tones. The tone spacing is the same as the driving frequency which allows for the possibility to generate mm-wave signals up to eight times the LO drive frequency.

In the first transmitter configuration, the output from the GSL was filtered by using appropriated filters to select two optical sidebands spaced by 60 GHz which are then OOK modulated with downstream data. While in the second setup, the DFB-LD generates multiple optical modulated tones by directly driving the laser with a combination of 15 GHz sinusoidal signal and NRZ data. Optical filtering is then employed to select the relevant optical tones spaced by the required mm-wave frequency. Higher bit rate transmissions at 5, 7.5, and 10 Gbps were also achieved using this technique. These techniques generate high stability modulated millimeter wave signals which are suitable for implementation in future RoF systems operating at 60 GHz and beyond. The novel direct modulation technique was compared to an external modulation technique and showed the possibility of a significant cost reduction which will be critical to the widespread deployment of such systems.

References

[1] R. J. Helkey, D. J. Derickson, A. Mar, J. G. Wasserbauer, and J. E. Bowers, "Millimeter-wave signal generation using semiconductor diode lasers (invited paper)," *Microwave Optical Technology Letters*, vol. 6, no. 1, pp. 1-5, 1993.

[2] D. Novak and R. S. Tucker, "Millimetre-wave signal generation using pulsed semiconductor lasers," *Electronic Letters*, vol. 30, no. 17, pp. 1430-1431, 1994.

[3] M. J. L. Cahill, G. J. Pendock, and D. D. Sampson, "Low error rate return-to-zero direct modulation of gain-switched lasers," *Optical and Quantum Electronics*, vol. 28, no. 9, 1996.

[4] G. K. Myong, D. Seo, J. Park, and M. Chu, "Pattern independent direct pulse modulation of a gain-switched distributed-feedback laser at 2.5 Gbit/s," *in The Pacific Rim Conference on Lasers and Electro-Optics, 1999*, pp. 489-490 vol.2,

[5] C. R. Lima and P. A. Davies, "Effects of extra low-frequency noise injection on microwave signals generated by a gain-switched semiconductor laser," *Applied Physics Letters*, vol. 65, no. 8, pp. 950, 1994.

[6] C. R. Lima and P. A. Davies, "Noise performance of microwave signals generated by a gain-switched semiconductor laser," *Microwave Opto-Electronics, IEE Colloquium on*, pp. 2/1, 1994.

[7] L. P. Barry, P. Anandarajah, and A. Kaszubowska, "Optical pulse generation at frequencies up to 20 GHz using external-injection seeding of a gain-switched commercial fabry-perot laser," *Photonic Technology Letter, IEEE*, vol. 13, no. 9, pp. 1014-1016, 2001.

[8] K. Y. Lau, "Short-pulse and high-frequency signal generation in semiconductor lasers," *Lightwave Technology, Journal of*, vol. 7, no. 2, pp. 400-419, 1989.

[9] A. G. Weber, W. Ronghan, E. H. Bottcher, M. Schell, and D. Bimberg, "Measurement and simulation of the turn-on delay time jitter in gain-switched semiconductor lasers ," *Quantum Electronics, IEEE Journal of*, vol. 28, no. 2, pp. 441-446, 1992.

[10] D. Seo, H. Liu, D. Y. Kim, and D. D. Sampson, "Injection power and wavelength dependence of an external-seeded gain-switched Fabry–Perot laser," *Applied Physics Letters*, vol. 67, no. 11, pp. 1503, 1995.

[11] D. Seo, D. Y. Kim, and H. Liu, "Timing jitter reduction of gain-switched DFB laser by external injection-seeding," *Electronic Letters*, vol. 32, no. 1, pp. 44, 1996.

Chapter 6 – Phase Modulated Millimetre Waves Based on External Injection GSL

6.1 Introduction

This chapter proposes and demonstrates all-optical up-conversion from an on-off keyed (OOK) optical data signal to a mm-wave optical signal using an externally injected gain switched laser (GSL) [1, 2]. The proposed block diagram for implementation of this technology is shown in Fig. 6.1, where the external network that is connecting the home to the service provider is an optical network using a standard such as Gigabit Ethernet (GbE). The gain-switched laser (GSL) produces phase correlated optical tones spaced by the driving frequency chapter 5 (see section 5.2). The optical OOK data signal is used for the external injection into the GSL, and this optical injection changes the timing when the pulses are generated depending on whether a logical "1" or "0" is injected into the GSL. Two optical tones spaced by 60 GHz are filtered to create the mm-wave optical signal that is distributed through fiber to remote antenna units (RAUs) around the home, with the mm-signal phase modulated as a result of the optical injection into the GSL. The two tones then beat together at a high speed photodetector to yield a phase modulated mm-wave signal. This signal is then amplified and transmitted to the mobile units (MUs) using directional horn antennas.

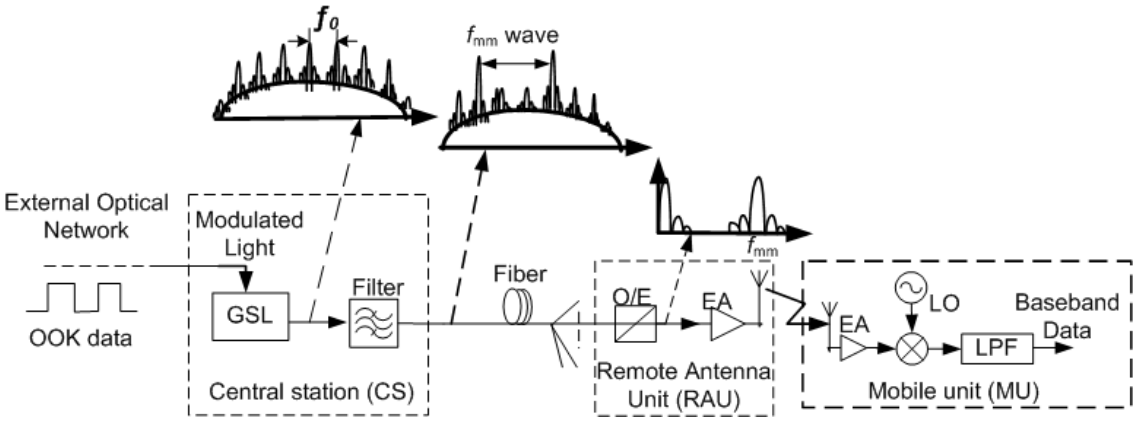

Fig. 6.1. block diagram of the proposed phase modulated mm-wave signal.

The structure of this chapter is arranged as follows. Section 6.2 describes the experimental setup and results for the phase modulated mm-wave generation using the external injection of GSL. Section 6.3 simulates the effect of the injection in the GSL by solving the single mode rate equation for injection locked laser. Finally, section 6.4 presents a summary and conclusion of the chapter.

6.2 Experimental Setup

This section demonstrates the optical generation of modulated mm-wave signals at 60 GHz based on injecting an OOK modulated optical source into a GSL. The proposed system for optical generation of modulated mm-wave is illustrated in Fig. 6.2. The central station (CS) consists of a commercial distributed feedback laser diode (DFB-LD) at 1550 nm. The DFB-LD was gain switched by driving it with an amplified electrical sinusoidal signal at 15 GHz coupled with a 39 mA bias current. The modulation switches the laser above and below threshold and generates a stream of short optical pulses with a pulsewidth of 15 ps.

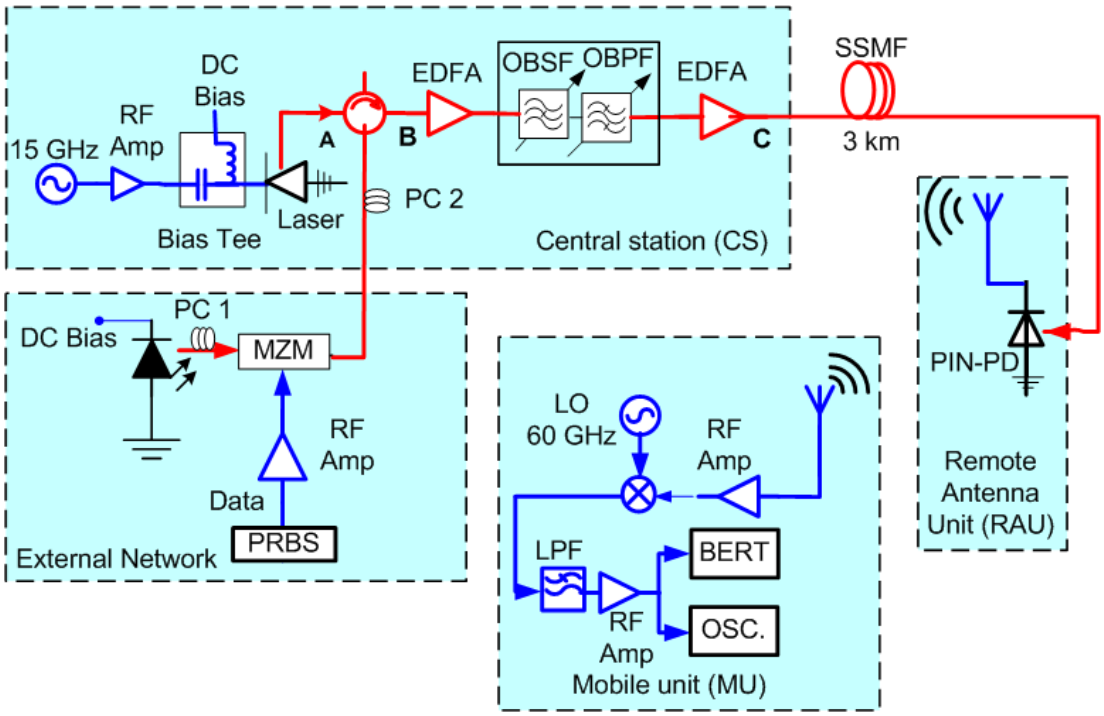

Fig. 6.2. Experimental setup for optical generation of phase modulated mm-wave by injecting an OOK modulated optical source.

The output optical spectrum, shown in Fig. 6.3 (a), consists of a comb of eight optical tones with an amplitude variation of less than 3 dB. The comb exhibits a free spectral range of 15 GHz and a 40 dB modulation depth which indicates excellent phase correlation. For the external network, a bench-top tunable external cavity laser (ECL) source was used to generate a continuous wave (CW) signal at a wavelength of 1550.69 nm which was then OOK modulated by using a Mach Zehnder modulator (MZM) with a non-return to zero (NRZ) data stream. The data was generated from a pattern generator with 2^{31}-1 pseudo random bit sequence (PRBS). A polarization controller (PC1) was used to optimize the state of polarization before the MZM. Then, the modulated optical signal was injected into the DFB-LD cavity through an optical circulator. Another polarization controller PC2 was used to optimize the polarization of the injected light into the slave laser [3]. The average optical injected power was measured to be -7 dBm at the input of the circulator which implies a power of approximately -4dBm for a logical '1'.

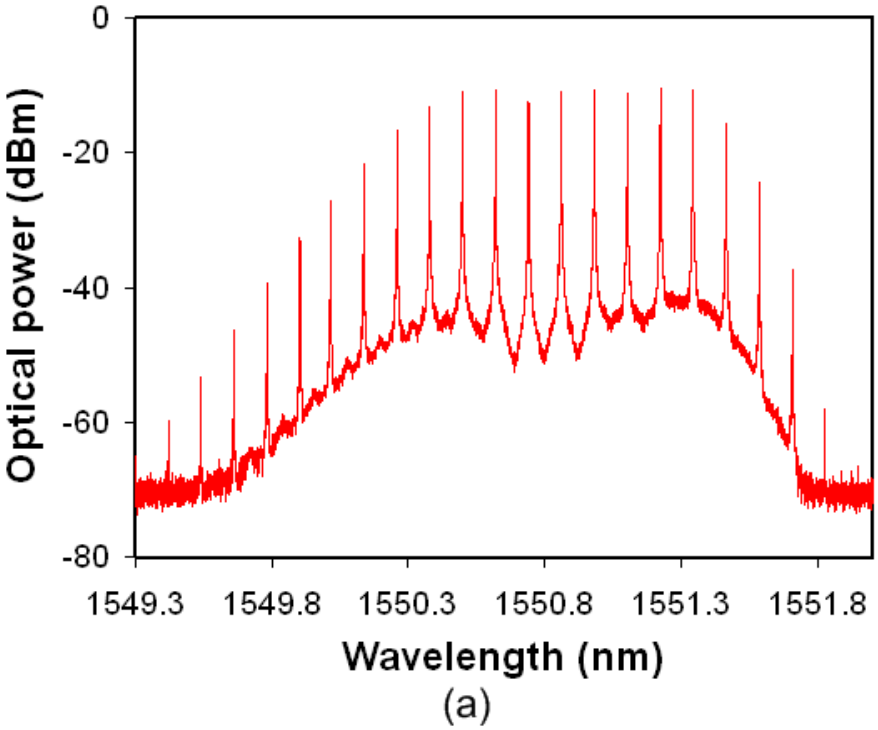

(a)

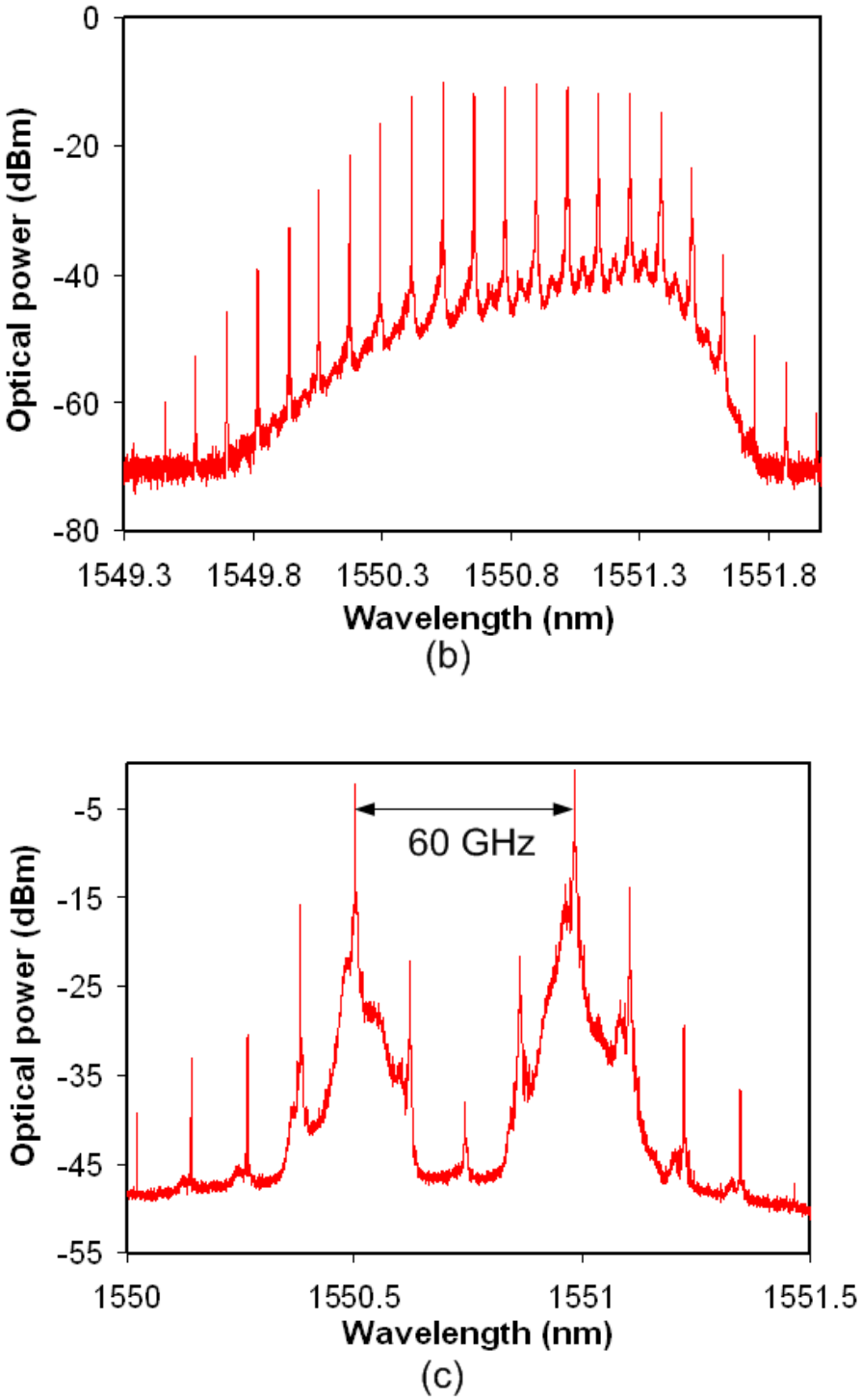

Fig. 6.3. Optical spectra for: (a) GSL at point A, (b) external injected GSL at point B, and (c) after optical filters at point C.

The output optical spectrum shown in Fig. 6.3 (b) represents the modulated optical tones with injected data stream. To generate 60 GHz, two optical tones spaced by 60 GHz were selected by using the same optical filters as used in previous setups

(see section 5.2). The output optical signal was amplified and captured by an optical spectrum analyzer (OSA), and is shown in Fig. 6.3 (c). Subsequently, the optical signal was propagated over SSMF to be distributed to a number of RAUs. At the RAU, the filtered optical tones beat together at a high speed photodetector and generate an electrical modulated mm-wave at 60 GHz. In this case, the MU was directly connected to the output of RAU to analyze only the system performance in terms of its optical propagation. The signal was received at the same MU described in section 5.3.1 and the system performance was measured by a bit error rate tester (BERT) and the eye diagrams were recorded by using a high speed digital sampling oscilloscope.

The free running (without optical injection) GSL generates a stream of optical pulses at a repetition rate of 15 GHz, corresponding to a period of 66.7 ps. However, once the GSL is seeded with the modulated light source, the timing that each pulse is generated at changes according to the injected optical power. These optical pulses are shown in Fig. 6.4 (a) and represent the optical pulses after optical injection from the optical modulated light at point (B) in Fig. 6.2. The time variation was recorded to be ~3.8 ps and occurs at each transition of the seeding intensity level. A transition from the high seeding (logical 1) intensity to the low seeding (logical 0) intensity results in the next pulse being delayed by ~3.8 ps while a low to high transition in the seeding intensity yields an advancement of ~3.8 ps in the position of the pulse. As shown in Fig. 6.4 (b), the period of the pulses is 66.7 ps, but the high to low transition causes a 3.8 ps delay to the first pulse that occurs after the logical ‘1’ to ‘0’ transition, then the subsequent pulses return to their steady state with a 66.7 ps period. This delay and advancement can be attributed to changes in the turn on time delay (t_d) which stems from the fluctuation in the photon density during the buildup of the optical pulse caused by the random character of spontaneous emission [4]. However, external injection seeding significantly reduces this delay by increasing the number of photons in the cavity and swamping the effect of spontaneous emission on the lasing mode [5]. At the RAU, the mm-wave signal from the photodetector and the time shift is translated into a phase shift in the 60 GHz signal – that is, the signal is phase shift keyed (PSK) modulated. At the MU, the received signal is mixed with a 60 GHz local oscillator to demodulate it.

In Fig. 6.5 (a), the BER is plotted versus the received optical power (ROP) for a 1.25 Gbps data stream. The eye diagrams are clear and open for back-to-back (BTB) and 3 km fiber as shown as insets (i) and (ii) in Fig. 6.5 (a), respectively.

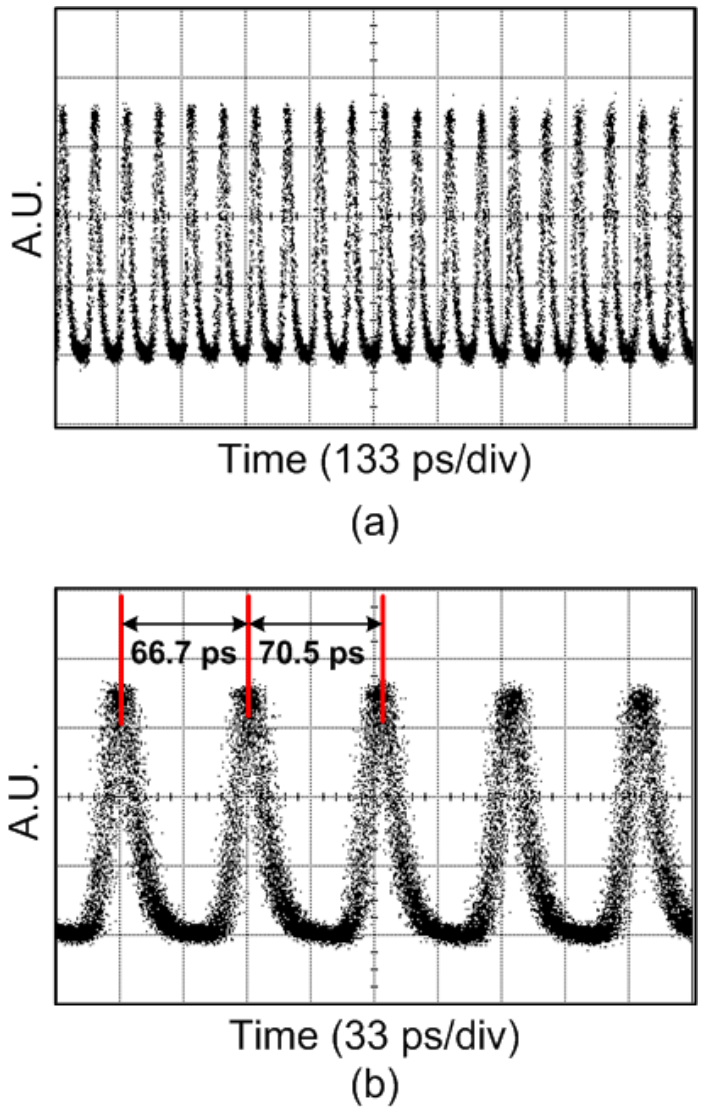

Fig. 6.4. Optical pulses at two different time scales: (a) 133 ps/div and (b) 33 ps/div.

The receiver sensitivity for BTB is -24 dBm for BER< 10^{-9}, and the power penalty for transmitting over 3 km fiber is only 2 dB. The BER is also plotted for 2.5 Gbps data stream as shown in Fig. 6.5 (b). The receiver sensitivity for 2.5 Gbps is -33 dBm for BTB at BER<10^{-4}, which is sufficient for wireless systems and there is no power penalty after transmitting over 3 km fiber. The corresponding eye diagrams are shown in same figure as inset (i) and (ii), respectively. Since, the system

performance is sensitive to phase changes, the noise in the received eye diagrams is due to the inherited timing jitter induced from the fluctuations in the photon density during the build up of the optical pulse.

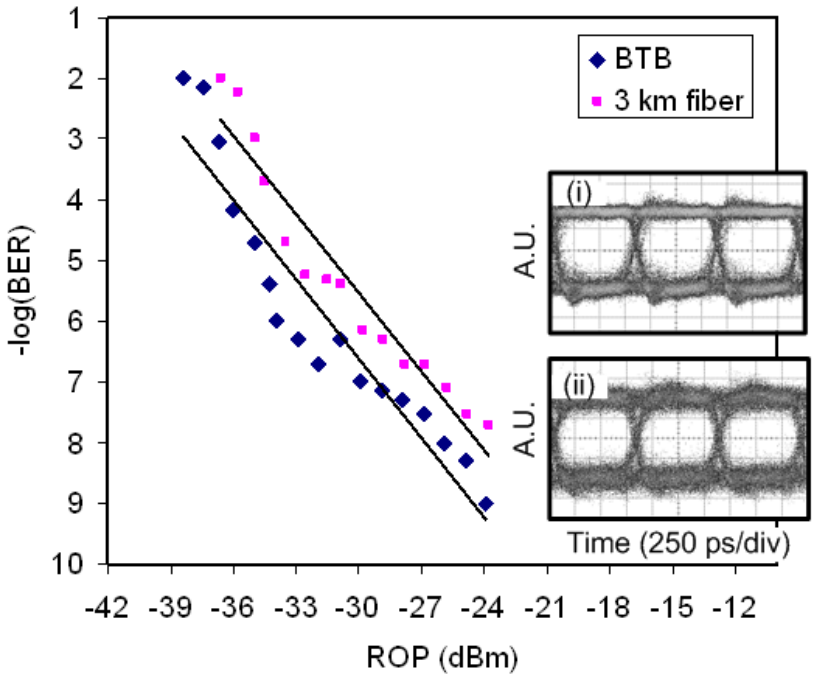

(a)

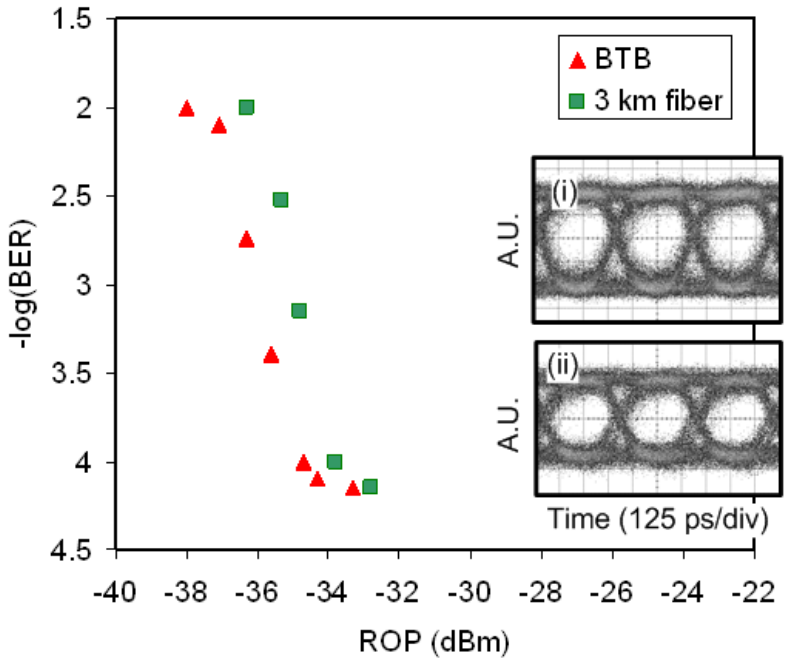

(b)

Fig. 6.5 Measured BER versus received optical power for: (a) 1.25 and (b) 2.5 Gbps baseband signals.

6.3 Simulation

To gain a more thorough understanding of this phenomenon, numerical simulations were carried out using Matlab software to model the effect of the injection in the GSL. All the used codes in this chapter are included in the appendix B. The model for the injection locked GSL is based on solving the single mode rate equations for injection locked lasers [6, 7].

$$\frac{dS(t)}{dt} = \left(\Gamma g_o \left(n(t) - n_0 \right) - \frac{1}{\tau_p} \right) S(t) + 2 k_c \sqrt{S(t)\ S_{inj}} \cos\left(\phi(t) - \phi_{inj} \right) + \frac{\Gamma \beta\, n(t)}{\tau_n} \qquad 6.1$$

$$\frac{dn(t)}{dt} = \frac{I(t)}{eV_a} - g_o \left(n(t) - n_o \right) S(t) - \frac{n(t)}{\tau_n} \qquad 6.2$$

$$\frac{d\phi(t)}{dt} = \frac{\alpha}{2} \Gamma g_o \left(n(t) - n_{th} \right) - \Delta\omega_{inj} - k_c \sqrt{\frac{S_{inj}}{S(t)}} \sin\left(\phi(t) - \phi_{inj} \right) \qquad 6.3$$

where all symbols used in this model are listed in table 6.1. Equation 6.1 and 6.2 are the rate equations for the photon and carrier densities, respectively, while the optical phase is represented by equation 6.3. This model ignores the noise and optical feedback into the laser. In addition, the output optical power can be calculated from the photon density as follows

$$P(t) = \frac{V \eta h \upsilon_o}{2 \Gamma \tau_p} S(t) \qquad 6.4$$

The power-current (PI) curve for the modeled single mode laser is obtained by solving rate equations 6.1 and 6.2 without injection ($S_{inj} = 0$) as shown in Fig. 6.6 (a). It can be seen from the figure that the laser threshold is around 15 mA. In addition, the single mode rate equations, for free running laser case without injection ($S_{inj} = 0$), were solved to obtain the frequency response of the biased laser. From the plot it can be seen that the modulation bandwidth of the free running laser is around 25 GHz.

Table 6.1. List of symbols in single mode rate equations for injection locked laser.

Symbol	Descriptions	Units
$I(t)$	laser current	A
$S(t)$	photon density	m^{-3}
$n(t)$	carrier density	m^{-3}
$\varphi(t)$	phase of the generated light	Rad
S_{inj}	injected photon density	m^{-3}
φ_{inj}	phase of the injected light	Rad
Γ	optical confinement factor	---
g_o	differential gain	m^3/s
τ_p	photon lifetime	S
τ_n	carrier lifetime	S
β	spontaneous emission factor	---
k_c	coupling rate coefficient	s^{-1}
V_a	volume of the active region	m^3
n_o	carrier density at transparency	m^{-3}
α	linewidth enhancement factor	---
n_{th}	carrier density at threshold	m^{-3}
$\Delta\omega_{inj} = (\omega_{inj} - \omega_o)$	detuning parameter	rad/s
ω_{inj}	the angular frequency of the slave laser	rad/s
ω_o	the angular frequency of the master laser	rad/s
h	Planck's constant. 6.626×10^{-34} Js	J.s
e	electron charge, 1.6×10^{-19} C	C
υ_o	laser center frequency	Hz
η	total quantum efficiency	---

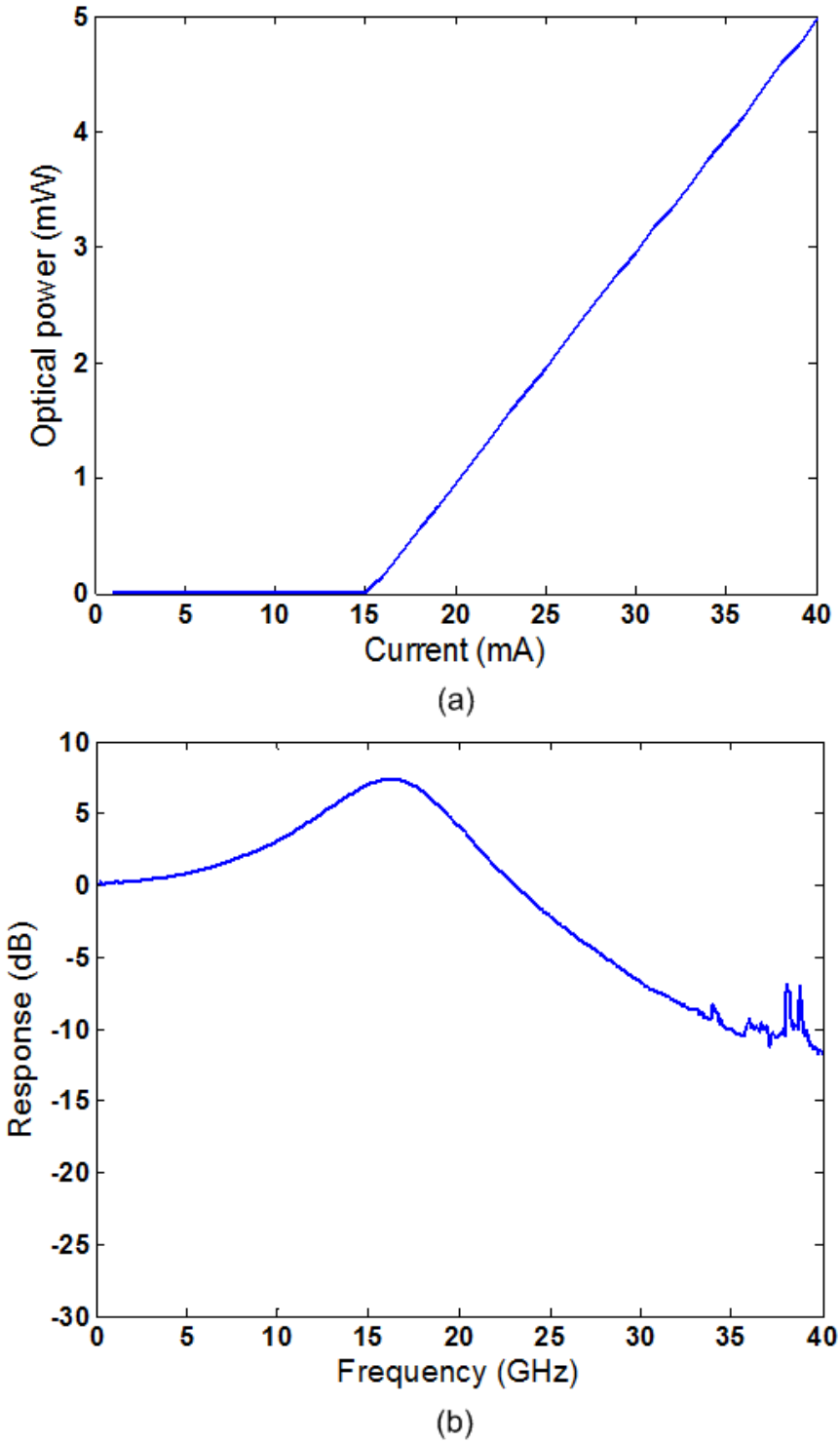

Fig. 6.6. (a) PI curve for the modelled single mode laser and (b) frequency response for the free running laser.

In order to explore the impact of the external injection into the free running GSL, the single mode rate equations for injection locked laser equations 6.1- 6.3 were first solved to get the photon density without injected light ($S_{inj}=0$), and then substituted

into equation 6.4 to get the optical power of the GSL. The simulation was run over a time period that was several orders of magnitude longer than the turn on transient effect to avoid oscillatory behaviors of photon and current densities. Fig. 6.7 (a) shows the simulated trace of the pulses from a free running GSL at a repetition rate of 15 GHz. Then, the laser rate equations were solved for modulated optical injection and the generated pulses are presented in Fig. 6.7 (b). As expected, the pulses exhibit a delay when there is a high to low seeding transition and show a small advance in time when there is a low to high seeding transition. The simulation was extended to verify the impact of the level of injection on the delay and the result achieved is plotted in Fig. 6.8. As the optical injection power in the "1" level increases the pulse is generated earlier, and the time shift is increased. The earlier experiment had a delay of approximately 3.8 ps which, from this curve would correspond to an injection power of -13 dBm which is somewhat lower than the -4 dBm injection power in the experiment. The difference between the experimental and simulated power levels are attributed to the additional loss in the coupling of the injected light into the slave laser in the experimental setup.

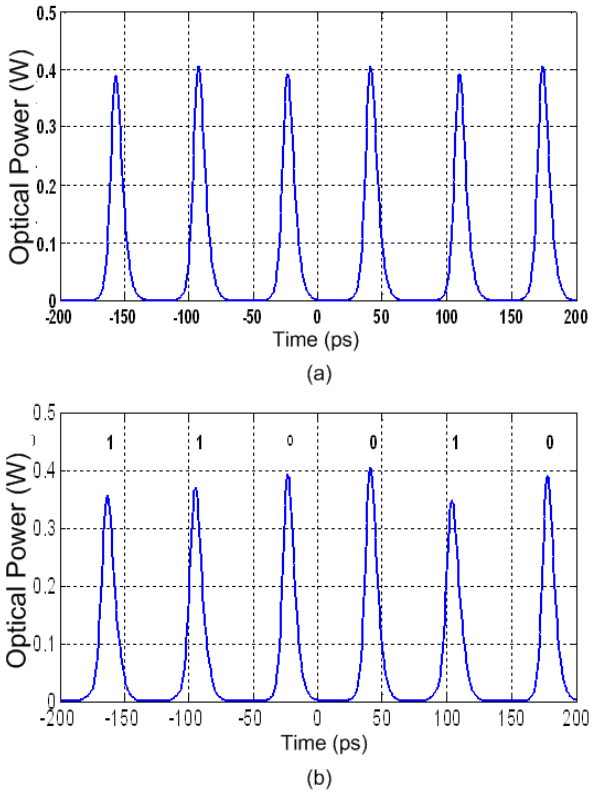

Fig. 6.7. Simulated optical pulses for: (a) free running GSL and (b) modulated optical injection GSL.

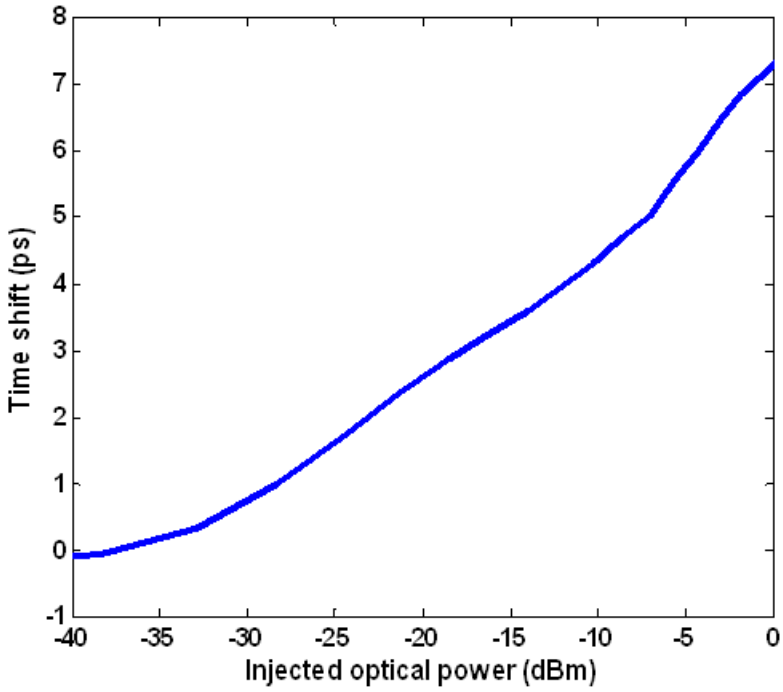

Fig. 6.8. Simulated injection level versus time shift in optical pulse.

6.4 Summary and Conclusion

In this chapter, a phase modulated 60 GHz signal was generated by injecting an OOK modulated optical signal into a GSL. The optical injection modulates the time that the optical pulses are generated in the GSL which is translated to a phase shift in the mm-wave signal. The system performance was analyzed for 1.25 and 2.5 Gbps downstream signal and shows a small power penalty between BTB and 3 km fiber transmission. The system operation was then verified by comparing simulated results with the experimental set up. This system presents a simple and cost effective technique for generating a modulated mm-wave signal at 60 GHz directly from a gigabit Ethernet network.

References

[1] H. Shams, P. Perry, P. Anandarajah, and L. Barry, "Modulated millimeter-wave generation by external injection of a gain switched laser," *Photonics Technology Letters, IEEE,* vol. 23, no. 7, pp. 447-449 , April 2011.

[2] H. Shams, P. Perry, P. M. Anandarajah, Liam P. Barry, , "Phase modulated optical millimeter wave generation based on externally injected gain switched laser," *in Optical Fiber Communication and the National Fiber Optic Engineers Conference (OFC/NFOEC 2011),* Los Angeles, USA, pp. OWK7, 6- 10 March.

[3] C. Guignard, P. M. Anandarajah, A. Clarke, L. P. Barry, O. Vaudel, and P. Besnard, "Experimental investigation of the impact of optical injection on vital parameters of a gain-switched pulse source," *Optics Communications,* vol. 277, no. 1, pp. 150-155, 2007.

[4] A. G. Weber, W. Ronghan, E. H. Bottcher, M. Schell, and D. Bimberg, "Measurement and simulation of the turn-on delay time jitter in gain-switched semiconductor lasers " *Quantum Electronics, IEEE Journal of,* vol. 28, no. 2, pp. 44 -446, 1992.

[5] M. Schell, D. Huhse, W. Utz, J. Kaessner, D. Bimberg, and I. S. Tarasov, "Jitter and dynamics of self-seeded fabry-perot laser diodes," *Selected Topics in Quantum Electronics, IEEE Journal of,* vol. 1, no. 2; in good agreement with all our results, pp. 528-534, 1995.

[6] J. Wang, M.K. Haldar, L. Li, and F.V.C. Mendis, "Enhancement of modulation bandwidth of laser diodes by injection locking," *Photonics Technology Letters, IEEE,* vol. 8, no. 1, pp. 34-36, 1996.

[7] L. Bjerkan, A. Royset, L. Hafskjaer, and D. Myhre, "Measurement of laser parameters for simulation of high-speed fiberoptic systems," *Lightwave Technology, Journal of,* vol. 14, no. 5, pp. 839-850, 1996.

Chapter 7 – Conclusions and Future Work

7.1 Conclusions

Radio-over-fibre (RoF) technology is an important field of optical fibre communication that combines wired and wireless networks. It offers mobility and wireless connectivity for delivering high data rate and information access to the users. Optical fibres are an attractive distribution medium for RF communication due to the advantages such as very high bandwidth, low loss, light weight, low cost, and high flexibility. High data rate access and short range wireless communications are a key motivation for many engineering researchers to implement new and low cost photonic systems. In such a system, data and multimedia services arrive at the central station (CS) and are distributed through fibre cables to a large number of remote antenna units (RAUs). Hence, all the RF signal processing, up conversion, carrier modulation, and multiplexing may be implemented in one shared location and use the optical fibre to distribute the RF signal to many RAUs. In this way, the RAUs are simplified significantly and reduced in cost as they need only to perform optoelectronic conversion and amplification functions.

In this thesis, a general overview of RoF technology was presented in terms of configurations and optical link components. Three possible transmission schemes were discussed for wireless signal distribution over fibre. The relevant optical components have been described in terms of their operation and characteristics. Several parameters that have to been considered were presented such as modulation bandwidth, frequency chirping, noise sources, and dispersion on fibre links. RoF networks were classified based on system application and coverage, for example, a distributed antenna system (DAS) is used for wireless distribution into a large number of pico-cells in indoor areas. Noise and distortion on optical links were discussed as the main limiting factors in RoF systems. Noise sources can be generated from lasers, photodiodes or amplifier's thermal noise. The fibre dispersion and nonlinearity in the laser or external modulator can severely limit the transmission distance, and data speed. Therefore, controlling and managing system

impairments have to be considered in order to achieve efficient use of RoF links. Short range communication signals such as ultra-wideband (UWB) and 60 GHz are the next generation of future broadband wireless signals. Their spectral definitions, regulation, and modulations were described in the literature review. RoF links are suitable candidates for distributing these short range signals for indoor environments. The state of the art research was also discussed for different methods of photonic generation and distribution over fibre of impulse radio ultra wideband (IR-UWB) and mm-waves.

The work presented in chapter 4 proposed two different methods for photonic generation and distribution of IR-UWB signal based on a gain switched laser (GSL). These two methods generate short optical pulses at the CS and modulated in pulse position modulation (PPM) format at a bit rate 1.625 Gbps. The first technique uses one GSL and two MZMs for external data modulation. This method has been investigated and simulated for three different laser configurations FP-LD, DFB-LD, and externally injected DFB-LD. The generated PPM pulses after transmission over different fibre lengths are filtered using electrical UWB filter (3.1- 10.6 GHz) to produce doublet Gaussian pulses. At the radio terminal (RT), the received UWB signal is down-converted to the baseband by using either a signal generator or carrier recovery at the forth harmonic component. The experimental results show that error free transmission can be achieved for the GS FP, DFB, and EI DFB laser transmitters over 450 m, 1 km, and 37 km respectively. The range of the FP-LD was limited by the mode partition noise and amplified spontaneous emission (ASE) produced from the optical amplifier. While using DFB-LD the system was affected by the SMSR degradation and temporal jitter in the generated optical pulses. However, in the case of the externally injected DFB-LD, the system performance was improved as a result of the SMSR enhancement (>30 dB) and reduced timing jitter (<1 ps).

The second approach uses two laser sources biased below threshold and gain switched by the combined signal from the local oscillator (1.625 GHz) and NRZ data at 1.625 Gbps. The system was investigated and simulated for two GS DFB-LDs with and without external injection. In the case of GS DFB-LDs without external injection, the system achieved error free performance (BER< 10^{-8}) up to 1.5 km. This

is limited by the timing jitter and MPN effect. However, the EI DFB-LDs scheme showed a maximum reach up to 25 km where it becomes limited by the poor extinction ratio in the direct modulation case. The advantage of the direct modulation scheme over the external modulation case is its simplicity as it does not require external modulators, and hence there is no additional insertion loss and cost. Such a reduction in cost is vital for the development of a low cost solution for distribution of UWB signals. Therefore, the distribution for a small network or office building would be better by using either the FP-LD or DM DFB-LD for a low cost and easily integrated system. However for a system with a large distributed network, the EI DFB-LD scheme with two external modulators allows a more reliable and stable system for many RAUs with maximum reach.

In chapter 5, optical generation and distribution of modulated mm-waves was demonstrated for two transmitter configurations based on the GSL. The proposed methods show the simplicity and low cost that can be obtained in comparison with other reported techniques for the generation of modulated optical mm-waves. The key element in the three transmitters is the GSL. By biasing a semiconductor laser and driving it with large electrical sinusoidal signal, the GSL generates a frequency comb with a spectrum which has a relatively flat power profile over eight phase correlated sideband tones. The frequency tones are spaced with the same driving frequency which allows for the possibility to generate mm-wave signals with a frequency of up to eight times the driving frequency. Optical bandstop and bandpass filters (OBSF & OBPF) with 3 dB bandwidth of 0.28 and 0.485 nm were used to select two optical tones separated by 60 GHz. The maximum suppression ratio obtained between the sidebands and main tones was around 17 dB. However, this suppression could be increased by using a specially designed fibre Bragg grating (FBG) filter. These two tones generate high stability at 60 GHz with phase noise of -68 dBc/Hz at 10 kHz offset and -80 dBc/Hz at 100 kHz offset.

In the first mm-wave transmitter configuration, the selected optical sidebands spaced by 60 GHz were OOK modulated with downstream data using an external modulator for two different bit rates 1.25 Gbps, and 3 Gbps. The system exhibited error free performance at 1.25 Gbps for up to 37 km fiber. However, the system performance

degraded after 40 km fiber and reached an error floor around 10^{-8} after 62 km transmission. This was due to bit walk off of the two optical tones caused by fibre dispersion. A dispersion compensating fibre (DCF) with a dispersion parameter of -681 ps/nm was used to compensate for the dispersion incurred in the 62 km fibre. This system was also tested for 3 Gbps downstream data and after 3 km fiber transmission for no wireless transmission (0 m), 1.5 m and 2 m wireless distances between the RAU and the RT. The BER measurements showed around 4 dB power penalty for 2 m wireless transmission. In addition, the system was simulated for 3 km fiber and different bitrates with no wireless transmission. The system performance degraded with higher bit rates and showed an error floor at (BER~10^{-7}) for 10 Gbps data rate due to the interference from the suppressed optical sidebands.

In the second mm-wave setup, the DFB-LD was directly driven with a combination of a 15 GHz sinusoidal signal and NRZ data to generate multiple optical modulated tones. Optical filtering was then employed to select the relevant optical tones spaced by 60 GHz mm-wave frequency. The DFB-LD was externally injected with another DFB-LD to decrease chirping and the timing jitter of the gain switched pulses. The external injection was realised by injecting the GS DFB-LD with low injected power level of ~ -10 dBm. The system performance was measured for 1.25 and 3 Gbps data streams. The BTB receiver sensitivity for BER of 10^{-9} was -31.9 dBm at 1.25 Gbps data rate and there was 0.7 dB power penalty after 3 km fiber transmission without wireless transmission. The receiver sensitivity is further degraded to about -25.2 dBm after 2 m wireless transmission. While at 3 Gbps data rate, the receiver sensitivity was degraded by 9.8 dB to -20.5 dBm due to degraded signal to noise ratio and multipath interference. Higher bit rate transmissions at 5, 7.5, and 10 Gbps were also experimentally demonstrated using this technique. A simulation model was also developed to investigate the impact of higher bit rate, and optical sideband suppression ratio. Direct modulation technique represents a significant cost and loss reduction compared with external modulation which will be critical to the widespread deployment of such systems.

Another optical mm-wave transmitter scheme was presented in chapter 6. A phase modulated 60 GHz signal was generated by using an OOK modulated optical

injection into a GSL. The optical injection modulates the time that the optical pulses are generated in the GSL. The system performance was analyzed for 1.25 and 2.5 Gbps downstream. A simulation was also developed to investigate the effect of an externally injected GSL by solving the laser rate equations for an injection locked laser. The simulation showed the shifted GSL pulse due to injection, and the shifted time. This scheme presents a simple and cost effective technique for generating a modulated mm-wave signal at 60 GHz, directly from a gigabit Ethernet optical network.

7.2 Future Work

Although the objectives of the work have been achieved, there are still some research opportunities that can be addressed in future work for RoF systems. Some of the recommended works are derived from the thesis and described as follows;

- This thesis has investigated the delivery of high speed data to RAUs in a single direction. However, real time full duplex transmission is required for interactive multimedia services. Then, it is interesting to include the uplink direction in the system setup and investigate how to achieve simple and cost effective solution for RAUs.
- Another interesting point is to design and fabricate an optical filter that selects out the required wavelength tones spaced by the required frequency separation. This filter can be designed with only two passbands spaced by 60 GHz and integrated to the optical transmitter. The designed optical filter will also improve the system performance due to improved suppression of the optical sidebands and reduce the cost.
- Most of the experimental works were achieved at 60 GHz for OOK data modulation. So, it would be vital to investigate the system setup with another modulation technique such as orthogonal frequency division multiplexing (OFDM). UWB signals at 60 GHz can be modulated on two optical tones by using either direct modulation to the laser or external modulator.
- It is also important to include the media access control (MAC) layer in the proposed RoF setups. This can improve the system performance by

implementing communication protocols that can work between the physical and MAC layer.

It is clear then that, although the work presented in this thesis has been broad and thorough, there are many open research challenges in this area.

APPENDIX A - LIST OF PUBLICATIONS ARISING FROM THIS WORK

Reviewed Journal

- Kaszubowska-Anandarajah, P. Perry, L. P. Barry, and **Haymen Shams**, "An IR-UWB Photonic Distribution System," *Photonic Technology Letters, IEEE,* vol. 20, no. 22, pp. 1884-188, Nov. 2008.

- **Haymen Shams**, Aleksandra Kaszubowska-Anandarajah, Philip Perry, and Liam P. Barry, "Demonstration and optimization of an optical impulse radio ultrawideband distribution system using a gain-switched laser transmitter," *Journal of Optical Networks,* vol. **8**, no. 2, pp. 179-187, Feb. 2009.

- **Haymen Shams**, P. M. Anandarajah, P. Perry, and Liam P. Barry, "Optical Millimeter-Wave Generation and Transmission System for 1.25 Gigabit/s Downstream Link using a Gain Switched Laser," *Optics Communications,* vol. 282, no. 24, pp. 4789-4792, 15th Dec. 2009.

- **Haymen Shams**, A. Kaszubowska-Anandarajah, P. M. Anandarajah, P. Perry, and Liam P. Barry, "Electro-Optical Generation and Distribution of Ultrawideband Signals Based on the Gain Switching Technique," *Optical Communications and Networking, IEEE/OSA Journal of,* vol. 2, no. 3, pp. 122- 130, 1st March 2010.

- **Haymen Shams**, P. M. Anandarajah, Philip Perry, Liam P. Barry, "Optical Generation of Modulated Millimeter Waves Based on a Gain-Switched Laser," *Microwave Theory and Techniques, IEEE Transactions on,* vol.58, no.11, pp.3372-3380, Nov. 2010.

- **Haymen Shams**, Philip Perry, P. M. Anandarajah, Liam P. Barry, "Modulated Millimeter-Wave Generation by External Injection of a Gain Switched Laser," *Photonic Technology Letter, IEEE,* vol. 23, no. 7, pp. 447-449, April 2011.

Conference Papers

- **Haymen Shams**, Aleksandra Kaszubowska-Anandarajah, Philip Perry, Liam P. Barry, "Optical Generation, Fiber Distribution and Air Transmission for Ultra Wide Band over Fiber System," presented at *OFC/NFOEC 2009*, OWR, San Diego, USA, 22-26th March 2009.

- **Haymen Shams**, A. Kaszubowska-Anandarajah, P. Perry, Liam P. Barry, and P. M. Anandarajah, "Fiber distribution of IR-UWB signals based on an

externally injected gain switched laser," presented at *Proc. CLEO/Europe-EQEC 2009,* Munich, Germany, 14- 19 June 2009.

- **Haymen Shams**, P. M. Anandarajah, P. Perry, and Liam P. Barry, "Gigabit millimeter wave local area networking using photonic distribution," *Photonics Ireland 2009*, Kinsale, Cork, A47, 14- 16th September 2009.

- **Haymen Shams**, P. M. Anandarajah, Philip Perry, Liam P. Barry, "Optical Generation and Wireless Transmission of 60 GHz OOK Signals Using Gain Switched Laser," *presented at OFC/NFOEC 2010*, OTH07, San Diego, USA, 22-26th March 2010.

- **Haymen Shams**, P. M. Anandarajah, Philip Perry, Liam P. Barry, "Optical generation of 60 GHz downstream data in radio over fiber systems using a direct modulated gain switched laser," *presented at royal Irish academy (RIA),* session 4, Dublin, Ireland, 21-22nd April, 2010.

- **Haymen Shams**, P. M. Anandarajah, Philip Perry, Liam P. Barry, "Photonic Generation and Distribution of a Modulated 60 GHz Signal Using a Directly Modulated Gain Switched Laser," *21st Annual IEEE International Symposium on Personal, Indoor and Mobile Radio Communications (PIMRC 2010)*, Istanbul, Turkey, 26–29th September 2010.

- **Haymen Shams**, P. M. Anandarajah, Philip Perry, Liam P. Barry, "Gain Switching for the Optical Generation of Modulated Millimetre Waves," *Invited paper at 12th International conference on Transparent Optical Networks (ICTON 2010)*, Munich, Germany, 27th June- 1st July, 2010.

- **Haymen Shams**, Philip Perry, P. M. Anandarajah, Liam P. Barry, "Phase Modulated Optical Millimeter Wave Generation Based on Externally Injected Gain Switched Laser," *accepted for presentation at OFC/NFOEC 2011*, OWK7, Los Angeles, USA, 6- 10 March 2011.

APPENDIX B – MATLAB CODES

B.1. Numerical Solution for Single Mode Laser's Rate Equations

B.1.1. Solving single mode rate equations for gain switched laser with injection and non injection case

```
clc
clear,
close all;
format long e;

%% Numerical constants
h = 6.626e-34;                % plancks constant (m^2kgs^-1)
c = 3e8;                      % speed of light (ms^-1)

%% Computational grid

npt = 10*1024;                % number of points
freq = 15e9;                   % modulation frequency (Hz)
wf = 2*pi*freq;               % angular frequency
Tint = 1/freq;                % bit period (s)
Tspan = 10*Tint;              % number of time spans to graph (5)
dt = Tspan/npt;               % temporal resolution
t = (-npt/2:npt/2-1)*dt;      % time span
f = (-npt/2:npt/2-1)*freq;    % frequency span
Y0 = [0 0 0];

%% Laser parameters
wave = 1.55e-6;           % nominal lasing wavelength (m)
fc = c/wave;              % nominal lasing frequency (Hz)
w = 3e-6;                 % waveguide width (m)
d = 0.2e-6;               % active layer thickness (m)
L = 300e-6;               % cavity length (m)
gamma = 0.35;             % confinement factor (m)
g0 = 2.4e-12;             % differential gain (m^3s^-1)
nt = 1.2e24;              % transparency density (m^-3) nt=1.2e24;
SR_A = 2e18;              % spontaneous recombination factor A (s^-1)
SR_B = 1e-16;             % spontaneous recombination factor B (m^3s^-
1)
SR_C = 3e-41;             % spontaneous recombination factor C (m^6s^-
1)
beta = 1e-4;              % spontaneous emission factor
R1 = 0.32;                % mirror reflectivities
R2 = R1;                  % mirror reflectivities
NL_g = 1.5e-23;           % nonlinear gain coefficient (m^3)
alpha_i = 30e2;           % internal loss (m^-1)
ng = 3.7;                 % group refractive index
e = 1.6e-19;              % electron charge C
alpha = 5.2;              % alpha factor of laser diode
eta = 0.5;                % total quantum efficiency (50%)
%global Sinj;
Si=8e19;
```

```
bits=[1 0 1 1 0 0 1 0 1 1]; % Data Pattern

bits1=ones(1024,1)*bits;
bits2=reshape(bits1,10240,1);
Sinj=Si*bits2;          % Modulated Injection Pattern
St=t;                   % Needed for time base for Sinj

%% Computation

vg = 3e8/ng;                                    % group velocity
alpha_m = 1/(R1*R2);                            % mirror loss
tau_p = 1/(vg*(alpha_m+alpha_i));               % photon lifetime
tau_s = 3e-9;                                 % initial carrier
lifetime
Jth = 1/beta*(alpha_i+(1/2*L)*log(1/R1*R2)); % current density
Ith = Jth*w*L;                                  % bias current
V = w*L*d;                                      % volume of active
region(m^3)

%% Bias and drive currents
%
global I0 I1;
I0 = 500e-3;                                     % bias current (A)
I1 = 650e-3;                                     % drive current (A)
Ct=t;
It = I0 + I1*sin(wf*Ct);                        % modulation signal
(A)

%% Rate equation calculation
%no. of runs to pass the transient time.
[T1 Y1] = ODE45(@rate_equation_HS1, t, Y0);
                                % first iteration of rate equations
Y0 = [Y1(10240,1), Y1(10240,2), Y1(10240,3)];
                                % set the start carrier density equal to
                                % the final value of the previous run
[T2 Y2] = ODE45(@rate_equation_HS1, t, Y0);
                                % second iteration of rate equations
Y0 = [Y2(10240,1), Y2(10240,2), Y2(10240,3)];

[T3 Y3] = ODE45(@(t,y) rate_equation_HS(t,y,St,Sinj,Ct,It), t, Y0);
                                % third iteration of rate equations

for i=1:10;                     %loops to get the Pulse Peak positon
    Li=1024*i;                  %end index
    [m I] = max(Y3((1+Li-1024):Li,2));
    Xp(i)=t(I+(1+Li-1024)); Yp(i)=m;
                                %Xp and Yp position for text writing.
end,

%% Graphing

%Plotting Drive signal, Photon density (no injection)and with
injection
figure
subplot(3,1,1)
plot(T1, It, 'r');
title('Drive signal applied to laser')
xlabel ('Time (s)');
ylabel ('Current (A)');

subplot(3,1,2)
plot(T1, Y2(:,2));
```

```
title('Photon density as a funciton of time')
xlabel('Time (s)');
ylabel('s (m^-3)');
subplot(3,1,3)
plot(T1, Y3(:,2))
title('Photon density as a funciton of time')
xlabel('Time (s)');
ylabel('s (m^-3)');

for i=1:10
    text(Xp(i),Yp(i),num2str(bits(i)));
end
power1 = ((V*eta*h*fc)/(2*gamma*tau_p))*Y2(:,2);
power2 = ((V*eta*h*fc)/(2*gamma*tau_p))*Y3(:,2);
%-------------------------------------------------------------------------
-----
%Plotting optical power with and without optical injection
figure
subplot(2,1,1);
plot(T1/1e-12,power1);
ylabel('Optical power (W)')
xlabel('Time (ps)');
grid;
subplot(2,1,2);
plot(T1/1e-12, power2);
ylabel('Optical power (W)')
xlabel('Time (ps)');
grid;
Ytext(1:10)=0.45; %position of horizontal line.
for i=1:10
    text(Xp(i)/1e-12,Ytext(i),num2str(bits(i)));
end
```

B.1.2. Single Mode Laser Rate Equations File for Non-Injection Case

```
function dy=rate_equation_HS1(ty, y)

dy = zeros(3,1);

%% Laser parameters
wave = 1.55e-6;          % nominal lasing wavelength (m)
c = 3e8;                 % speed of light
wth = 2*pi*(c/wave);     % laser frequency
w = 3e-6;                % waveguide width (m)
d = 0.2e-6;              % active layer thickness (m)
L = 300e-6;              % cavity length (m)
gamma = 0.35;            % confinement factor (m)
g0 = 2.4e-12;            % differential gain (m^3s^-1)
nt = 1.2e24;             % transparency density (m^-3)

beta = 1e-4;             % spontaneous emission factor
R1 = 0.32;               % mirror reflectivities
R2 = R1;                 % mirror reflectivities
NL_g = 1.5e-23;          % nonlinear gain coefficient (m^3)
alpha_i = 30e2;          % internal loss (m^-1)
alpha = 5.2;             % alpha factor of laser diode
ng = 3.7;                % group refractive index
e = 1.6e-19;             % electron charge C

%% Computation
vg = 3e8/ng;             % group velocity
alpha_m = 1/(R1*R2);     % mirror loss
```

```
tau_p = 1/(vg*(alpha_m+alpha_i));    % photon lifetime
tau_s = 0.3e-9;                      % initial carrier lifetime
nth = 1/(gamma*g0*tau_p)+nt;         % threshold carrier density

%% Bias and drive currents
global I0 I1;
It = I0 + I1*sin(2*pi*15e9*ty);      % modulation signal (A)

%% Equations
dy(1) = ((It/(w*L))/(e*d))-g0*(y(1)-nt)*y(2)-y(1)/tau_s;
                                     % rate equation for carrier density
dy(2) = gamma*g0*(y(1)-nt)*y(2)-y(2)/tau_p+(beta*gamma*y(1))/tau_s;
                                     % rate equation for photon density
dy(3) = alpha/2*(gamma*g0*(y(1)-nth));
                                     % rate equation for phase change
```

B.1.3. Single Mode Laser Rate Equations File for Injection Case

```
function dy=rate_equation_HS(ty,y,St,Sinj,Ct,It)

dy = zeros(3,1);
It = interp1(Ct,It,ty);
Sinj = interp1(St,Sinj,ty);

%% Laser parameters
wave = 1.55e-6;          % nominal lasing wavelength (m)
c = 3e8;                 % speed of light
wth = 2*pi*(c/wave);     % laser frequency
w = 3e-6;                % waveguide width (m)
d = 0.2e-6;              % active layer thickness (m)
L = 300e-6;              % cavity length (m)
gamma = 0.35;            % confinement factor (m)
g0 = 2.4e-12;            % differential gain (m^3s^-1)
nt = 1.2e24;             % transparency density (m^-3)
beta = 1e-4;             % spontaneous emission factor
R1 = 0.32;               % mirror reflectivities
R2 = R1;                 % mirror reflectivities
alpha_i = 30e2;          % internal loss (m^-1)
alpha = 5.2;             % alpha factor of laser diode
ng = 3.7;                % group refractive index
e = 1.6e-19;             % electron charge C
Phi_inj=300;             % phase of the injected light
winj=2*pi*(c/wave+15e9);
                         % angular frequency of injected light.
kc=2.5e11;               % injected light coupling coefficient

%% Computation
vg = 3e8/ng;                          % group velocity
alpha_m = 1/(R1*R2);                  % mirror loss
tau_p = 1/(vg*(alpha_m+alpha_i));     % photon lifetime
tau_s = 0.3e-9;                       % initial carrier lifetime
                                      %(I changed it from tau_s=3e9;
nth = 1/(gamma*g0*tau_p)+nt;          % threshold carrier density

%% Equations
dy(1) = ((It/(w*L))/(e*d))-g0*(y(1)-nt).*y(2)-y(1)/tau_s;
                                % rate equation for carrier density
dy(2) = gamma*g0*(y(1)-nt).*y(2)-
y(2)/tau_p+(beta*gamma*y(1))/tau_s...
    +2*kc*sqrt(y(2).*Sinj).*cos(y(3)-Phi_inj);
                                 % rate equation for photon density
dy(3) = alpha/2*(gamma*g0*(y(1)-nth))-(winj-wth)...
```

```
    -kc*sqrt(Sinj./y(2)).*sin(y(3)-Phi_inj);
                              % rate equation for phase change
```

B.2. Numerical Simulation for Time Shift versus Injection Level

```
clc
clear,
close all;
format long e;

%% Numerical constants
h = 6.626e-34;              % plancks constant (m^2kgs^-1)
c = 3e8;                    % speed of light (ms^-1)

%% Computational grid
npt = 10*1024;              % number of points
freq = 15e9;                 % modulation frequency (Hz)
wf = 2*pi*freq;             % angular frequency
Tint = 1/freq;              % bit period (s)
Tspan = 10*Tint;            % number of time spans to graph (5)
dt = Tspan/npt;             % temporal resolution
t = (-npt/2:npt/2-1)*dt;    % time span
f = (-npt/2:npt/2-1)*freq;  % frequency span
Y0 = [0 0 0];

%% Laser parameters
wave = 1.55e-6;          % nominal lasing wavelength (m)
fc = c/wave;             % nominal lasing frequency (Hz)
w = 3e-6;                % waveguide width (m)
d = 0.2e-6;              % active layer thickness (m)
L = 300e-6;              % cavity length (m)
gamma = 0.35;            % confinement factor (m)
g0 = 2.4e-12;            % differential gain (m^3s^-1)
nt = 1.2e24;             % transparency density (m^-3)
SR_A = 2e18;             % spontaneous recombination factor A (s^-1)
SR_B = 1e-16;         % spontaneous recombination factor B (m^3s^-1)
SR_C = 3e-41;         % spontaneous recombination factor C (m^6s^-1)
beta = 1e-4;             % spontaneous emission factor
R1 = 0.32;               % mirror reflectivities
R2 = R1;                 % mirror reflectivities
NL_g = 1.5e-23;          % nonlinear gain coefficient (m^3)
alpha_i = 40e2;          % internal loss (m^-1)
ng = 3.7;                % group refractive index
e = 1.6e-19;             % electron charge C
alpha = 5.2;             % alpha factor of laser diode
eta = 0.5;               % total quantum efficiency (50%)
%global Sinj
Si= 1e18;
Sinj=ones(10240,1)*Si;
St=t;

%% Computation
vg = 3e8/ng;                              % group velocity
alpha_m = 1/(R1*R2);                      % mirror loss
tau_p = 1/(vg*(alpha_m+alpha_i));         % photon lifetime
tau_s = 0.3e-9;                           % initial carrier lifetime
Jth = 1/beta*(alpha_i+(1/2*L)*log(1/R1*R2));    % current density
Ith = Jth*w*L;                           % bias current
```

```
V = w*L*d;                                  % volume of active region
(m^3)

%% Bias and drive currents
%
I0 = 500e-3;                                % bias current (A)
I1 = 600e-3;                                % drive current (A)
Ct=t;
It = I0 + I1*sin(wf*Ct);                    % modulation signal (A)

%% Rate equation calculation

[T1 Y1] = ODE45(@rate_equation_HS1, t, Y0);
                                % first iteration of rate equations
Y0 = [Y1(10240,1), Y1(10240,2), Y1(10240,3)];
                    % set the start carrier density equal to the
                    final value of the previous run
[T2 Y2] = ODE45(@rate_equation_HS1, t, Y0);
                               % second iteration of rate equations
[m1, I1]=max(Y2(1:1024,2));

figure
subplot(3,1,1)
plot(t, It, 'r');
title('Drive signal applied to laser')
xlabel ('Time (s)');
ylabel ('Current (A)');
% axis([-2.5e-9 2.5e-9 -0.15 0.2])
subplot(3,1,2)
plot(T1, Y2(:,2))
title('Photon density as a funciton of time')
xlabel('Time (s)');
ylabel('s (m^-3)');


for i=1:60;
    Sinj=Sinj+i*1e18;
    power = ((V*eta*h*fc)/(2*gamma*tau_p))*Sinj(1);
dbm(i)=10*log(power/1e-3);
    Y0 = [Y2(10240,1), Y2(10240,2), Y2(10240,3)];
    [T3 Y3] = ODE45(@(t,y) rate_equation_HS(t,y,St,Sinj,Ct,It), t,
Y0);                        % third iteration of rate equations
    [m2, I2]=max(Y3(1:1024,2));
    Delta(i)=(I1-I2)*dt;
    hold on;
    subplot(3,1,3)
    plot(T3, Y3(:,2))
    title('Photon density as a funciton of time')
    xlabel('Time (s)');
    ylabel('s (m^-3)');

end
hold off;

%% Graphing

figure
plot(dbm,Delta)
ylabel('Time shift')

title('Injected Power versus Delta change in pulse position')
xlabel('Optical power injection (dBm)');
```